Contents lists available at ScienceDirect

Arabian Journal of Chemistry

journal homepage: www.ksu.edu.sa

Review article

In-depth review of synthesis of hydroxyapatite biomaterials from natural resources and chemical regents for biomedical applications

Precious Osayamen Etinosa [a], Obinna Anayo Osuchukwu [b,k,*], Emeka Obiora Anisiji [c], Mohammed Y. Lawal [d], Sikiru Adepoju Mohammed [d], Opeyemi Isaac Ibitoye [e], Peter Gbenga Oni [f], Victor D. Aderibigbe [g], Toyin Aina [h], Damilola Oyebode [i], Solomon C. Nwigbo [j]

[a] Department of Mechanical Engineering, Worcester Polytechnic Institute, 100 Institute Road, Worcester, MA 01609, USA
[b] Department of Mechanical Engineering, Bayero University, Kano 700241, Kano State, Nigeria
[c] Department of Mechanical and Mechatronics Engineering, Federal University, Otuoke 562103, Nigeria
[d] Department of Mechanical Engineering, Nigerian Defence Academy, PMB, 2109 Kaduna, Nigeria
[e] Department of Biology and Biotechnology, Worcester Polytechnic Institute, 100 Institute Road, Worcester, MA 01609, USA
[f] Department of Chemistry and Biochemistry, Worcester Polytechnic Institute, 100 Institute Road, Worcester, MA 01609, USA
[g] Department of Chemistry, University of Wyoming, 1000 E University Ave, Laramie, WY 82071, USA
[h] Department of Biomedical Engineering, College of Engineering, Afe Babalola University, Ado Ekiti KM 8.5 Afe Babalola Way, 5454 Ado Ekiti, Ekiti State, Nigeria
[i] Center for Molecular and Cellular Bioscience, University of Southern Mississippi, 118 College Dr, Hattiesburg, MS 39406, USA
[j] Department of Mechanical Engineering, Nnamdi Azikiwe University, Awka 420007, Anambra State, Nigeria
[k] Multifunctional Materials Laboratory, Shell Chair Office in Mechanical Engineering, Ahmadu Bello University, Zaria, 810212 Samaru Zaria, Kaduna State, Nigeria

ARTICLE INFO

Keywords:
Biomedical
Bioactive
Mechanical properties
Sol-gel
Tissue engineering
Synthesis technique

ABSTRACT

Hydroxyapatite (HAp) is a popular ceramic biomaterial, which has extensively been employed in numerous biomedical applications. It has drawn the attention of scientists primarily owing to its properties similar to the bones and teeth of human beings. Due to its organic similarity, HAp has exceptional biocompatibility and can activate osteoconduction and osteoinduction occurrence. Hence, HAp has been used in a broad collection of healing applications extending from common dental implant, and bioactive coatings on grafts to purposefully premeditated drug delivery methods, and even for tissue engineering (TE) applications. The production method is essential in controlling the physicochemical properties of HAp, which in turn affects its mechanical and biological properties. The anticipated physiognomies of HAp can be accomplished using a suitable technique of production and sources. This in-depth review discussed the various natural sources of HAp, and synthesis techniques for producing HAp, alongside their advantages and disadvantages, applications, and essentials of HAp for therapeutic applications. From the review, it was found that the sol–gel route is preferred over other routes because of its even molecular mixing, high purity of products, low production temperature, and ability to synthesize nanosized particles of HAp. As a result, it is provisional that upon the cautious blend of key considerations such as sources, synthesis technique, and production parameters for the manufacture of natural HAp (NHAp), mechanical properties can be improved and the product can be employed as a drug delivery system. These are important extents for the prospect of the research.

1. Introduction

Ceramics belongs to the family of biomaterials employed in biomedical engineering (BE). Because of their flexibility in production, high compressive strength, variable porosity, and bioactive qualities in the body, ceramics are often employed as implant materials (Liu and Yang, 2014; Osuchukwu et al., 2023, 2022a, b). This type of biomaterial can be synthesized from bovine bones (B) (Osuchukwu et al., 2022c, 2021; Obada et al., 2022) and catfish (C) bones (Osuchukwu et al., 2022d, 2023; Osuchukwu et al., 2023), Nevertheless, hydroxyapatite (HAp) and porous coating materials are the most often used therapies today (Aldousari et al., 2018). The goal of using a coating layer is to

* Corresponding author.
E-mail addresses: poetinosa@wpi.edu (P.O. Etinosa), oao1800004.pme@buk.edu.ng (O.A. Osuchukwu).

https://doi.org/10.1016/j.arabjc.2024.106010
Received 16 October 2023; Accepted 2 October 2024
Available online 16 October 2024

achieve effective osseointegration and critical bone-implant interaction. Researchers have continued to investigate the production of hydroxyapatite (HAp) scaffolds for bone tissue applications in recent years because of their important bioactivity and osteoconductivity (Apostu et al., 2018).

HAp is an inorganic bio-ceramic component of natural bones and teeth with high biocompatibility, osteoinductivity, surface area (100 m^2 g^{-1}), and bioactivity (Awasthi et al., 2021; Figueiredo et al., 2010; Kamalanathan et al., 2014). Hydroxyapatite has the following characteristics: The apatite molecular formula is $Ca_{10}(PO_4)_6(OH)_2$, which is similar to that of human apatite and has Calcium – Phosphate ratio of 1.67. When used for bone repairs, HAp has been demonstrated to be the most stable biomaterial with these fundamental properties by numerous researchers (Niakan et al., 2017). Natural hydroxyapatite can be produced from fish, camels, horses, and cattle or bovine bones. It can also be produced from limestone, plants, algae, and eggshells (Abukawa et al., 2006; Abifarin et al., 2019; Obada et al., 2020; Niakan et al., 2015; Goto and Sasaki, 2014; Pal et al., 2017; Ramirez-Gutierrez et al., 2017; Ramesh et al., 2016; Edralin et al., 2017). Laonapakul (Wu et al., 2017) listed some of the physiochemical, mechanical, and biological characteristics of HAp, and some of the methods for producing HAp. The biomaterial, HAp, have mechanical properties that are most similar to those of human bone tissue (Laonapakul, 2015). Hydroxyapatite has low fracture toughness and flexural strength, which prevents it from being used as a graft material on a large scale in orthopaedics and dentistry (Hench, 1998).

Sol-gel process (Layrolle et al., 1998), chemical precipitation (Loo et al., 2008), hydrothermal reaction, and solid-state reaction (Sobczak et al., 2009) are a few of the routes that can be utilized to manufacture hydroxyapatite powder. Using these techniques, varied morphologies, stoichiometric patterns, grain sizes, and crystallinity levels of HAp powder were produced (Sobczak et al., 2009). Sintering is a widely accepted technique for synthesizing HAp (Ramesh et al., 2011; Farokhi et al., 2018; Lu and Mikos, 1996; De Groot, 1980; Tan et al., 2013)]. According to Stea et al. (1995), the HAp produced by the sintering process developed a very strong bond with bone tissue. According to other researchers, microwave, spark plasma, and conventional muffle furnace sintering are the three main categories of HAp sintering techniques. Using thermal decomposition, Odusote et al. (2019), produced HAp from bovine bone. Before processing the bones, hot water was used to de-fat the bones. To eliminate the organic phase, the bones were calcinated at 750 °C to obtain HAp. The results showed that hydroxyapatite may be inexpensively derived from a natural source, such as bovine bone, and can be used as a restorative biomaterial for dental implants and replacement of hard tissues (Odusote et al., 2019). The dimensions, natures, and crystalline segments of the extracted HAp are all impacted by the extraction procedures, according to Ravaglioli and Krajewski (1991). According to Sobczak et al. (2009), the method for creating HAp powders from waste is intriguing because of its economic worth and environmental benefits. They also noted that the HAp is resistant to being readily overwritten by human tissues because of its inherent resemblance to human bone.

Song et al. (2023) reviewed some approaches for the plan and production of bionic scaffolds to enhance bone defect restoration, roles of artificial intelligence (AI) and medical imaging in supporting clinical treatment. Considering the low subsistence rate and poor variation efficacy of stem cells, as well as the inadequate integration of implanted stem cells, limited the restoration of bone injuries. Hao et al. (2024) fabricated magnetic special HAp to fix mesenchyme stem cells into a three-dimensional hybrid spheroid for modelling bone tissue. This method can overcome the low subsistence rate and poor variation efficiency of stem cells, as well as imbalanced interface fusion problems. In their work, Dang et al. (2024) examined the structure of the soft-hard tissue interface of the periodontium and the factors that influence the development of this interface. They also looked at significant guiding paths and biomimetic restoration techniques (such as controlling the fate of seed cells, planning bionic scaffolds, and scheming functional hydrogels) in interfacial tissue engineering. Oryan and his colleagues (Oryan et al., 2014) concluded that bone implanting is one of the most generally employed alternatives to bone restoration.

To minimize the cost of producing pure HAp from natural sources, from the open literature, no research has been made about the utilization of animal matrix of non-separated biowastes and catfish bones derived hydroxyapatite (% wt, as shown in the graphical abstract). The accessibility of these bones as the natural resources of HAp makes the study motivating. Hence, this paper targets to accomplish a review of different synthesis methods of HAp to minimize the cost of producing HAp from natural sources that will be used for different biomedical applications such as bone defect fillers and tissue engineering scaffolds, implant coating, pins for anchoring tooth implants and drug delivery systems and also for other important purposes (Osuchukwu et al., 2021; Oonishi, 1991). This review centres on the recent studies of the sources of HAp, and production techniques of HAp fabrication for different biomedical applications (bone fillers and tissue engineering scaffolds, implant coating arrangement, and drug delivery methods).

2. Natural sources of hydroxyapatite

2.1. Hydroxyapatite from fishbone sources

The production of fish waste, such as scales and bones, has significantly increased due to the rising global fish consumption (Kris-Etherton et al., 2002). In fisheries, salvaging fish scales and bones aids HAp extraction and decreases solid waste (Tang, 2021). The catfish fish bone (Fig. 1) is a fantastic source for synthesizing HAp since it is rich in calcium, phosphate, and carbonate (Panda et al., 2014).

Fish bones and scales have been pretreated utilizing a variety of techniques. Boiling is a popular pretreatment procedure used to eliminate fatty flesh and undesirable residue on the scale and bone (Pal et al., 2017; Akram et al., 2014; Sunil and Jagannatham, 2016). Moreover, the fishbone or scale is processed by rinsing in tap water (Panda et al., 2014), then soaked in low concentrations of hydrochloric acid (0.1–1 M HCl) to deproteinize the material, and then washed in tap water (Pon-On et al., 2016). Before further processing, fish scales and bones were often broken up or ground into pieces (Laonapakul, 2015). Sol-gel process (Layrolle et al., 1998), chemical precipitation (Loo et al., 2008), hydrothermal reaction (Krishnamra and Tang, 2016), calcination (Kongsri et al., 2013), and solid-state reaction (Sobczak et al., 2009) are a few of the methods that can be utilized to manufacture hydroxyapatite powder.

Fig. 1. Typical catfish bones (Osuchukwu et al., 2021).

It was discovered that Pb^{2+}, Cu^{2+}, Cd^{2+}, and Ni^{2+}, among other metals and radionuclides, can be removed by fish bone apatite to levels below the noticeable points. The removal of chromium from groundwater by fish bone apatite has been investigated by Ozawa and Suzuki (Ozawa and Suzuki, 2002). In this review, the majority of the techniques utilized to extract HAp from fishbones used the calcination technique, either as the only process or in conjunction with other techniques (Sun et al., 2017; Londoño-Restrepo et al., 2016; Raghavendra et al., 2015; Hussin et al., 2022; DileepKumar et al., 2022; Liu et al., 2018; Ahmed et al., 2022). Sunil and Jagannatham (2016) employed a low-cost method to produce HAp from fish bones by a simple heat treatment route. The produced pure HAp had traces of Ca, P, O, and Mg. At 600–1000 °C, the powders yielded large fused crystals of ≈200 nm. Surya et al. (2021) extracted HAp from the bones of Sardinella fish via an alkaline hydrolysis technique. The scanning electron microscope (SEM) showed an agglomerates of fine and rod-like crystals with a structure of dense thick particles. Fourier transform infrared spectroscopy (FTIR) spectral bands revealed some functional groups present in the produced HAp. Irfan et al. (2021) produced HAp from fish bones, the fracture analysis was performed using the 2-parameter and 3-parameter Weibull functions to confirm the best suitable results.

With traditional sintering methods, Obada et al. (2023) produced porous kaolin-based ceramic assisted materials. Using the compaction load of 10–20 MPa, the assisted materials were compacted and sintered at 900 and 1000 °C. The hardness and fracture toughness values of 0.409 GPa and 0.835 MPa $m^{1/2}$ were obtained. Sathiyavimal et al. (2020) produced HAp from fish bones. The fishbones were dried overnight at 75 °C in a hot air oven. The bones were broken up into little pieces after drying, and calcination was carried out for 4 h at 900 °C. The calcined bones were then pounded into a fine powder using a mortar and pestle. The fine powder of the HAp was kept at 4 °C for a maximum of 8 weeks for characterization. The XRD result (Fig. 2) revealed the attendance of strong diffraction peaks at 2θ positions of 18.02°, 28.65°, 29.37°, 34.08°, 39.27°, 47.12°, 50.78°, 54.29°, 62.56° and 64.33°, signifying reflections from (1 0 0), (1 0 2), (2 1 0), (2 1 1), (1 3 0), (2 2 2), (1 3 2), (0 0 4), (2 4 1) and (5 0 2) crystal planes, respectively.

Pamungkas et al. (2019) produced HAp from fish bones using thermal calcination, but the powder has impurities. Nano-HAp was

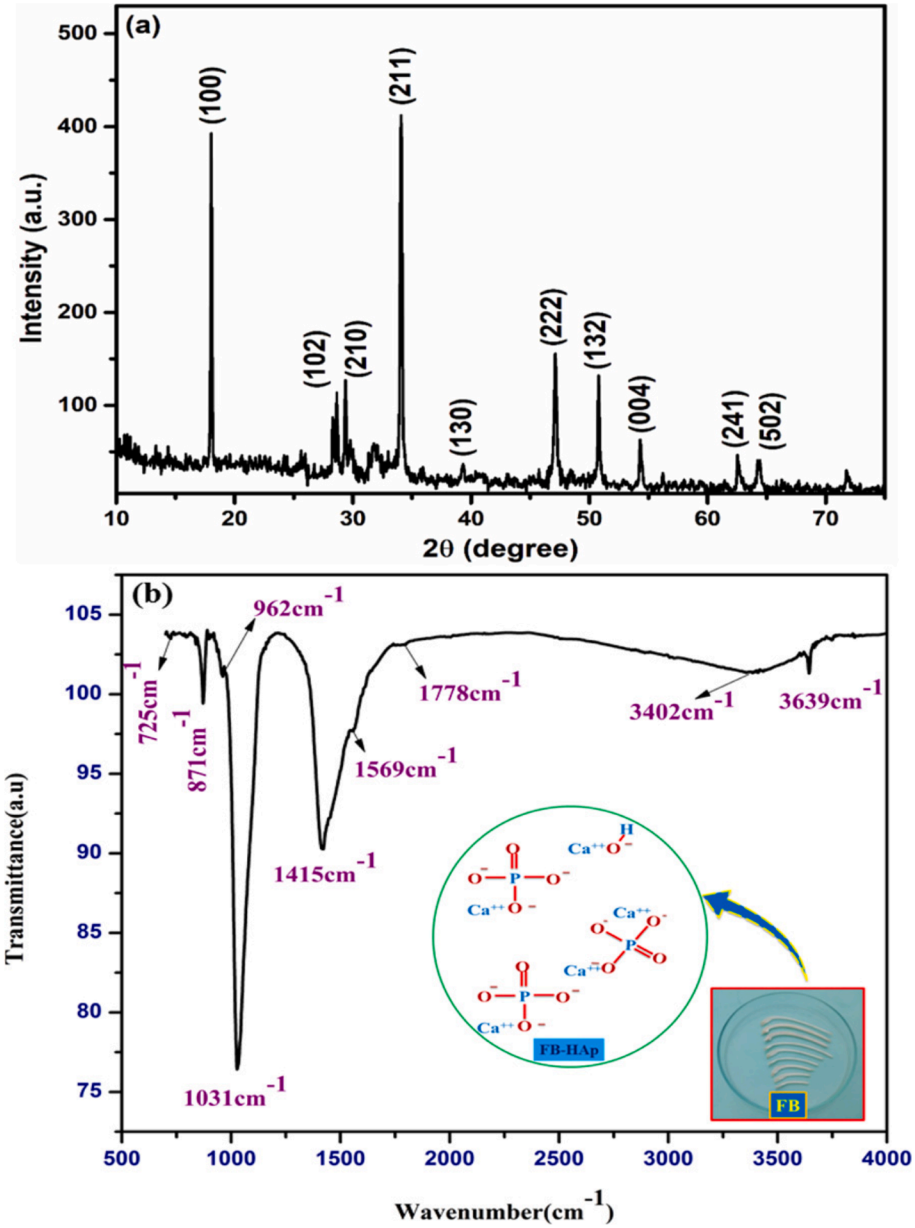

Fig. 2. XRD pattern of fish bone HAp showing different peaks (Sathiyavimal et al., 2020).

synthesized from fish scales by an alkaline heat treatment route. The produced NHAp has a Calcium-to-Phosphate (Ca/P) molar ratio of 1.67 (Sathiskumar et al., 2019).

In another work, a poly-coated HAp scaffold was produced from cuttlefish bone. Hydrothermal conversion of aragonitic cuttlefish bone into HAp was attained at 200 °C retaining the cuttlebone design. The phosphate precursors and treated bones underwent hydrothermal treatment to achieve a Ca/P ratio of 1.67. The bones were then dried at 105 °C after being cooked in deionized water. The compressive strength of 0.88 MPa and the elastic modulus of 15.5 MPa were reported for human trabecular bones. The SEM image showed a sponge-like microsphere (Milovac et al., 2014). HAp was mined from fishbone biowaste via a thermal calcination process (Ahamed et al., 2022). The coprecipitation procedure was used to produce NHAp from fishbone, and its antibacterial characteristics were studied. The temperature variations used were 30, 60, 80, and 100 °C. At a temperature of 100 °C, the highest XRD spectra were seen, with nanoscale size ranging from 37.32 to 49.27 nm. The FTIR's functional groups revealed the attendance of OH, CO_3^{2-}, and PO_4^{3-}. The calculated Ca/P ratio was 1.71, which is greater than 1.61. The antibacterial properties result were significant to *Escherichia coli* and *Staphylococcus aureus* (Hariani et al., 2020).

To determine the best quality and most affordable nano-calcium powder for suggestion to the stakeholders, Wardani et al. (2020), synthesized HAp from 6 fish classes, including tilapia, catfish, grouper, snapper, tuna, and kingfish mackerel. A process involving alkali was used to synthesize the HAp. The grouper bone had a particle size of 281.4 nm, which was larger than the tilapia bone, which had the best particle size of 87.37 nm. The average phosphorus composition varied from 10.73 % for kingfish mackerel to 15.99 % for grouper, according to the EDX results, and the average calcium composition ranged from 21.51 % for the snapper to 34.37 % for grouper. The Ca/P ratio of 1.41–1.66 was obtained (Wardani et al., 2020). Abdullah et al. (2023) extracted HAp from Black Tilapia fish bones and scales. Natural hydroxyapatite was mined using a straightforward method at a calcination temperature of 600–1000 °C. They concluded that natural hydroxyapatite found in fish scales and bones can promote apatite formation and exhibit good biocompatibility. Scale and fishbone hydroxyapatite are nontoxic and have worthy biocompatibility (Fendi et al., 2023).

Akpan et al. (2020) produced biological HAp from catfish bones via the thermal process. XRD analysis revealed that a high crystallinity HAp of 99.9 % was produced corresponding to the structural properties of fluorapatite with crystallite size of about 37.1 nm. The grains seen in the morphology (Fig. 3a) were slightly lengthy spherical particles with seemingly weak connectivity, a less agglomerated structure and a Ca/P ratio of about 1.58. The EDX result (Fig. 3b) showed that the elements present in these particles are Ca, P, Mg, O and C. The atomic ratio of Ca/P was estimated as 1.58 which is close to the theoretical stoichiometric ratio of Ca/P (1.67).

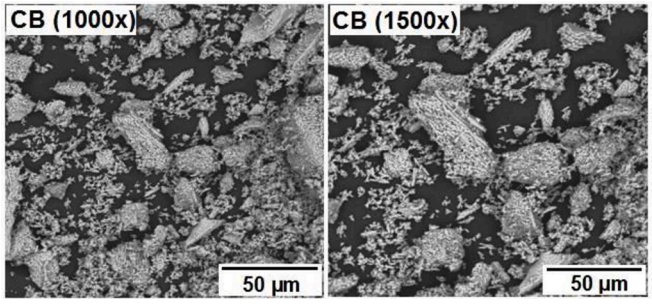

Fig. 3a. SEM Pictures of the HAp produced from catfish bones (Akpan et al., 2020).

2.2. Hydroxyapatite from bovine bone sources

To synthesize HAp from bovine bone (Fig. 4), various techniques such as heat decomposition, calcination, or both with one or more additional techniques have been used (Abukawa et al., 2006; Oonishi, 1991). The bones are heated up to 1400 °C in the furnace during the calcination process to eliminate some organic elements like proteins, lipids, fat, pathogens, etc. (Oonishi, 1991; Heidari et al., 2020; Hariani et al., 2020). Alkaline hydrothermal hydrolysis was used by Barakat et al. to extract HAp from bovine bone. The isolated HAp generated nanoflake HAp with a Ca/P ratio of 1.86 after five hours of heating at 250 °C. They further asserted that using subcritical water, nanoflake HAp with a Ca/P ratio of 1.56 could be produced (Barakat et al., 2009). Odusote et al. (2019) produced pure HAp from bovine bone samples after pretreatment. The bones were calcined at 750 °C. It was then sintered at 1300 °C into a block for hardness measurement. Thermal decomposition was used by Hosseinzadeh et al. (2014) to produce HAp from bovine bones. The bones' lipids were removed, and the bones were then crushed into powders. The powders were then heated for 24 h at 170 °C before being divided into two samples. Samples A and B were then heated at 750 °C and 850 °C, respectively, for 6 h. The results showed that triang (TCP) HAp was produced following complete impurity elimination. The Ca/P ratio at 850 °C was 1.5 lower than the 1.67 Ca/P ratio attained at 750 °C. The pellets for the compressive strength test were formed at 150, 160, and 170 MPa of compression pressure. A compressive strength of 10.82, 17.56, and 23.41 MPa were attained after the samples were sintered at 1200 °C. They concluded that the HAp produced is comparable to those used in tissue engineering and drug delivery applications.

In a study by Han et al. (2022), via a combination of acid/alkali treatment, and calcination process HAp was extracted from bovine bone. The FTIR result revealed the presence of carbonate and phosphate functional groups. The XRD and SEM analysis showed a hexagonal crystalline structure of HAp with a size of 120 ± 12.5 nm. Some important elements like Ca, P, Mg, Na, and Sr were present in the produced HAp powder. Recent studies showed the new means for synthesizing HAp from bovine bone. The bovine bones were sliced and boiled in an opened chamber after boiling them in a pressurized tank, soaked with ethanol (Demir-Oğuz et al., 2023; Wu et al., 2023; Lukina et al., 2023, Md Dali et al., 2023). In research by Barua et al. (2019), after pretreatment to remove impurities from bovine bones, HAp was synthesized by thermal decomposition. The SEM picture showed agglomeration of HAp particles with porous morphology. The Ca/P ratio of 1.71 was obtained from EDX, while an average particle size of around 68 nm was calculated with the aid of ImageJ software. HAp was produced from bovine bones by calcination. The powders calcined at 700 °C and 900 °C indicated the existence of HAp. At 900 °C, the Ca/P ratio was 1.70, while at 1100 °C β-TCP was formed which influenced the Ca/P ratio with an irregular morphology shape. Trace elements like Ca, Mg, Sr, Na, K, and Zn existed (Dillon et al., 2019).

HAp was produced from bovine bone by thermal synthesis at 900 °C. The HAp at 900 °C was characterized using XRD and FTIR analysis. Using a metallic mortar and pestle the bones were ground to powders and sieved with a 100 µm mesh sieve. The powders were sintered at 900 °C after being pelletized under a 3 KN load. The obtained crystallite size was 14.18 nm, and the XRD result formed at angle 2θ was 32.54. The porosity was 47.78 %, while the hardness and compressive strength values were 35.87 MPa and 0.39 MPa, respectively (Mohd Pu'ad et al., 2020). Three samples of HAp were fabricated from bovine bones. The bones were treated with temperatures of 100, 160, and 220 °C and a compaction load of 24.54 Bar was used to pelletize them for compressive tests. The compressive strength at 100 °C was the highest. The results can be seen in Table 1 below (Abdelmoneim et al., 2022). Azzallou et al. (2022) produced NHAp from waste of bovine bone via thermal decomposition at 800 °C for 2 h.

Zhang et al. (2023) used a hydrothermal technique to produce HAp

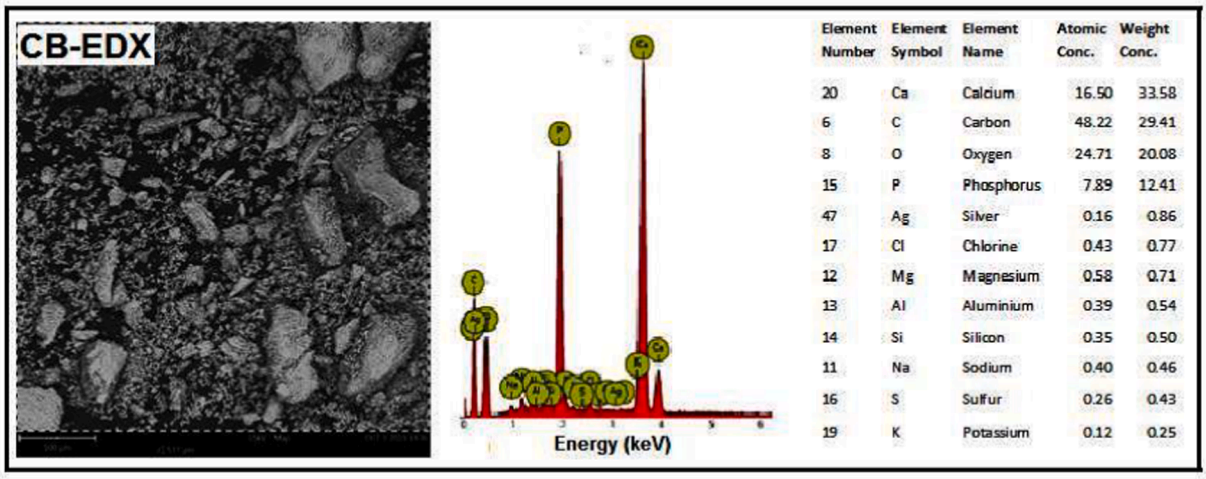

Element Number	Element Symbol	Element Name	Atomic Conc.	Weight Conc.
20	Ca	Calcium	16.50	33.58
6	C	Carbon	48.22	29.41
8	O	Oxygen	24.71	20.08
15	P	Phosphorus	7.89	12.41
47	Ag	Silver	0.16	0.86
17	Cl	Chlorine	0.43	0.77
12	Mg	Magnesium	0.58	0.71
13	Al	Aluminium	0.39	0.54
14	Si	Silicon	0.35	0.50
11	Na	Sodium	0.40	0.46
16	S	Sulfur	0.26	0.43
19	K	Potassium	0.12	0.25

Fig. 3b. SEM/EDX picture of catfish bones-derived HAp at 900 °C (Akpan et al., 2020).

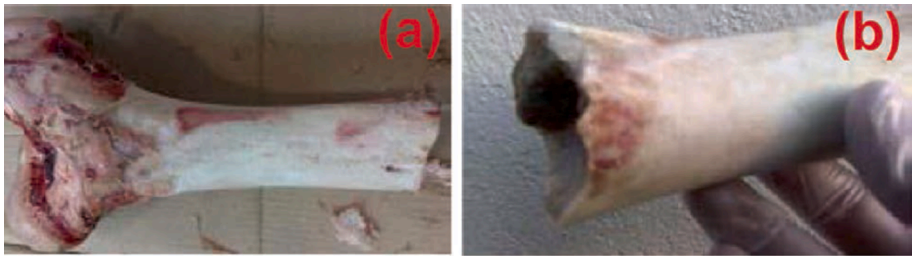

Fig. 4. A typical bovine bone (Hosseinzadeh et al., 2014).

Table 1
Mechanical and Characterization parameters of bovine HAp (Abdelmoneim et al., 2022).

S/N	Compaction load (Bar)	Processing temperatures (°C)	Compressive strength (MPa)	Mean (MPa)	HAp shape	Weibull modulus, *m* (MPa)	Pore sizes (μm)
1	24.54	100	0.47–5.13	2.14 (±1.19)	Fibrous-like	2.2	100–650
2	24.54	160	0.40–1.9	0.93 (±0.4)	Irregular	2.71	100–650
3	24.54	220	0.19–1.28	0.53 (±0.29)	Irregular	2.18	100–650

scaffolds from bovine bones for bone tissue engineering. The study demonstrated the benefit of the hydrothermal process as an economical and ecologically friendly way of valorizing bio-waste, precisely cattle bones. The created HAp showed beneficial characteristics for a comprehensive range of biomedical applications. Using the laser sintering method, natural HAp was extracted from bovine bone for biomedical uses (Alahnoori et al., 2023). Yu et al. (2023) produced HAp via pyrolysis of bovine bone for lead (Pb) removal. The results revealed that under low and high initial lead concentrations, 94.1 % and 74.68 % of removal were observed. HAp was produced from bovine bones and converted into nanoparticles in a ball mill before being subjected to uniaxial and isostatic pressing into discs. The results achieved better mechanical properties for biomedical applications (Minim et al., 2023). Atemni et al. studied the physicochemical properties of bovine and chicken bones, using two different calcination temperatures of 600 and 1000 °C. At 1000 °C, the XRD crystalline phase of the produced HAp powders matches pure HAp, and a Ca/P ratio of 1.66 was obtained. They concluded that the HAp could be used as a biomaterial in bone implanting and other biomedical applications (Atemni et al., 2023). Through some in vitro testing, histological anatomy testing, and immunohistochemical testing, the effect of the secretome addition to the bovine hydroxyapatite (BHAp) as a bone graft candidate was detected (Gusti et al., 2023).

2.3. Hydroxyapatite from shell sources

Eggshells are one of the best sources of calcium that can be obtained, and using this type of unadulterated calcium helps to strengthen the bones (King'Ori, 2011; Tsai et al., 2006; Javaid and Kaartinen, 2013). The eggshells, which have 95 % calcium, support strong teeth (Rivera et al., 1999). Clamshells also contain significant amounts of plant micronutrients and calcium (Sano et al., 2012; Núñez et al., 2019; Yu et al., 2020). HAp can be synthesized from snail shells, eggshells, cockle shells, clam shells, sea shells, and mussel shells (Fig. 5) using any of the following synthesis techniques Calcination, Hydrothermal, Mechano-chemical, Sol-gel precipitation, a Combination of techniques (Suresh Kumar et al., 2020; Santhosh and Prabu, 2013; Bambaeero and Bazargan-Lari, 2021; Adak and Purohit, 2011; Zuliantoni et al., 2022; Kumar et al., 2015; Shavandi et al., 2015; Shariffuddin et al., 2013; Citradewi et al., 2021; Azis et al., 2015; Hassanzadeh-Tabrizi et al., 2021).

Tsai et al. (2006) synthesized HAp from eggshells. Calcining eggshells effectively produced pure NHAp as a calcium source through the wet chemical precipitation. A temperature range of 800–1400 °C was used for sintering HAp pellets in the open air. Vickers hardness, fracture toughness, and sample characteristics were assessed. The results revealed that pure phase HAp was achieved and remained stable at 1250 °C. In contrast, secondary phases of α-TCP and Tetracalcium

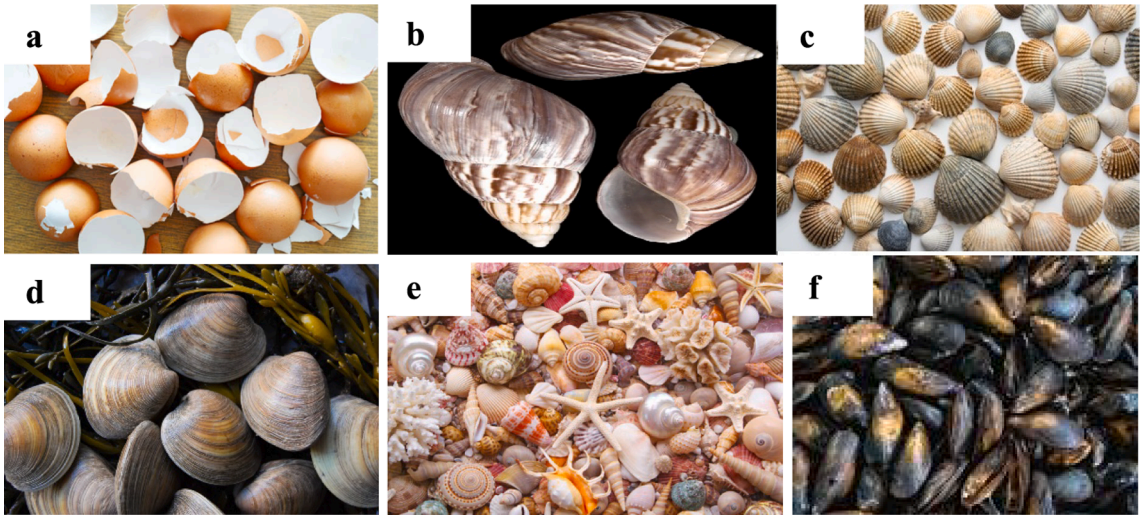

Fig. 5. Pictures of shells of (a) Egg; (b) Snail; (c) Cockle; (d) Clam; (e) Sea; and (f) Mussel (Suresh Kumar et al., 2020; Santhosh and Prabu, 2013; Bambaeero and Bazargan-Lari, 2021; Adak and Purohit, 2011; Zuliantoni et al., 2022; Kumar et al., 2015; Shavandi et al., 2015; Shariffuddin et al., 2013; Citradewi et al., 2021; Azis et al., 2015; Hassanzadeh-Tabrizi et al., 2021; Pal et al., 2019; Alif et al., 2018).

Phosphate (TTCP) were seen at 1300 –1350 °C and disintegrated around 1400 °C. At 1250 °C, a comparatively high density of 97.4 % was attained in the pure HAp. Due to the tiny grain size of 0.33 μm obtained at 1000 °C, a fracture toughness of 1.14 MPa.$m^{1/2}$ and hardness value of 4.96 GPa were achieved (Apostu et al., 2018).

Using a quick microwave irradiation technique, nano-crystalline HAp was generated from mussel shells wastes by Shavandi et al. (2015). After a suitable pre-treatment and an irradiation stage in a microwave with a power of 1.1 kW, mussel shells were transformed into rod-like nano-crystalline HAp particles of 30–70 nm long using 0.1 M EDTA as a chelating agent for 30 min. The thermal study (Fig. 6) revealed that synthesized HAp was remarkably stable at 1000 °C, and the XRD and FTIR studies revealed that the powdered HAp is highly pure. In addition, the HAp sample displayed a linked and porous shape, indicating that it can be applied to bone tissue engineering procedures.

With the aid of a brand-new pyrolysis-wet slurry precipitation procedure, HAp was fabricated from mussel shells. Methylene blue, a model textile wastewater chemical, and its azo dye breakdown products were destroyed at an initial rate of 2.5 × 10^{-8} mol L^{-1} min^{-1} by the synthesized HAp, which showed strong photocatalytic activity. The post-reaction HAp's FTIR analysis (Fig. 7) confirmed surface PO_4^{3-} group depletion (Shariffuddin et al., 2013). HAp was synthesized through a hydrothermal process with cockle shell waste as the precursor. By varying the temperatures and reaction times under a simple state, the cockle shells were calcined, hydrated, and carbonated to produce precipitated calcium carbonate. This calcium carbonate was then combined with diammonium hydrogen phosphate to produce HAp. The XRD peaks demonstrated that the described procedure may successfully produce HAp with a hexagonal crystal structure with the highest peak at 44.5. The HAp had about 17.8 m^2/g specific surface area. To examine the electronic condition of doped Ag, an XPS study was carried out and the full XPS spectrum showed the major peaks of elements present in the results which gave the range of electron volts present (i.e. Ag 3d5/2 and Ag 3d3/2 located in the range of 365–370 eV and 372–376 eV, respectively). The high-resolution TEM result pointed well-resolved lattice bounds, which were detected at the distances of 0.35, 0.28, and 0.17 nm (Azis et al., 2015). HAp was produced from cockle shells by Razali et al. (2016) via calcination and hydrothermal techniques. By calcining the cockle shells at 450 °C and 800 °C for 2 h, calcite was created. The samples of calcite calcium carbonate underwent hydrothermal treatment at 110 °C after being treated with diammonium hydrogen phosphate. The derived HAp had nanoparticles with rod-like and needle-like structures at 450 °C and 800 °C respectively.

Zuliantoni et al. (2022) derived HAp from the snail shells using hydrothermal method. The XRD crystallography was comparable to commercial HAp. The SEM result at different magnifications revealed that the fine particles of apatite compound merge with different sizes. The HAp had cube-like or needle-like particles (Fig. 8). They assumed that the change in crystal structures and lattice parameters resulted in the difference in microstructure. The HAp particles ranged from 26.9 μm to 322 μm. The FTIR (Fig. 9) of the synthetic and snail HAp showed O—H bonds stretching at the peaks 3458 and 3452 cm^{-1} respectively. The C—O, P—O, and CO_3^{2-} bonds were formed in both at different wave peaks.

HAp was manufactured from snail shells by calcination and wet chemical precipitation methods after pre-treatment to remove dust particles. Before grinding with milling balls, the clean snails were dried for 24 h in an oven at 100 °C. The derived HAp was sintered in the furnace at a temperature of 1000 °C for 4 h (Ahmed et al., 2022). Strontium (Sr)-doped hydroxyapatite was produced from clam shells using the hydrothermal method. The effects of Sr doping on the XRD results were minimal. Sr replaced Ca and gradually increased the elastic modulus of the produced HAp from 130 to 137 GPa. All of the samples were found to be non-toxic based on the *in vitro* cytotoxicity of the sintered specimen against a mouse osteoblast cell line (Pal et al., 2019). Alif et al. produced synthetic HAp using clamshells, which initially had agglomerated spherical-shaped particles that changed to rodlike shapes as the calcination temperatures was increased (Alif et al., 2018).

Lenita researched on hydrothermal and precipitation methods for synthesizing HAp from clamshells (Herawaty, 2014). The precipitated and the hydrothermal HAps have Ca/P ratios of 1.71 and 2.03 respectively. The former had spherical-polygonal particles with an average diameter of 10–20 nm, while the latter resulted in nanorods with dimensions of 15–20 nm in diameter and 40–60 nm in length. Using clamshells, Bramhe et al. produced HAp that ranged from longer nanorods to one-dimensional nanowires with a high aspect ratio. It has previously been proposed that the temperature of heat treatment led the crystals to developed in a single direction, leading to the creation of nanorods (Bramhe et al., 2014). To study the crystallization and degradation qualities, Afriani et al. filled a composite scaffold with cockle shell hydroxyapatite and silica. At room temperature, stirring for 2.5 h at 300 rpm produced a homogeneous calcium and phosphate solution. The sample was then sintered at 900 °C for 5 h. It was discovered that the silica had delayed the hydroxyapatite/silica composite's

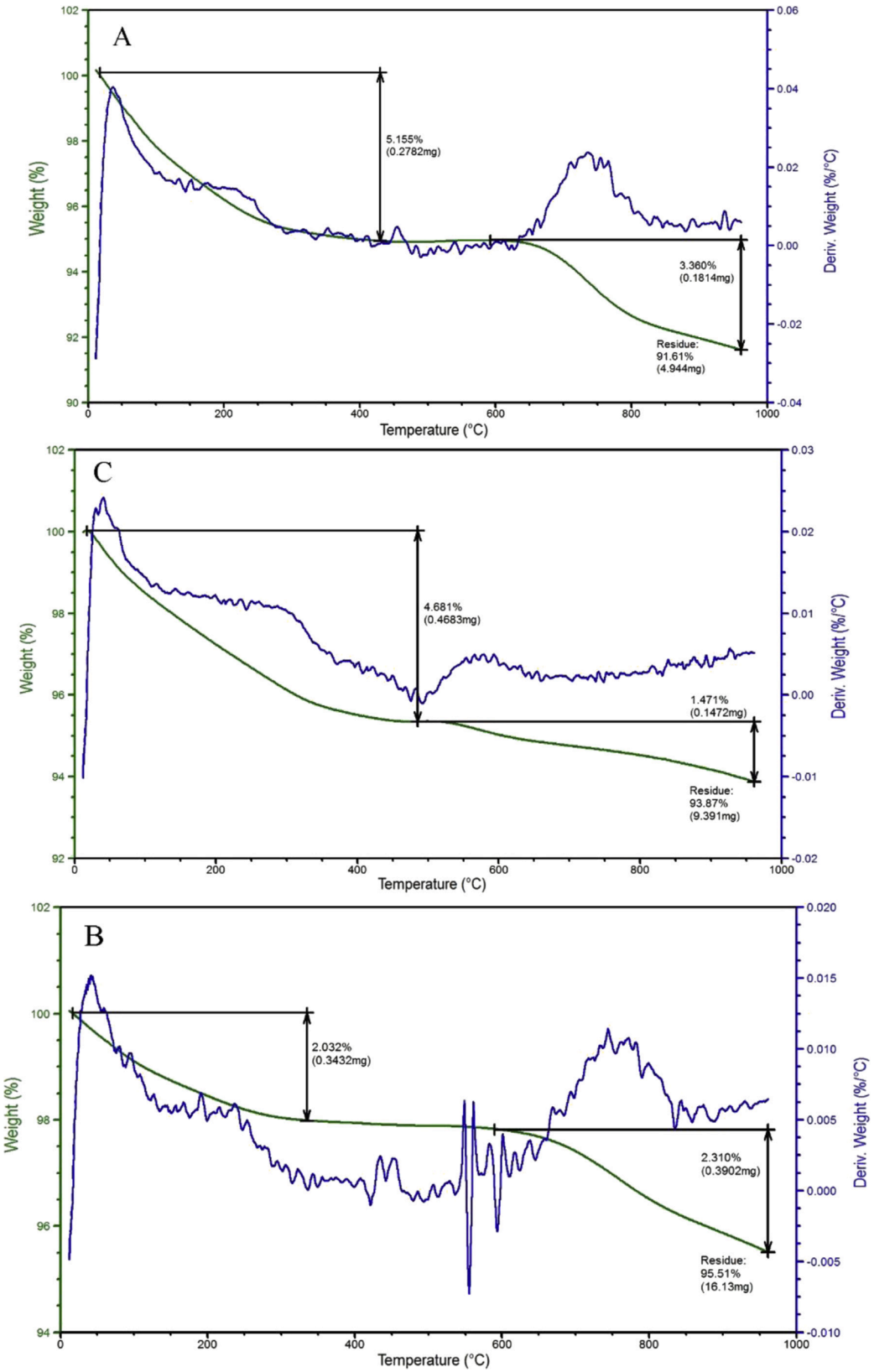

Fig. 6. Thermal Analysis of Mussel HAp (Shavandi et al., 2015).

breakdown process (Afriani et al., 2019).

Sultana et al. (2021) employed a UV-mediated solid-state technique to produce HAp from eggshells without heat. They recommended employing the UV-irradiation method at room temperature, followed by ball milling, to produce hydroxyapatite. The XRD peaks showed the presence of pure HAp and peaks matched with Miller Indices with hexagonal shape. Both the FTIR and Raman spectroscopic analysis revealed that all the typical bands points, as well as the Raman shifts, are

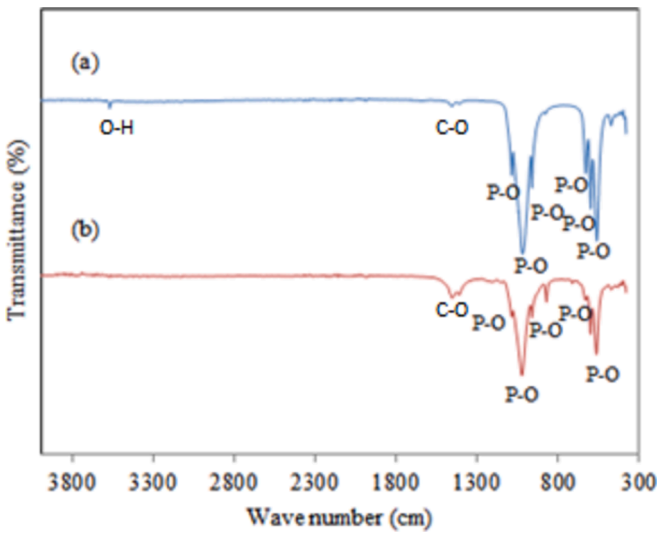

Fig. 7. FTIR result of mussel-derived HAp (Shariffuddin et al., 2013).

typical HAp. In a study by Wu et al., microwave irradiation was effectively used to produce HAp wads. Magnesium and strontium were found in the HAp, which was predicted to support the material's biodegradability and may have applications in the field of bone implants (Wu et al., 2021). Hsu et al. (2023) produced spherical-shaped HAp from crab shells via alkali treatment and hydrothermal reaction at different temperatures. At the temperature of 200 °C the average particle size was about 20–40 nm. From the results, the XRD diffraction peaks corresponded to the HAp phase. The *in vitro* tests after 7 days showed apatite deposits on the whole surfaces of the HAp coatings, showing that the HAp retains admirable bioactivity. Hussain and Sabiruddin (2023) produced HAp powders from Indian clam seashells via hydrothermal process. Firstly, calcium oxide (CaO) was produced by calcining the clam seashells at 900 °C. Tri-calcium phosphate was suitably combined with the produced seashell-based calcium oxide in demineralized water. To carry out the hydrothermal processes, the colloidal solution was further heated at a temperature of 1000 °C for a range of times. The findings suggested that a key factor influenced the various properties, particularly the as-produced HAp's phase amount, was the hydrothermal reaction's heating period. An increase in the heating period increased the HAp's crystallography.

Using SEM and XRD, Lee et al. (2012) studied the physical properties of synthetic HAp (sHAp) and HAp from the eggshell (eHAp). The XRD peaks (Fig. 10) agreed with the SEM results (Fig. 11). The results revealed that the synthetic HAp had a smaller grain size than the eggshell HAp.

Fatimah et al. (2024) produced a novel HAp by in-situ co-precipitation monitored by the hydrothermal technique using a cockle shell as a biogenic calcium source. The crystalline structure of the HAp was identified in both samples and associated with Miller Indices reflection planes of pure hydroxyapatite (Fig. 12). The TEM analysis (Fig. 13) confirmed the presence Ag_3PO_4 phase. It showed well-resolved lattice fringes seen at different distances associated with the plane of Ag_3PO_4. The alteration of HAp surface morphology from a porous structure to a random chunk structure was observed in the SEM result (Fig. 14). Surface evaluation using XPS of the Ag_3PO_4/HAp sample reveals that the survey represents Ca, P, and Ag are the elements poised of the material (Fig. 15a). Deconvolution to the Ca 2p spectrum (Fig. 15b) revealed two prominent peaks ascribed at 346.0 and 349.7 eV corresponding to Ca $2p_{3/2}$ and Ca $2p_{1/2}$, respectively.

Durucan and Brown (2000) employed reagent-grade calcium carbonate ($CaCO_3$) and thermally generated calcium pyrophosphate ($Ca_2P_2O_7$) to produce α-TCP. A complete reaction was indicated by an enthalpy of 133 kJ/mol, and different pushed and powder samples produced different amounts of heat overall throughout the conversion of HAp. As the hydrolysis temperature was increased from 37 °C to 56 °C, the time required for the full reaction decreased to roughly 6.5 h from 18 h. A significant increase in tensile strength was observed after hydrolysis. The average values were 9.36 ± 0.4 MPa and 9.30 ± 0.5 MPa, respectively. The fracture strength were from 0.52 MPa to 0.82 MPa, while the density was about 70 %.

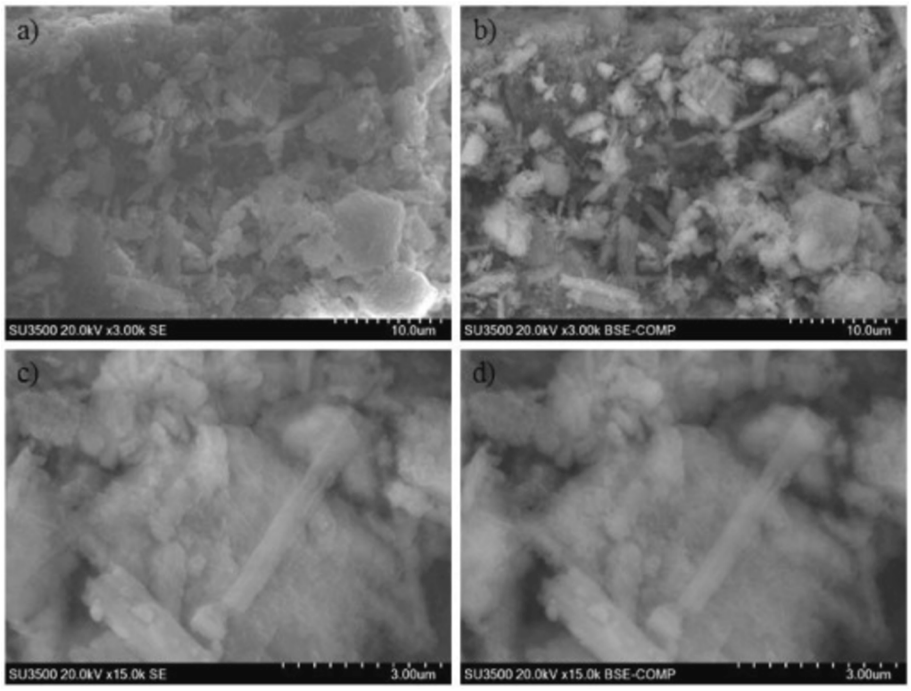

Fig. 8. SEM image of snail shell powder calcined at 700 °C with magnification, (a) 3000×, SE mode; (b) 3000×, BSE mode; (c) 15,000×, SE mode; (d) 15,000×, BSE mode (Zuliantoni et al., 2022).

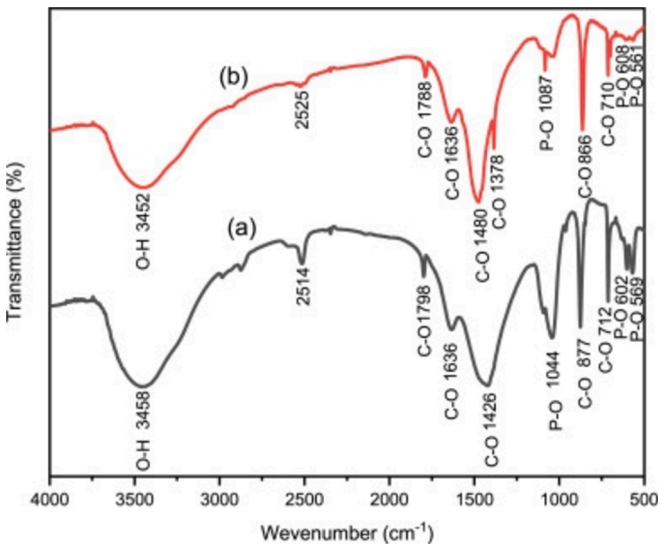

Fig. 9. Typical FTIR Spectra of HAp Powder (a) commercial HAp and (b) Snail HAp (Zuliantoni et al., 2022).

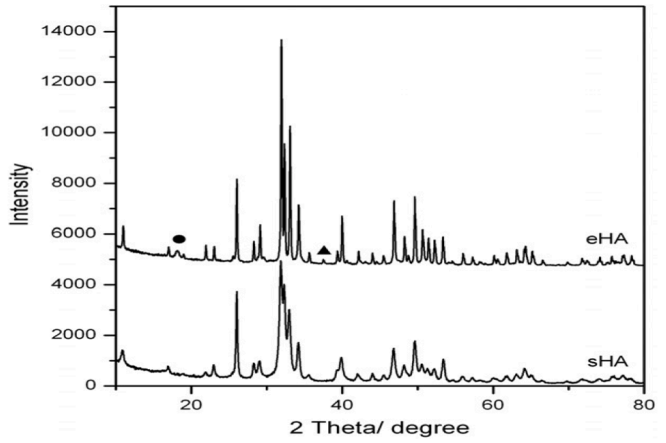

Fig. 10. Typical XRD of synthetic and eggshell HAp (Lee et al., 2012).

2.4. Hydroxyapatite from other sources

Fruit peels, wood, flowers, stalks, leaves, and leaves are thought to be ideal for extracting HAp. A large portion of natural HAp is derived from limestone as the main mineral source (Memarpour et al., 2019; DileepKumar et al., 2022). Three different types of fruit wastes – grape, sweet potato, and pomelo peels – were converted into ultrapure HAp nanoparticles using the hydrothermal approach by Wu et al. (2013). Pomelo peelings were used to extract the HAp, which showed good characteristic ratios and physical forms similar to those of the crystalline HAp crystals found in human bones. The mangoes, grapes, and ripe tamarind used to carry out the fruit extracts were all locally cultivated. The fruits were first peeled and the seeds were removed. The pulp was then washed by submerging it in distilled water, weighed, and macerated using a ratio of 10 ml of distilled water from the starting weight. With the aid of distillation funnels and filter paper, the macerated product was filtered. The resultant filtrate was then manually ground into a fine powder and utilized as a template for the synthesis of HAp after being dried at 40 °C to eliminate any remaining water. The three samples have similar XRD patterns with no additional crystalline phase in the HAp which proved that the use of different biomolecules did not prevent the production of HAp phases. The XRD patterns peaks (Fig. 16) showed that the HAp particles were tiny and had low crystallinity, two properties that are similar to those of bone apatite that occurs naturally. They concluded that the presence of carbonate is a method of lattice defect in the HAp, which might be responsible for its low crystallinity, as confirmed by the XRD data. As observed in the SEM scan (Fig. 17a), the attendance of biomolecules alters the sizes and forms of the HAp. The HAp that was produced from grape peel extract demonstrated higher aggregation.

With an increase in reaction time up to 72 h, the needle-like shape changed into a rod-like shape and the phase ratio reduced, as shown in Fig. 17(b). The researchers concluded that the occurrence may be due to high carbonate content. They also observed that the HAp produced from pomelo peel extract demonstrated good phase ratios with physical structures similar to those of the crystalline HAp shapes of normal bone. The crystallite sizes of the HAp after 72 h were 32, 49, and 12 nm for grape, sweet potato, and pomelo peel extracts respectively. The EDS (Fig. 18) analysis showed that the Ca/P molar ratios were between 1.57 and 1.77.

Roy et al. (2023) described a methodical synthesis of a mixed metal nanocomposite made of strontium copper and manganese oxide by encasing the result in hydroxyapatite produced from fish bones (food waste) and using papaya fruit extract as the starting material. The substance inside the capsule can function as a photocatalyst, as seen by the speed with which dyes degrade. Azaryan et al. (2023) studied the effect of of nano-hydroxyapatite (nHAp) prepared via *Elaeagnus Angustifolia* extract to improve the relative manifestation of immunomodulatory/dentin–pulp regeneration genes in DPSCs. Jaganathan & and Sithique produced a new bioactive Chitosan-Lignin/n-Hydroxyapatite/Opuntia ficus-indica -Fruit gum (Cs-Lg/n-Hap/OFI-Fg) biocomposite. The biological properties were assessed for the biocomposites. The anticancer results showed that a biocomposite with a 5 g/ml concentration had a substantial effect against bone cancer cells, demonstrating that the as-obtained composites may be more beneficial for treating bone defects (Jaganathan and Sithique, 2023). Using eggshell waste as a calcium source and Muntingia calabura leaf extract as a solvent, HAp was created. According to FESEM, the generated nanoparticles resembled irregular rods, and the growth of HAp was confirmed by the results of EDX and XPS (Vinayagam et al., 2023). Orange peel pectin was obtained by microwave irradiation and added to chicken bone HAp with the use of ultrasonic and ball milling. At sintering temperature of 1250 °C, a high relative density of 85.53 % and Vickers hardness of 3.53 GPa were achieved (Teoh et al., 2023).

Analytical grade and aqueous solutions were made by dissolving reagents in deionized water to produce HAp using the emulsion technique. All sample preparation solutions had a Ca/P ratio of 1.67. The XRD result showed that all the diffraction peaks represent pure hexagonal phase HAp. The length and width of the nanorods were above 280 nm and 10–20 nm respectively when pH was 7.0 (Jahangir et al., 2019). Using eggshells, bio-based HAp were produced via sonochemical method using phosphoric acid as the source of phosphorus and bio-based calcium carbonate particles . The eggshells were the source of calcium and they were washed and ball-milled to nanoscale size before being heated in a tube furnace to produce calcium oxide (CaO) particles. These CaO were stirred in water for 24 h at 25 °C to yield calcium hydroxide. The two particles were irradiated with a high-intensity ultrasonic horn for 2 h at 10 °C in distilled water. The results revealed that the HAp were porous (~20–50 nm), and thermally stable at 750 °C. The produced HAp had a surface area of 58.8 m^2/g. They concluded that the HAp is suitable for biomedical applications (Hassan et al., 2014).

Mesoporous HAp was produced from $Ca(NO_3)_2{\cdot}4H_2O$ and H_3PO_4 via a double emulsion method according to the reaction below (Hassan et al., 2014):

$$10Ca(NO_3)_2.\,4H_2O + 6H_3PO_4 + 20NH_4OH \rightarrow Ca_{10}(PO_4)_6(OH)_2 + 20NH_4NO_3 + 22H_2O(a)$$

Biobased HAp was prepared by double emulsion technique using bitter

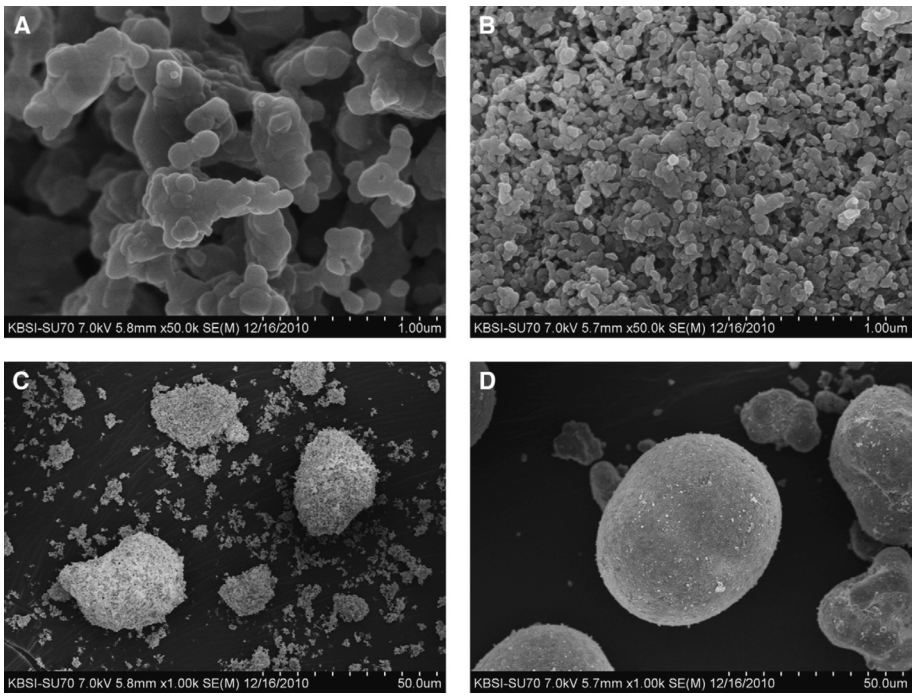

Fig. 11. Typical SEM results of (A) HAp from eggshell; (B) synthetic HAp; (C) eggshell HAp at low magnification & (D) synthetic with smaller particle size (Lee et al., 2012).

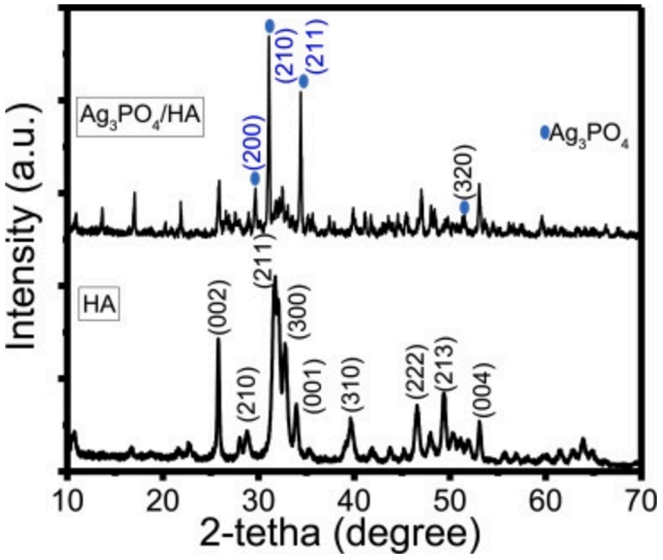

Fig. 12. XRD patterns of Ag_3PO_4/HAp and HAp (Fatimah et al., 2024).

almond oil and span 80 surfactants. The morphology of the as-synthesized HAp and its clinical efficacy were evaluated using some analyses. The nanocarriers' monodispersity and average dimension of 418 nm were discovered by DLS. Zeta potential studies revealed an average surface charge of − 34.5 mV, confirming their outstanding stability and viability for long-term storage. TEM and SEM images (Fig. 19) revealed their spherical and porous form. The FTIR result confirmed the attendance of HAp (Aslani et al., 2024). Phosphoric acid and calcium carbonate particles extracted from eggshells were employed in the sonochemical fabrication of bio-based HAp nano-particles as given below (Aslani et al., 2024):

$$CaCO_3 \rightarrow CaO + CO_2\uparrow (b)$$

$$CaO + H_2O \rightarrow Ca(OH)_2 (c)$$

$$5Ca(OH)_2 + 3H_3PO_4 \rightarrow \frac{1}{2}Ca_{10}(PO_4)(OH)_2 + 9H_2O \quad (d)$$

Table 2 below is the summary of synthesis techniques and some important results according to some researchers.

3. Hydroxyapatite synthesis techniques

According to different researchers, several synthesis techniques have been employed for the production of HAp including the precipitation technique (Santos et al., 2004), sol–gel method (Chai and Ben-Nissan, 1999), hydrothermal technique (Manafi and Joughehdoust, 2009), multiple emulsion technique (Kimura, 2007; Murray et al., 1995), sonochemical technique, (Tas, 2000; Thamaraiselvi et al., 2006), and hydrolysis technique (Shirkhanzadeh, 1998). These processes, which are solution-based reactions, are carried out at various temperatures using a variety of apparatus, solvents, and chemicals. Here, several additives are used to control precipitation. These approaches produced HAp particles traditionally with regular geometry and tiny size, in contrast to the dry process which produces HAp powders with erratic form and huge size. See Fig. 20 for some of these techniques ((Morey and Niggli, 1913; Lukina et al., 2023, Md Dali et al., 2023, Memarpour et al., 2019, Wu et al., 2023)).

Pramono and Puspitasari (2024) used a wet chemical synthesis method in assisted with a sonication technique to produce HAp from scallop shell waste. FTIR, SEM, and XRD were used to characterise the hydroxyapatite samples. The HAp sample contained a single phase and a tiny crystal size, according to the XRD data. The hydroxyapatite sample had an ellipse-like grain form, according to the SEM data. The XRF analysis revealed that t the HAp sample's chemical composition consists primarily of calcium and phosphate. The hydroxyapatite sample that underwent sonication exhibited an absorption spectrum, as indicated by the FTIR results. HAp was produced from cuttlefish shell waste via microwave hydrothermal technique. The bones were crushed and calcined at temperature of 900 °C to obtain calcium oxide (CaO). Afterwards, the

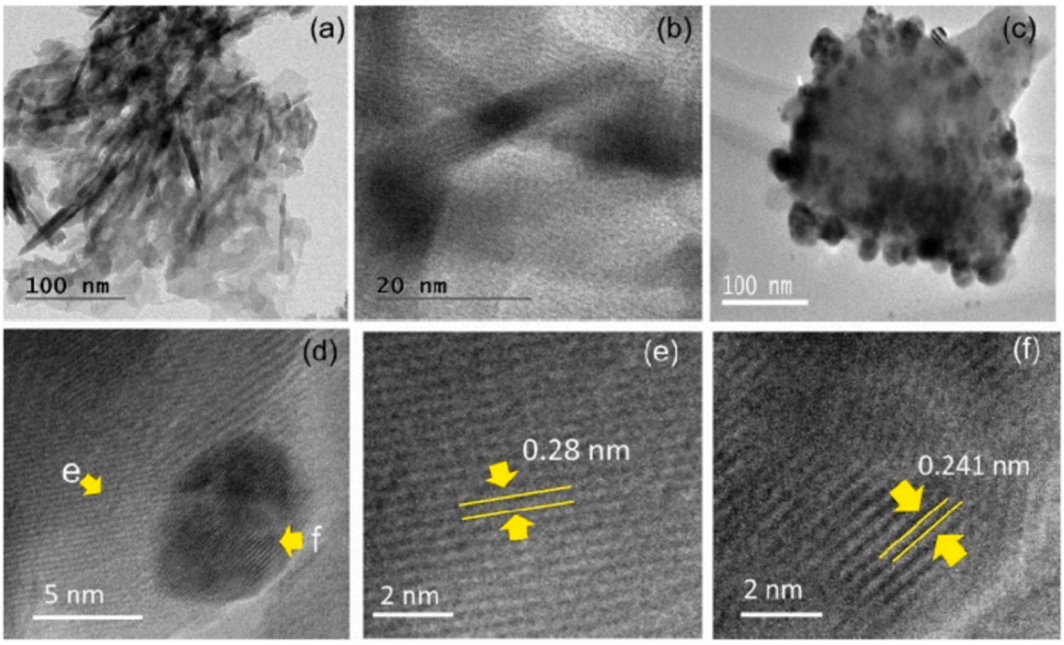

Fig. 13. (a–b) TEM images of HAp with different magnifications, (c–d) TEM images of Ag_3PO_4/HAp with different magnifications, (e). High-resolution TEM image of HAp with (2 1 1) lattice fringes, (f) High-resolution TEM image of Ag_3PO_4 with (2 1 0) lattice fringes (Fatimah et al., 2024).

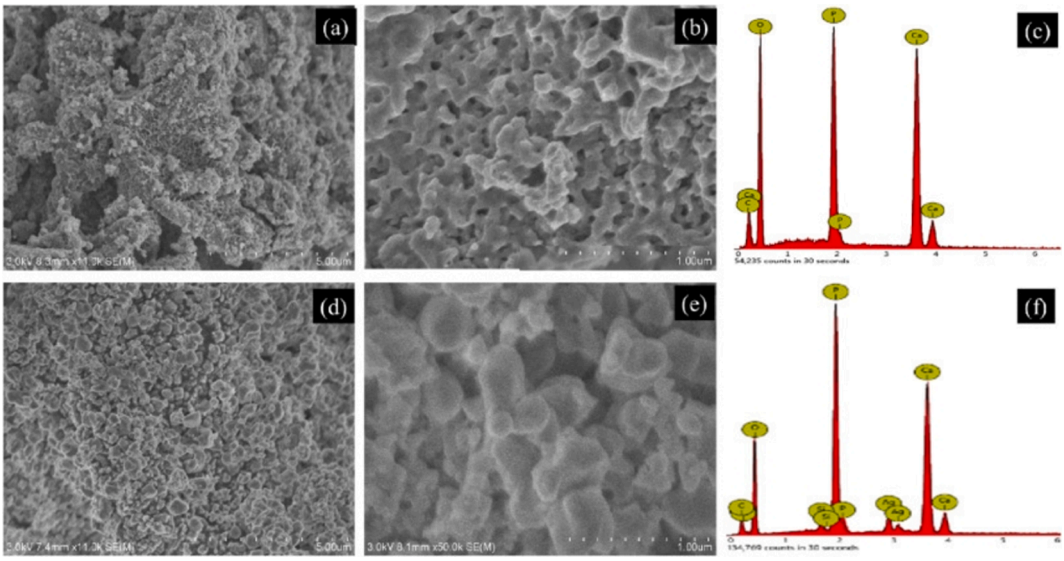

Fig. 14. (a–b) SEM images of Cockle shell HAp with different magnifications, (c) EDX spectrum of HAp, (d–e) SEM images of Ag_3PO_4/HAp with different magnifications, (f) EDX spectrum of Ag_3PO_4/HAp (Fatimah et al., 2024).

CaO was processed by microwave hydrothermal to obtain HAp powder and was characterised using FTIR, XRD, SEM, EDX, and thermogravimetric analysis. The Ca/P ratio of the HAp was 1.7 with higher crystallinity. The TGA analysis displayed the highest weight loss of 16.57 %. They concluded that the cuttlefish shell waste is a good raw material for producing HAp (Nurbaiti et al., 2024). Méndez-Lozano et al. (2024) produced HAp flakes via a microwave-aided hydrothermal method. The achieved flakes recommended promising bids as a substrate for placing titanium dioxide (TiO_2) films by chemical vapour deposition with metal–organic sources. Some synthesis methods for the production of HAp are discussed below.

3.1. Sol-gel method

One of the earliest proposed methods for the production of HAp was the sol–gel method. However, only a small number of studies have explicitly explored the creation of HAp nanoparticles using sol–gel technique. The sol–gel process has the advantage of molten-level reactant mixing, improving the chemical homogeneity of the resultant powder (Chai and Ben-Nissan, 1999; Fatimah et al., 2024; Durucan and Brown, 2000; Hassan et al., 2014; Aslani et al., 2024; Hasan et al., 2024; Pramono and Puspitasari, 2024). Due to the possibility of good control over process parameters, the sol–gel approach is an active modality for the synthesis of nanophase-HAp (Anbalagan Balamurugan et al., 2006). According to reports, HAp materials produced using the sol–gel method are effective at enhancing contact and stability at artificial/natural bone

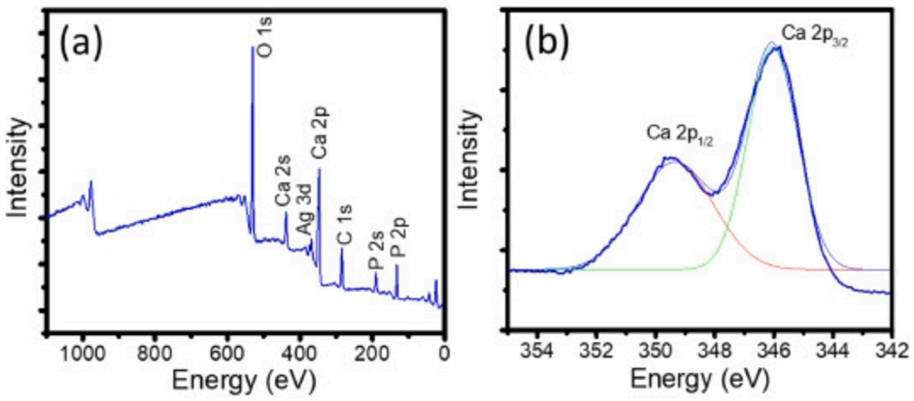

Fig. 15. (a) Survey spectrum & (b) Ca 2p spectrum (Fatimah et al., 2024).

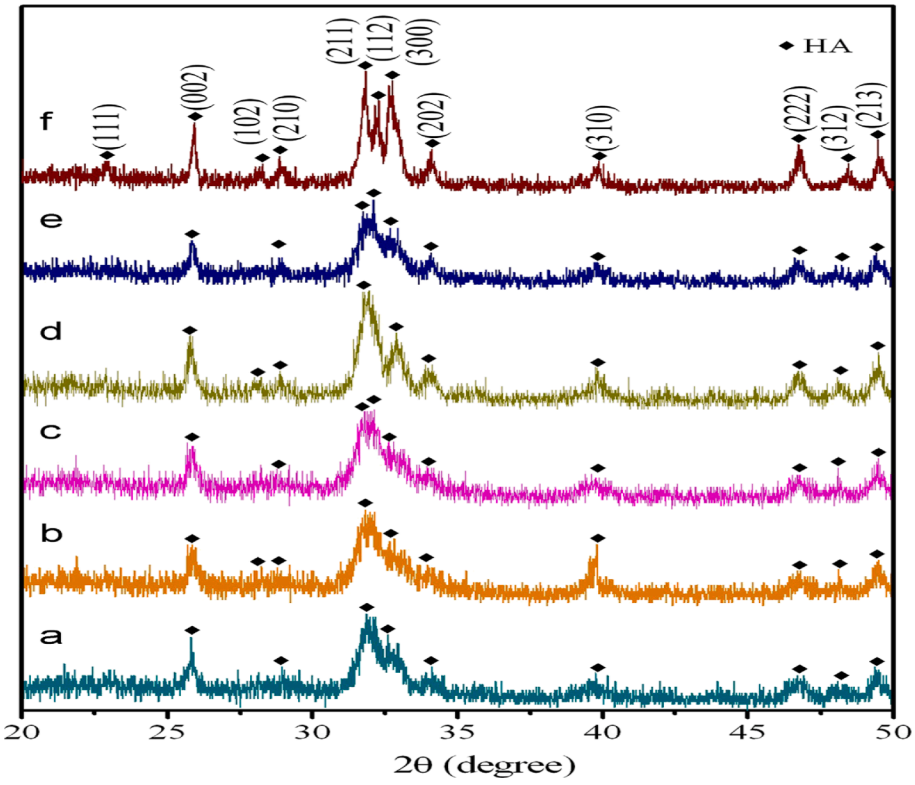

Fig. 16. XRD patterns of (a) Grape peel, 24 h; (b) grape peel, 72 h; (c) sweet potato peel, 24 h; (d) sweet potato peel, 72 h; (e) pomelo peel, 24 h and (f) pomelo peel, 72 h (Wu et al., 2013).

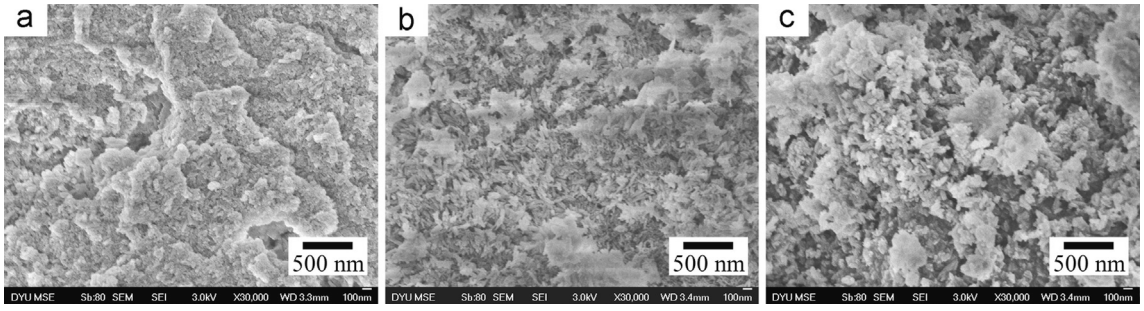

Fig. 17a. SEM images of hydroxyapatite produced from (a) Grape peel, (b) sweet potato peel and (c) pomelo peel (Wu et al., 2013).

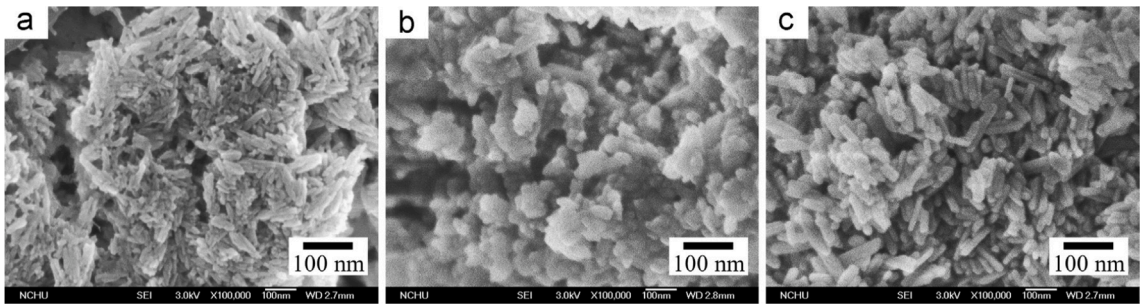

Fig. 17b. SEM images of hydroxyapatite produced (a) Grape peel, (b) sweet potato peel and (c) pomelo peel, at 150 1C for 72 h (Wu et al., 2013).

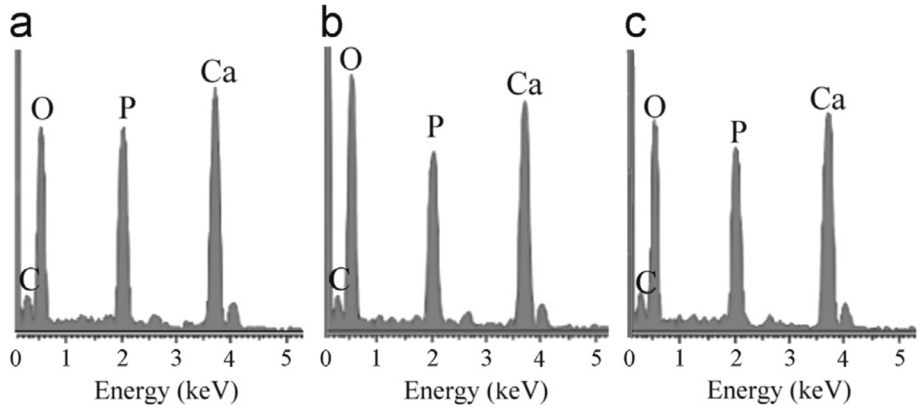

Fig. 18. EDS analyses for HAp produced from (a) Grape peel, (b) sweet potato peel and (c) pomelo peel (Wu et al., 2013).

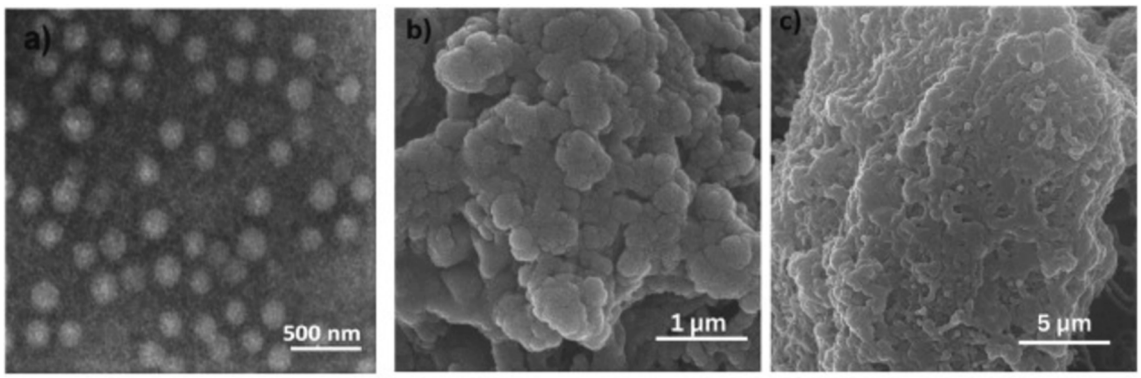

Fig. 19. (a) TEM (b) FE-SEM and (c) FE-SEM pictures of HAp produced via emulsion method (Aslani et al., 2024).

interfaces in both *in vitro* and *in vivo* studies (Li and De Groot, 1994).

Other significant advantages of the sol–gel process include the formation and fusing of the arranged crystals at low temperatures. According to recommendations, HAp crystals should be made using a variety of synthesis methods at temperatures above 1000 °C, while temperatures of hundred degrees lower are necessary for calcination and sintering of sol–gel HAp, which results in a decrease in degradation for the duration of sintering. Furthermore, a powder obtained through a usual sol–gel method often produces a stoichiometric structure with a large surface area and a small cluster size (varying from 50 nm to around 1 µm, based on the processing parameters) (Kumar and Kalainathan, 2010; Sanosh et al., 2009; Bigi et al., 2004; Kuriakose et al., 2004; Bezzi et al., 2003). The primary drawbacks include the presence of a secondary phase, which is commonly calcium oxide (CaO), and some of the starting materials' high costs, particularly those of alkoxide-based precursors (Eshtiagh-Hosseini et al., 2007; Hsieh et al., 2001; Jillavenkatesa et al., 1999).

For the sol–gel synthesis of HAp, various calcium and phosphorus precursor combinations have been used. The sol–gel approach was used by Anbalagan Balamurugan et al. (2006) to manufacture pure monophasic-HAp. A Ca/P ratio of 1.67 was reported. According to the elemental analysis performed using EDXS and EELS, the powder that was calcined at 900 °C possesses monophasic stoichiometric HAp. Bigi et al. (2004) studied the morphological changes of sol–gel-produced nanostructured HAp. In ethanol, $Ca(NO_3)_2{\cdot}4H_2O$ and $(NH_4)2HPO_4$ were made pliable. A new organic convertor was introduced: polyethylene glycol. After being heated up to 1100 °C for 4 h, the surface characterization results indicated the presence of amorphous HAp, a dry gel precursor, and mono-phase HAp. Bezzi et al. produced pure HAp powder using the sol–gel procedure. A Ca/P ratio of 1.667 was obtained. To eliminate $Ca(OH)_2$ and CaO in the produced HAp powder, the process was controlled at 600 °C. X-ray diffractometry and a high-precision phenolphthalein test were used to confirm the elimination of CaO. The morphology picture of the produced powder at 800 °C showed some

Table 2
Summary of synthesis techniques.

Serial	Synthesis Method	Sources of HAp	Mechanical Properties Results	Crystallographic Results	Refs
1.	Sol-gel	a. Fishbonesb. Bovine bonesc. Mussel shells	Hardness = 0.409 GPa Fracture Toughness = 0.835 MPa $m^{1/2}$.N/AN/A	Hexagonal shape Crystallinity = 85 % Ca/P ratio = 1.66 Crystallite size = 40–60 nm. FTIR's functional groups OH, CO_3^{2-}, and PO_4^{3-}. Ca/P ratio – 1.67. The highest peak is on 2θ = 31.9001. FTIR's functional groups OH, CO_3^{2-}, and PO_4^{3-}. Hexagonal shape Crystallinity = 87 %. Crystallite size = 48.38 nm. Shape – Hexagonal. The highest peak on 2θ – 34.Ca/ P ratio – 1.70 Crystallinity – High. Crystallite size – 30–70 nm FTIR – O—H groups, stretching mode at 3570 cm^{-1} and vibration at 630 cm^{-1}	(Obada et al., 2023) (Pamungkas et al., 2019) (Shavandi et al., 2015)
2.	Hydrothermal	a. Fishbones. b. Bovine bones. c. Eggshells. d. Cockle shell e. Snail shells. f. Clam shellsg. Crab shells.h. Fruits peels	a. N/A b. Compressive strength – 23.41 MPa c.Compressive Strength – 0.88 MPa and elastic modulus – 15.5 MPa. d. N/A e. N/A f. Elastic Modulus – 130 to 137 GPa. Fracture toughness – High.g. N/Ah. N/A	a. Ca/P ratio = 1.67 FTIR's functional groups OH, CO_3^{2-}, and PO_4^{3-}. b. Ca/P ratio – 1.71 Shape – Sponge-like microsphere Crystallite size – 37.32–49.27 nm. c. Ca/P ratio – 1.86. Nanorod shape. Crystallinity – high. Crystallite size – 300 nm. FTIR – O—H present. d. Ca/P ratio – 1.67. Crystallite size – 12–16.5 nm. The XRD highest peak on 2θ – 44.5. Binding energy – 365 eV–372 eV. Shape – Hexagonal FTIR's functional groups are P—O, OH, CO_3^{2-}, and PO_4^{3-}. e. Shape – Cube-like/rod-like. Particles size – 26.9 μm–322 μm. FTIR functional groups of C—O, P—O, and CO_3^{2-} bonds were formed at different wave peaks. The XRD's highest peak on 2θ – 52.5. Crystallinity – Better Crystal size – 73.55 nm. f. Shape – Spherical and rod-like. The average length of the rods varies from 130 to 170 nm and width varies from 30 to 50 nm. Density – 3.04 g/cc–3.50 g/cc.Ca/ P ratio – 1.47–1.71. FTIR – Bending modes of lattice H_2O, OH^-, CO_3^{2-}, and PO_4^{3-}. Crystallite size – 35–69 nm. g. Average particle size – 20–40 nm. Shape – Spherical. XRD peak at 2θ – 34.77. FTIR – C—O, OH^-, N—H, CO_3^{2-}, and PO_4^{3-}. Crystallinity – High. h. FTIR functional groups – Carbonate, Phosphate, asymmetric stretching of CH_2 and CH_3 and OH. Crystallinity – Low. XRD peaks – Broad. Shape – Needle-like/Rod-like. The diffraction peak at 2θ – 26.04°. Crystallite size – 32, 49, and 12 nm.Ca/P ratio – Between 1.5 & 1.77.	(Sathiyavimal et al., 2020) (Hariani et al., 2020) (Sano et al., 2012) (Azis et al., 2015) (Azis et al., 2015) (Pal et al., 2019) (Hsu et al., 2023) (Wu et al., 2013)
3.	Chemical Precipitation	a. Bovine bone b. Eggshells.c. Mussel Shells.	a. Hardness – 35.87 MPa Compressive strength – 0.39 MPa b. Fracture toughness –1.14 MPa.$m^{1/2}$ and hardness –4.96 GPac. N/A	a. Shape – Hexagonal Crystallite size – 14.18 nm. XRD result formed at angle 2θ – 32.54. Porosity – 47.78 %. b. Crystallinity 97.4 % Shape – rod-like Ca/P ratio – 1.65 Grain size – 0.33 μm. c. Ca/P ratio – 1.66.	(Mohd Pu'ad et al., 2020) (Tsai et al., 2006) (Shariffuddin et al., 2013)

(*continued on next page*)

Table 2 (*continued*)

Serial	Synthesis Method	Sources of HAp	Mechanical Properties Results	Crystallographic Results	Refs
				Mass loss – 40 to 48 %. C—O, $^{-}CO_3^{2-}$, OH^{-}, PO_4^{3-} present in the FTIR result.	
4.	Sonochemical	a. Egg Shells. b. Eggshell + H_3PO_4 c. Cockle shell + KH_2PO_4.d. Snail shells + $(NH_4)_2HPO_4$	a. N/A b. N/Ac. N/Ad. N/A	a. Shape – Hexagonal. FTIR bands – $CaCO_3$, CO_3^{2-}, and PO_4^{3-}, Bending mode H-O—H. XRD result formed at angle 2θ – 31–35. b. Shape – Neddle-like. Crystallite size – 30–50 nm. Surface area – 58.8 m^2/g. Stable at 750 °C. c. Shape – Needle-like. Crystallite size – 12 – 20 nm. d. Shape – Needle-like/Rod-like. Crystallite size – 12–17 nm.	(Sultana et al., 2021) (Hassan et al., 2014) (Li et al., 2021) (Li et al., 2021)
5.	Hydrolysis	Calcium carbonate ($CaCO_3$) and thermally synthesized calcium pyrophosphate ($Ca_2P_2O_7$)	Fracture strength – 052–0.82 MPa. Tensile strength – 9.309.36 MPa.	FTIR bands – Absorbed water, OH^{-}, HPO_4^{2-}, and PO_4^{3-}. Shape – Irregular. Density – 70 %. Enthalpy – 133 kJ/mol	(Durucan and Brown, 2000)
6.	Emulsion	a. $Ca(NO_3)_2{\cdot}4H_2O$ and $(NH_4)_2HPO_4$b. Poly(acrylic acid)/Polyethylene glycol	a. N/Ab. N/A	a. Shape – Hexagonal Spherical/Nanorod. Crystallite size < 70 nm Length of the nanorods – 200–280 nm and width – 10–25 nm.Ca/ P ratio – 1.67. b. Shape – FTIR bands – O—H, C═O, C—O, COOH, C—N, N—H and PO_4^{3-}. The highest XRD result formed at an angle 2θ – 75.8. Crystallinity – Low.Peaks – Reduced.Crystalline structure (Face centred cubic) .	(Wang et al., 2019) (Aslani et al., 2024)

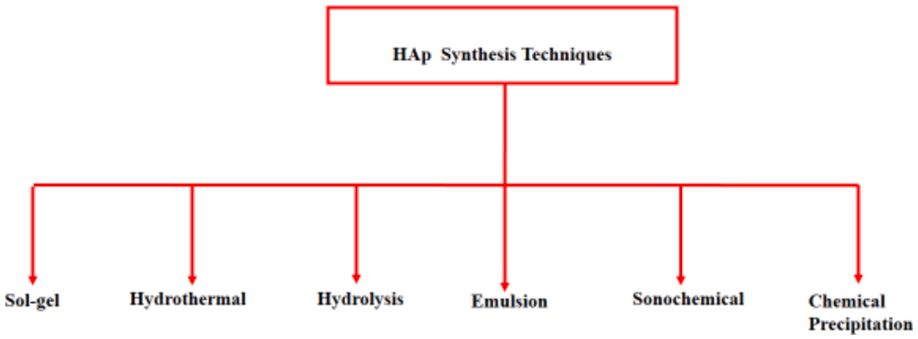

Fig. 20. Some wet methods for hydroxyapatite synthesis (Morey and Niggli, 1913).

agglomeration (Fig. 21). The mean particle size was around 0.8 nm, while the specific surface area, estimated by the Brunauer–Emmett–-Teller technique were 7–11 m^2/g. The FTIR spectrum displayed the typical OH^{-} and PO_4^{3-} vibration peaks as well as the weak CO_3^{2-} group bands, and also very weak bands, indicating that it is slightly B-carbonated HAp, as would be expected given that the sol–gel route used organic reagents (Bezzi et al., 2003).

Baladi et al. (2023) produced HAp via a sol–gel approach with lemon extract and studied its cancer activities in the human body. The cancer cells of *in vitro* cell death was observed and this inveterate that the as-produced HAp expressively reduced the percentage of cells that stayed alive. A coating of Silver-Fluoride-HAp (Ag-FHAp) on stainless steel substrates via the sol–gel technique was studied. The FESEM images and Mapping analysis were used to confirm the nano-scale size and uniform particle distribution in the Ag-FHAp structure, respectively, while the FTIR results showed HAp development in the achieved structure. They concluded that these structures are suitable materials for orthopaedic graft casing to reduce infection risk during surgical therapy (Jirofti et al., 2023). Sirajunisha et al. (2023) synthesized reduced Graphene oxide – HAps via sol–gel method. Using an Abalone shell with the aid of the sol–gel route, Cheng et al. (2023) developed a low-cost and ecologically friendly HAp for the removal of MO from simulated wastewater. Research on Graphene-Improved HAp Film on Dolomitic Marble via sol-gel process was carried out by Wang et al. (2023). Sol-gel method in an aqueous media was used by Monteiro et al. (2023) to produce hydroxyapatite nanoparticles without the need for additives. Pure HAp with average particle sizes of 24 and 53 nm, respectively, were produced by calcining samples at 600 and 750 °C. Additionally, the samples that were calcined at 900 and 1050 °C produced −calcium phosphate specifically and had average particle sizes of 118 and 732 nm, respectively. Ulfah et al. (2024) created a coating of Silver-Fluoride-Hydroxyapatite (Ag-FHAp) on Stainless Steel Substrates (SSS) using the sol–gel technique. In summary, Fig. 22 below is a setup for a typical sol–gel process.

Using the citric acid sol–gel combustion technique, TenHuisen and Brown (1998) produced nanocrystalline HAp powder from calcium nitrate, diammonium hydrogen phosphate, and citric acid. XRD, SEM, and Transmission Electron Microscope (TEM) were used to characterize the

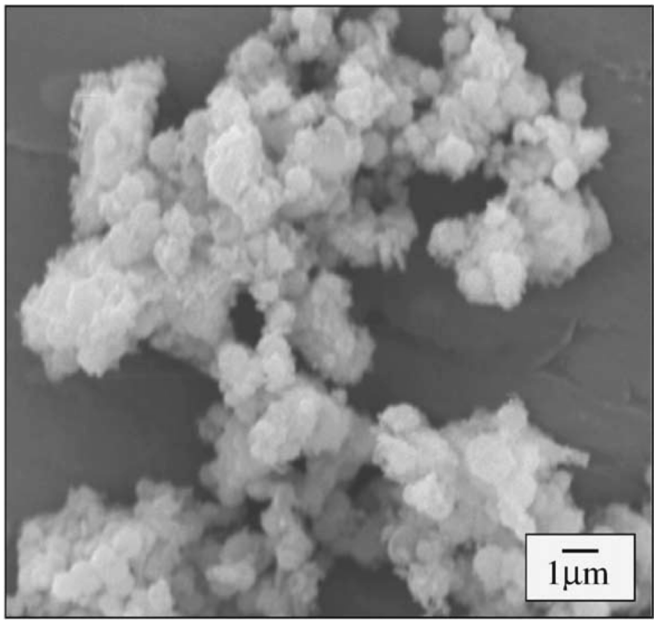

Fig. 21. Typical sol–gel SEM result of hydroxyapatite (Bezzi et al., 2003).

synthesized powder. The results showed that the dried gel was feathery and porous resembling bread. The dried gel showed an extremely amorphous character powder with grain size between 80 and 150 nm and an effective diameter of 494.6 nm. The XRD pattern of the resulting bioceramic sintered at 1200 °C for 3 h was pure HAp even after 3 h and other phases obtained were β-$Ca_3(PO_4)_2$ (β-TCP), α-$Ca_3(PO_4)_2$ (α-TCP) and CaO. The SEM result showed some agglomeration. The open porosity of the resulting HAp ceramic was 19 % and flexural strength of 37 MPa was obtained. Terbium-doped CaP nanocrystalline powders were synthesized by the citric acid sol–gel combustion routine. The phase composition, morphology, and luminescent properties of the produced powders were studied by XRD, SEM, TEM, fluorescence spectrophotometer, and microscopy. At 700 °C, Tb-doped CaP nanocrystalline powders were pure HAp and β-TCP. SEM and TEM observations (Fig. 23) showed that the 4 % Tb-doped CaP nanocrystalline powders are about 50–150 nm spherical particles. The 4 % Tb-doped CaP nanocrystalline powders exhibited the strongest emission at 548 nm ($\lambda_{excitation}$ = 240 nm) and strong green fluorescence under fluorescence microscopy (Sturgeon and Brown, 2009).

3.2. Hydrothermal method

Several ceramic materials, including HAp, can be synthesized using the hydrothermal process, which was firmly identified as an essential technology for the synthesis of materials in the 20th century (Suchanek and Riman, 2006; Yang and Park, 2019; Shi et al., 2020; Cao et al., 2022; Sankar and Kumar, 2021). The reaction of chemicals in an aqueous solution at a raised temperature and pressure is typically used to identify the hydrothermal process as one of the most popular methods for preparing HAp. Simply put, hydrothermal synthesis can be thought of as chemical precipitation in which the aging stage is conducted inside an autoclave or pressure vessel at a high temperature that is normally over the boiling point of water (Nurbaiti et al., 2024; Méndez-Lozano et al., 2024; Cao et al., 2022; Zhang and Darvell, 2010; Cihlar and Castkova, 2002; Ioku et al., 2002; Yasukawa et al., 1999; Zhu et al., 2009; Manafi and Rahimipour, 2011). However, as the hydrothermal pressure or temperature rises throughout the treatment, the Ca/P ratio for the precipitates increases (Sadat-Shojai, 2009; Zhang and Zhang, 2011; Guo et al., 2005; Neira et al., 2008; Zhang and Darvell, 2011; Lee et al., 2011; Lin et al., 2011).

It is known that HAp nanoparticles made under hydrothermal conditions are largely stoichiometric and have a high degree of crystallinity (Tsiourvas et al., 2011; Xu et al., 2011; Zhang and Zhang, 2011; Du et al., 2009; Kandori et al., 2009). Nevertheless, the hydrothermal procedure is more expensive than some of the other synthesis approaches since high

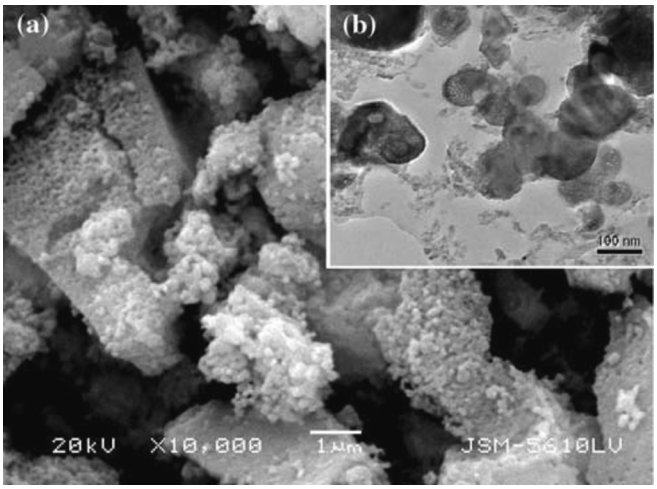

Fig. 23. Typical micrographs of Tb-doped HAp (a) SEM result & (b) TEM result (Sturgeon and Brown, 2009).

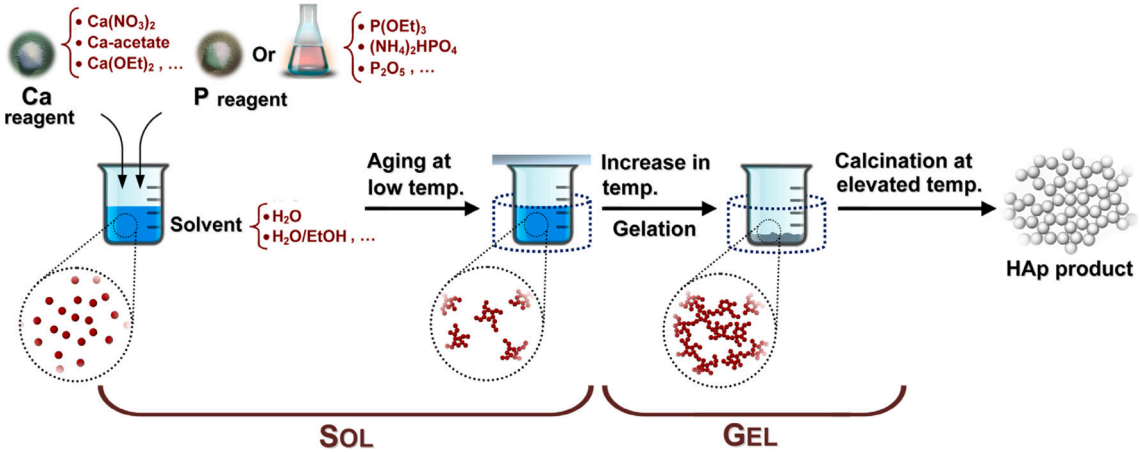

Fig. 22. A typical sol–gel process for the production of hydroxyapatite (Sadat-Shojai, 2009).

temperature and pressure calls for expensive equipment. The hydrothermal method's inadequate capacity to control the morphology and size distribution of nanoparticles is by far its worst drawback. In reality, particles produced by a typical hydrothermal method are typically irregular, spherical, or rod-like, with a very broad size distribution (Zhang et al., 2009; Wang et al., 2007; Muthu et al., 2022; Prasad et al., 2023; Anandan and Jaiswal, 2023). Fig. 24 depicts the basic hydrothermal technique preparation procedures. Under normal circumstances, a chemical that is weakly soluble or insoluble is dissolved and then recrystallized by the process (Yoshimura and Suda, 2017; Morey and Niggli, 1913).

Doped HAp-nanopowders were fabricated using the hydrothermal technique. The study proposed a low-cost, straightforward method for producing doped nanopowders in large quantities (Yang and Park, 2019). Manafi & and Rahimipour (Sadat-Shojai, 2009) employed a hydrothermal process to produce HAp. The produced HAp had diameters of 25–50 nm and lengths of 120–130 nm. They concluded that this method can be used to fabricate HAp for different uses. The microwave hydrothermal approach was used by Kumar et al. (2018) to quickly produce mesoporous hydroxyapatite nanocrystals with regulated size, shape (needle-, rod-, and fiber-like), and surface area. HAp powder was produced by the hydrothermal process and its effects on the structure and properties of the produced HAp were studied (Yoshimura and Suda, 2017). Roohani et al. (2021) synthesized HAp from eggshells using a hydrothermal process. The HAp's shape was hexagonal with a Ca/P ratio of 1.67. Condino et al. (2018) fabricated HAp from pig bone using the hydrothermal method. Potassium hydroxide (KOH) was used to deproteinize and remove fats from the bones for 24 h.

3.3. Hydrolysis method

The hydrolysis technique is used in the production of HAp (for example, dicalcium phosphate and tricalcium phosphate) from different sources. It is frequently referred to as the "water ionization method, which produces hydroxide (OH^-) and hydrogen ions (H^+) (Service, 2000; Torres-Mansilla et al., 2023; Zubieta-Otero and Rodriguez-Garcia, 2023; Pu'ad et al., 2020). As a result, when Ca/P compound is hydrolyzed with water or an organic solvent (like 1-butanol, ethanol, alcohol, 1-hexanol, propane diol, 1-octanol, or ethylene glycol) while being heated and stirred, a non-stoichiometric (i.e. Ca/P ratio more than 1.67) HAp is generated (Atemni et al., 2023; Service, 2000; Petrakova et al., 2021; Bordbar-Khiabani et al., 2023; Fedotov and Komlev, 2022). The dissolving and precipitation methods are widely used to convert Ca/P compounds into HAp through water hydrolysis (Seredin et al., 2022). In addition, the dissolution of Ca/P compounds and subsequent precipitation strategies are also involved in the formation of HAp crystals via a variety of additional synthesis processes (Seredin et al., 2023; Murata et al., 2023).

The hydrolysis of octacalcium phosphate (OCP) has also received some attention in the last decades (Niu et al., 2017; Miyatake et al., 2009; Oizumi et al., 2021). The preparation of HAp particles, however, has not been particularly interested in this type of conversion over the past ten years. This is likely due to the slow rate of OCP hydrolysis and/or the high ability of OCP to incorporate impurity species, including additives and foreign ions used in its transformation to HAp (Sadat-Shojai, 2009). However, the hydrolysis procedure is regarded as a separate technique when one wants to turn a ready-made or commercially available Ca/P into HAp (Graham and Brown, 1996; Pieters et al., 1998; Ressler et al., 2023; Ito et al., 2008; Shih et al., 2005; Shih et al., 2004; Morgan et al., 2000; Štulajterová and Medvecký, 2008; Lakrat et al., 2023; Zinicovscaia et al., 2023). Under specific conditions, Tetracalcium phosphate (TCP) can be achieved via hydrolysis according Refs (Fulmer and Brown, 1998; Karalkeviciene et al., 2023; Monma and Kamiya, 1987; Kim et al., 2005; Medvecky et al., 2022; Madanayake et al., 2021). It has been confirmed that the increased reaction temperature during hydrolysis affects the HAp surface area and the crystals (Duminis and Shahid, 2021; Laky et al., 2023).

By hydrolysing-TCP, Lakrat et al. (2023) produced calcium-deficient HAp, and the effects on it were carefully examined. In solvothermal environments, the hydrolysis reaction was carried out in solutions with varying additive concentrations in aqueous and different aqueous-organic media. It has been proven that the type and quantity of organic additives affect the product's shape and phase purity. Model morphology varied depending on the quantities of particular organic additions, ranging from plate- to rod-like. In alkaline solutions with a pH of 10.8 and a temperature of 39 °C, the hydrolysis of brushite into HAp has been investigated both with and without the addition of calcium ions. The result demonstrated that temperature and pH had a significant impact on HAp precipitation. After prolonged hydrolysis, the solution lacking Ca^{2+} contained calcium phosphates in their most stable state (Shih et al., 2005). Bigeye snapper bone hydroxyapatite synthesis under ideal acid hydrolysis settings was studied, along with the effects of synthesis period (10–60 min) and HCl concentration (2.0–5.0 % w/v) on yield and hydroxyapatite characteristics. The SEM results revealed irregular shape, wide surface area, and roughness of the produced HAp (Chahal et al., 2023). Fig. 25 is a typical hydrolysis technique process.

3.4. Emulsion technique

The specific regulation of morphology, size, and size distribution of grains or particles is exceptionally essential and indeed challenging; particularly when one intends to fabricate nanomaterial with

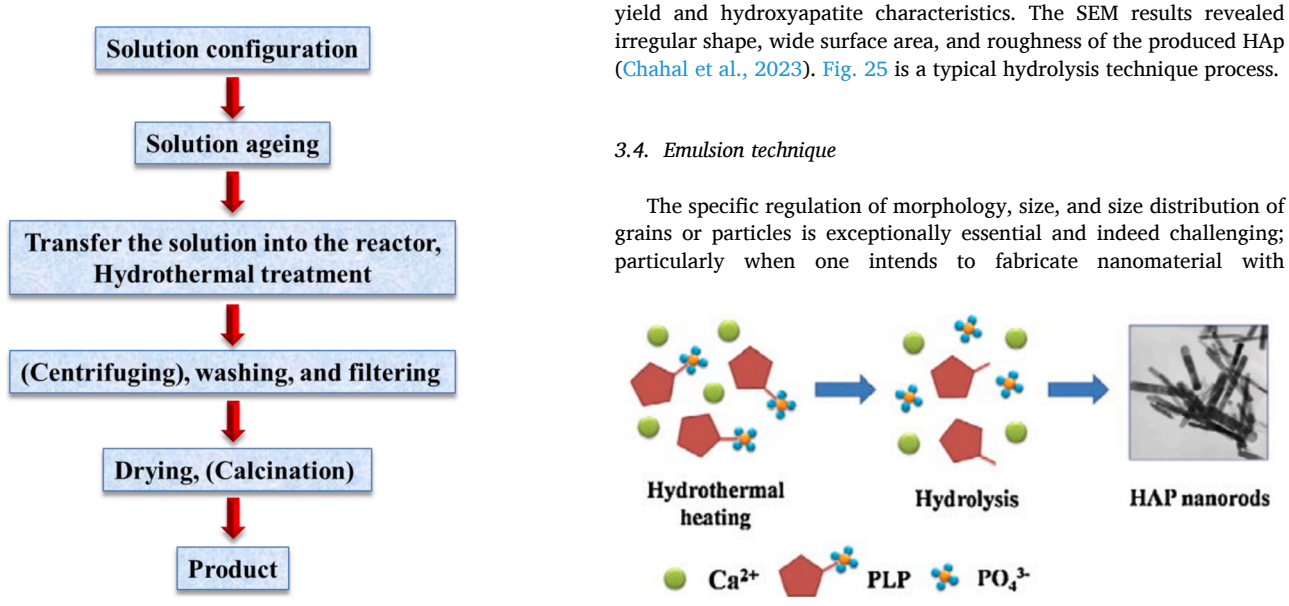

Fig. 24. The basic hydrothermal technique preparation procedures (Yang and Park, 2019).

Fig. 25. A typical hydrolysis technique for the production of hydroxyapatite nanorods (Wang et al., 2023).

insignificant agglomeration and accumulation. The emulsion handling of HAp particles was originally used to enhance the bunching and to confine the development of solid agglomerates according to Murray et al. (1995), but this method is currently a matter of excessive attention not only to make an agglomerate-free ceramic powder but also to regulate the microstructure and morphology of resultant particles. Certainly, amid many diverse synthesis procedures established for HAp production, the emulsion technique is recommended to be more effective in decreasing the particle size, guiding the morphology, and regulating the agglomeration of HAp particles (Mehnath et al., 2022). Furthermore, ease and slight production situations lacking any high-temperature necessities in the main process make the emulsion method the right technique. The emulsion route relies strappingly on the kind of surfactant(s) employed and the concentration of the surfactant (s) in the liquid medium (Murray et al., 1995; Chahal et al., 2023; Arjama et al., 2021). Fig. 26 below is a picture showing the main three emulsification processes,

From Fig. 26, the emulsion route can be done through three main methods: water-in-oil emulsion, oil-in-water emulsion, and water-in-oil-in-water dual emulsion. However, the production of HAp is generally done through the water-in-oil method recorded for approximately 70 % of all literature connected to the emulsion method for the production of HAp. The water-in-oil emulsion is centred on a clear reverse micro-emulsion method having inverse micelles diffusing in a constant oil stage according to Lett et al. (2015). A “water pool” on hold in the oil phase is formed by each micelle, which is made up of solution droplets encircled by certain surfactant molecular groups. The reaction between calcium and phosphate ions leads to the creation of HAp crystals with the addition of the second microemulsion containing a different reagent (Sofronia et al., 2014). The advantages of this technique include (Kimura, 2007): (1) a common stimulated reservoir is adequate to be adopted as a reactor, hence, any exceptional device is needless. (2) Low production temperatures at approximately room temperature are functional. (3) The aqueous phase is effortlessly characterized. (4) Absorption is faster when linked to solid dosage methods.

The pH-shock wave approach was used to produce HAp using a microemulsion process. The result revealed that an A-type carbonate HAp was produced at 650 °C which crystallized in units with equal dimensions without internal porosity. Sintering was thought to occur above 900 °C, producing a system of higher particles that included pure HAp and −tricalcium phosphate (Saha et al., 2009). To improve the method of processing HAp, Murray et al. (1995) derived HAp powders by emulsion-refining the gelatinous calcium phosphate in an O/W emulsion. The obtained powder exhibited both higher green and sintered density at temperatures above 800 °C. The SEM picture via the emulsion method (Fig. 27 a) showed some inter-agglomerate voids, exhibited by the difference in sintering, resulting in the creation of large, crack-like pores, which act as the strength-limiting microstructural defects in the usually produced HAp (Fig. 27b). Fracture strength of 170 4–12.3 MPa was obtained compared to 70 ± 15.4 MPa for the usual method.

Wang et al. (2023) established a new method for producing mesoporous HAp via double emulsion droplets as microreactors. The results showed a unique production method for adjusting the nanoscale porosity and the morphology of HAp. Sun et al. (2007) scrutinized the nanoemulsion procedure as a way to produce carbonated hydroxyapatite nanospheres which can be employed to create composite tissue engineering scaffolds. HAp nanoparticles were fabricated via emulsion of the liquid membrane system. A high Ca/P ratio of 2.0 was obtained with an unwanted reaction of high Ca^{2+}. The surface area decreased as reaction and calcination temperatures increased. The specific surface area decreased from 227 to 58 m^2/g following thermal treatment at temperatures ranging from 450 to 750 °C (Alam et al., 2024).

By a reaction in a microemulsion method soothed by a surfactant (sodium bis-2-ethyl hexyl succinate), hydroxyapatite nanoparticles were produced. The characterization results showed the production of pure HAp and the creation of additional calcium phosphate compounds was confirmed (Lett et al., 2015). A new biomimetic approach to manufacture for crystal growth at the aqueous level was proposed by Mehnath et al. (2022). de Andrade et al. (2023) presented a surfactant-free method for the production of polyester-based microparticles packed with HAp nanoparticles by the O/W emulsion procedure. Lai et al. (2008) proposed a fresh method for making super-hydrophilic membranes by interpolating HAp with graphene oxide and operating vacuum filtration. The suggested HAp membrane showed a new way of filtering out oil and water and grips favourable potential for application in that area. Minaev et al. (2022) produced Poly(lactic acid)/hydroxyapatite core–shell nanoparticles by a surfactant-free emulsification technique and the osteoblast variation performance was assessed.

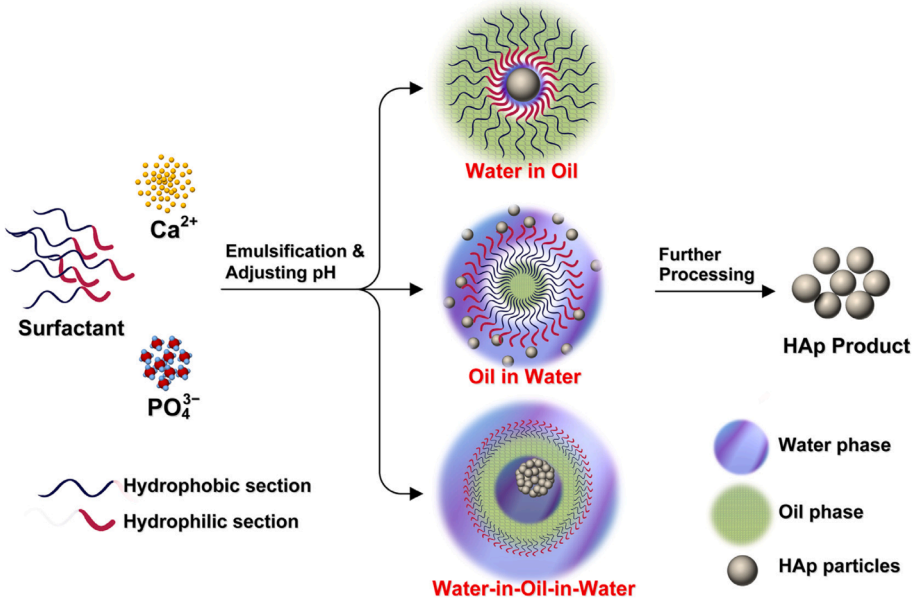

Fig. 26. Typical Emulsion processes for the production of hydroxyapatite (Sadat-Shojai, 2009).

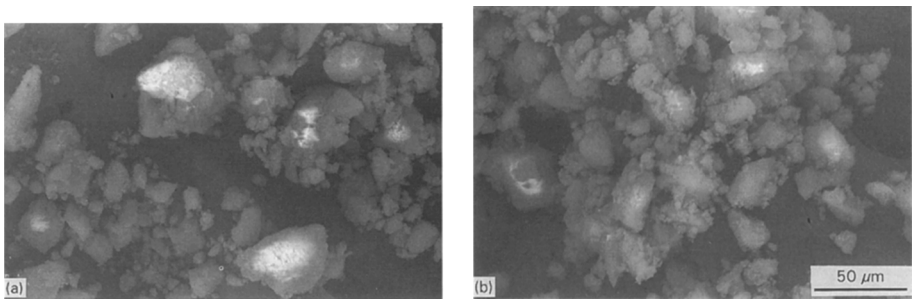

Fig. 27. SEM image of (a) Usual Produced HAp and (b) Emulsion Produced HAp (Murray et al., 1995).

3.5. Sonochemical technique

One of the early methods for producing nanomaterials was sonochemistry (Jirofti et al., 2023). In the field of research known as sonochemistry, molecules react chemically when strong ultrasonic radiation is used. In other words, Sonochemical techniques, which do give nanosized results centered on the chemical reactions triggered by powerful ultra-sound radiation (Lee et al., 2022).

According to Fig. 28, audile cavitation in an aqueous phase, where the formation, growth, and disintegration of microbubbles occur, is the physical mechanism underlying sonochemical synthesis (Zhao et al., 2014; Gedanken, 2004; Mai et al., 2017; Jevtic et al., 2008; Han et al., 2009). To speed up mixed reactions between liquid and solid reactants, chemical reactivity is undoubtedly stimulated (Noruzi et al., 2023; Anwar et al., 2023). Recent research has shown that sonication can accelerate the growth of HAp crystals by up to 5.5 times (Burdusel et al., 2023). Additionally, it has been claimed that HAp nanoparticles made via a sonochemical process preserve crystals that are more uniform, slighter, and cleaner with only a minimal amount of agglomeration (Kim and Saito, 2001; Nguyen et al., 2023; Rouhani et al., 2010). Due to their increased surface area, these nanoparticles can specifically improve the sintering kinetics and, consequently, the mechanical characteristics of the final product. By using urea as an organic converter and ultrasonic precipitation, Giardina and Fanovich (2010) produced a needle-like nanocrystalline HAp. They discovered that urea addition encourages the production of HAp nanoparticles.

The ultrasonic approach makes it simple to produce nanomaterials according to Zhang et al. (2009). Kuznetsov et al. (2008) produced HAp from mussel shells via an ultrasonic-assisted route and Fe^{2+}/Fe^{3+} ions were incorporated. The characterization result showed that the fused ions did not alter the purity of the HAp. Also, in Simulated Bidy Fluid (SBF) studies, the produced material demonstrated acceptable bone regeneration ability. To produce natural HAp (NHAp), Poinern et al. used ultrasonic irradiation, after calcination. They studied how ultrasound affected the production of nanoparticles and discovered that following treatment, ultrafine NHAp powders (30–36 nm) were produced as a result of physical and chemical interactions. The secondary ultrasonic operating circumstances, which might have contributed to the emergence of more bubbles and cavities, were not disclosed by the authors (Cao et al., 2005).

Sonochemistry and microwave technology were employed by Qiao et al. (2011) to produce NHAp and generate mesoporous structures that potentially imitate volcanic rocks. They pointed out that their findings were preliminary because the study is still underway. They did not disclose the operating parameters or characterizations, however, this technique may be novel and useful in manufacturing mesoporous nanoparticles. Agalya et al. (2022) used a hydrothermal alkaline treatment in conjunction with an ultrasonic wet milling process to produce and characterize HAp from pig bones. The bones were first defatted, and then they were cleaned with potassium hydroxide (KOH) aqueous solution for 24 h to get rid of any filth or oil, followed by 100 W of ultrasonic handling. The results of the characterization showed that the particle size decreased with increasing ultrasound intervals, demonstrating the mechanism by which micro agglomerates are eroded and fragmented into nanoparticles. The X-ray results showed that the HAp nanocrystals were not altered by any of the techniques used to clean and produced the nanoparticles. Additionally, the presence of Mg, Na, K, and Zn was noted in smaller amounts, and the isolation processes used to produce the HAp nanoparticles had no impact on the trace elements concentrations.

Alkaline cleaning has been shown to have an impact on the organic matter, crystallinity, and stoichiometry of the hydroxyapatite structure by Poinern et al. (2011) through their study of alkaline cleaning at high concentrations and prolonged exposure times. A new HAp magnetic nanocomposites was produced as an organized point drug delivery via ultrasound-supported precipitation technique. The results proved that the produced nanocomposites can be active means of transportation for the continuous delivery of an antihypertensive drug known as atenolol (Liang et al., 2013).

Hasan et al. (2024) studied the effectiveness of the ultrasonic method for the production of HAp from cockle shells. Ultrasonic was used to clean and dry them in an oven at 50 °C for 2 h. Using a mortar and pestle, the dried shell was crushed before being ground at 5000 rpm in hammer mills with a 0.5 μm sieve net. After dissolving 1 g of shell powder in 100 mL of 0.1 M EDTA, 0.06 M of phosphoric acid (H_3PO_4) was gradually added. After adding 1 M of sodium hydroxide (NaOH) to bring the

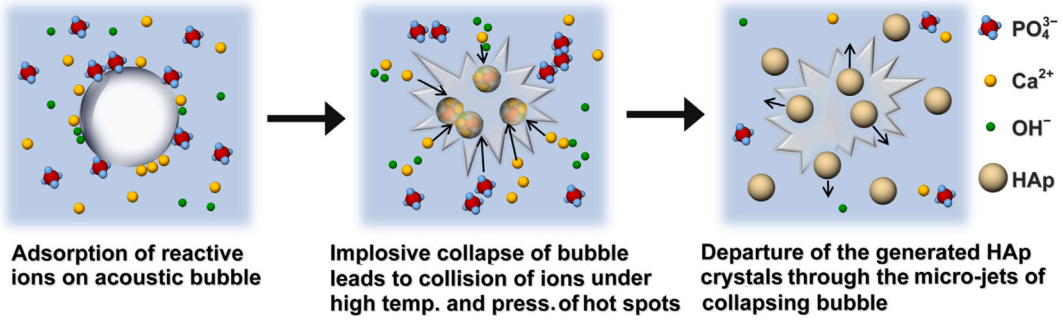

Fig. 28. A typical sonochemical technique of HAp (Lee et al., 2022).

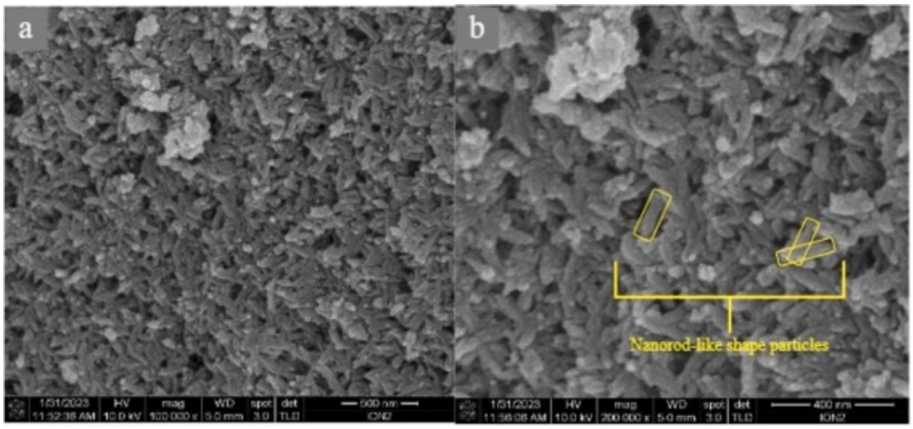

Fig. 29. Typical FE-SEM of HAp produced through ultrasonic technique (Hasan et al., 2024).

solution's pH down to 13, it was shaken for an extra hour at 27 ± 1 °C. X-ray diffraction (XRD) spectroscopy and Field Emission-Scanning Electron Microscopy (FE-SEM) with an energy-dispersive X-ray spectroscopy (EDX) detector were used to analyse the morphological and elemental structures of HAp. According to the FE-SEM result (Fig. 29), the extracted HAp exhibited hexagonal crystal structure, elongated-oriented growth, and nanorod- and fibre-like agglomeration particles. The positively charged calcium and EDTA interact to create an electrostatic force on the a-axis, which drives growth along the c-axis and affects the orientation of the crystal growth. The produced HAp peaks corresponded to the Miller indices with slight phase transition in HAp during recrystallization, but the changes were insignificant (Hasan et al., 2024).

3.6. Chemical precipitation technique

The common and broadly researched method for the production of HAp is the precipitation method. This method is also known as wet precipitation or chemical precipitation. This method is preferred usually to produce HAp in distinction to other methods. Because the comparatively huge quantity of HAp can be produced using the precipitation method without organic cleaners at a low cost (Santos et al., 2004; Liang et al., 2013; Zubieta-Otero and Rodriguez-Garcia, 2023; Brzezińska-Miecznik et al., 2015; Naseri et al., 2023; Nayak, 2010). However, the precipitation process is typically carried out at pH levels greater than 4.2, and temperatures range from room temperature (25/27 °C) to one near the boiling point of water (<100 °C) (Mendez-Lozano et al., 2022; Shum et al., 2009). Fig. 30 depicts the steps required for the chemical precipitation of HAp along with the suggested parameters to regulate the characteristics of the HAp powder. Chemical precipitation using a variety of calcium- and phosphate-containing reagents, such as calcium hydroxide or calcium nitrate as the Ca^{2+} source and diammonium hydrogen phosphate as the PO_4^{3-} source, can be used to produce HAp nanoparticles. A traditional procedure involves maintaining a stoichiometry Ca/P ratio of HAp while adding each reagent dropwise to the next and gently stirring continuously. The next step is to wash, filter, dry, and crumble the suspension into a powder or age it under atmospheric pressure (Zhou et al., 2008; Jarudilokkul et al., 2007; Tao et al., 2007; Swain and Sarkar, 2011; Afshar et al., 2003; Kong et al., 2002).

HAp produced via simple precipitation still has a Ca/P ratio of more than 1.67 and ill crystallized and irregular in shape (Sadat-Shojai et al., 2013; Gómez-Morales et al., 2001; Fomin et al., 2009). Many elements are assumed to cause these disadvantages, with the high chemical affinity of HAp to some ions. The complex nature of the CaP crystals, hydrogen-bonded interfaces amongst the HAp particles, and the part of the kinetic parameters, which are liable on the investigational settings, prevail over the thermodynamic parameters (Gibson and Bonfield, 2002; Verwilghen et al., 2009). For example, the non-stoichiometric characteristics may arise due to vacancies in the crystal lattice (Kumta et al., 2005; Zhang and Zhu, 2005), the exchange of diverse ions like Ca, K, and Cl (Verwilghen et al., 2009; Koutsopoulos, 2002), or the attendance of extra phases (Verwilghen et al., 2009; Palazzo et al., 2009), etc. Hence, a specific regulator over the processing settings is normally recommended for the production of a powder with slight deficiencies. The pH data and temperature used in the precipitation reaction and/or the aging phase are the greatest perplexing factors. Certainly, to achieve a mono-crystal HAp with high phase purity, the precipitation reaction is commonly carried out at a high pH or a high temperature, or together. At whatever time the pH value needs to be reduced (e.g. for a precise morphology), the temperature should be raised and the other way round (Mendez-Lozano et al., 2022; Liou et al., 2004; Iafisco et al., 2011; Liu et al., 2001; Zhang and Lu, 2007; Okada and Furuzono, 2007; Koumoulidis et al., 2001). This leads to an intense reduction in the attendance of phase impurities (e.g. dibasic calcium phosphate anhydrate and octacalcium phosphate (OCP)), occasioning HAp as a principal phase (Mendez-Lozano et al., 2022; Catros et al., 2010; Okada and Furuzono,

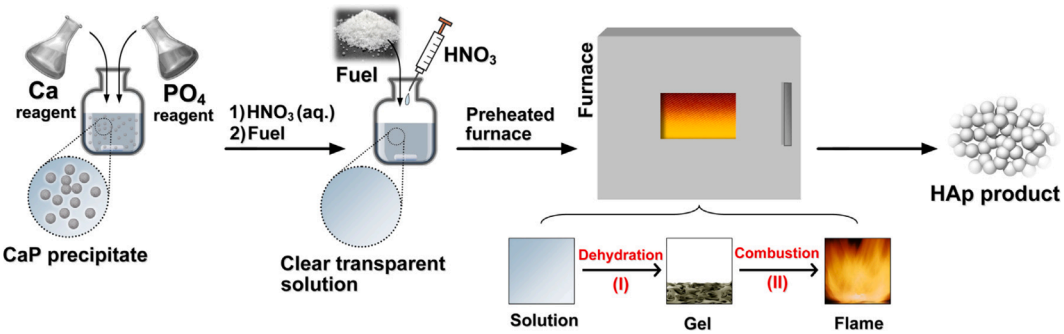

Fig. 30. Seps required for the chemical precipitation of hydroxyapatite (Nayak, 2010).

2007; Koumoulidis et al., 2001; Chen et al., 2005).

Using a wet chemical technique nano-sized calcium-scarce apatitie crystals with Ca/P ratios from 1.5 to 1.67 were produced and of needle-like shape with 5–10 nm in breadth and 40–50 nm in length was detected. The findings indicated that the apatite with a Ca/P ratio of 1.67 had the highest FTIR amplitude and that the structural disorder increased in the following order: 1.67 > 1.5 > 1.6 > 1.55. The structural study also reveals dissimilar chemical and biological characteristics between these nano-crystals with a Ca/P ratio from 1.5 to 1.67 (Zhang and Zhu, 2005). HAp muttonchops produced via regular precipitation technique were thermally treated in the atmosphere. The phase structure showed that the HAp achieved was morphologically stable at higher temperatures less than 1200 °C, while a phase change of the HAp occurred apparently at around 1200 °C. When compared with the chemical composition and crystallinity, the thermal stability of the HAp may well be employed as a reinforcing material in dense and porous HAp ceramics (Okada and Furuzono, 2007). New porous HAp panes with high pore homogeneousness were produced by a self-assembly nonaqueous precipitation technique. The produced HAp are greatly active carbonate apatite and hexagonal (Wang and Shaw, 2007).

HAp nano-sized particles were produced via chemical precipitation in calcium chloride and ammonium hydrogen phosphate aqueous solutions. The effect of temperature, sintering period, and calcination on the crystallinity and morphology of the HAp nanoparticles were studied. From the results, crystallinity and crystallite size increased with temperature and maturation period. According to the characterization results, HAp nanoparticles' altered morphology was related to their crystallinity. The high crystallinity of HAp led to the nanoparticles' uniform shape and smooth surface. After being calcined at 650 °C for 6 h, HAp powders dramatically increased in crystallinity (Catros et al., 2010). HAp of diverse morphologies was produced via the direct decomposition of calcium lactate pentahydrate chelates with

Table 3
Summary of synthesis techniques advantages and disadvantages.

Serial	Synthesis techniques	Advantages	Disadvantages	Limitations	Refs
1.	Emulsion	– Common stimulated reservoir. – Low production temperatures. – The aqueous phase is effortlessly characterized. – Absorption is faster when linked to solid dosage methods. – High phase purity of HAp.	– Expensive. – Low Crystallinity of HAp.Ca/P ratio less than 1.67.	Many Chemicals are required.	(Osuchukwu et al., 2021; Kimura, 2007; Ponomareva et al., 2010)
2.	Hydrothermal	– High degree of crystallinity. – Can be used to produce pure Hap – high purity and fine particle size powders in a short time	– Inadequate capacity to control the morphology and size distribution of nanoparticles. – Requires expensive	High temperatures and pressures are required.	(Osuchukwu et al., 2021; Zhang et al., 2009; Wang et al., 2007; Muthu et al., 2022; Prasad et al., 2023; Anandan and Jaiswal, 2023; Yoshimura and Suda, 2017; Morey and Niggli, 1913).
3.	Sol-gel	– Convenient operation – Simple synthesis process – Controllable particle size. – Molten-level reactant mixing, improving the chemical homogeneity of the resultant powder – Formation and fusing of the arranged crystals at low temperatures. – Produces a stoichiometric structure with a large surface area.	– Different HAp morphology. – Presence of a secondary phase, which is commonly calcium oxide (CaO)	Some of the starting materials' high costs, particularly those of alkoxide-based precursors.	(Osuchukwu et al., 2021; Kumar and Kalainathan, 2010; Sanosh et al., 2009; Bigi et al., 2004; Kuriakose et al., 2004; Bezzi et al., 2003)
4.	Hydrolysis	– HAp can be derived with required physicochemical properties. – Can be used at low temperatures. – Pure HAp can be obtained. – Moderate chemicals required. – Nanosized particles can be achieved.	– Expensive. – Different morphology of HAp.	The slow rate of OCP hydrolysis and the high ability of OCP to incorporate impurity species, including additives and foreign ions used in its transformation to HAp.High temperature affects the surface area.	(Osuchukwu et al., 2021; Sadat-Shojai, 2009; Service, 2000; Torres-Mansilla et al., 2023; Zubieta-Otero and Rodriguez-Garcia, 2023; Pu'ad et al., 2020)
5.	Sonochemical	– Nanosized HAp can be achieved. – Accelerate the growth of HAp crystals by up to 5.5 times. – Increased surface area. – Improve the mechanical characteristics of the final product.	– Formation, growth, and disintegration of microbubbles occurs. – Low purity of end products. – Unstable Ca/P ratio.	Particle size decreased with increased mechanical activation duration.High temperature	(Noruzi et al., 2023; Anwar et al., 2023; Burdusel et al., 2023; Kim and Saito, 2001; Nguyen et al., 2023; Rouhani et al., 2010; Giardina and Fanovich, 2010)
6.	Chemical Precipitattion	– Huge quantity of HAp can be created. – Low cost. – Nanosized HAp can be achieved.	– pH levels greater than 4.2, and temperatures range from room temperature.	High pH level.High temperature.	(Santos et al., 2004; Liang et al., 2013; Zubieta-Otero and Rodriguez-Garcia, 2023; Brzezińska-Miecznik et al., 2015; Naseri et al., 2023; Nayak, 2010)

dipotassium hydrogen phosphate in hydrothermal settings. The suggested method permits the exact controller of the HAp crystals morphology and produces purity, which is crucial for biomedical applications. The produced HAp had the form of muttonchops, hexagonal rods, nanoparticles, flowers, and cylinders (Zhang et al., 2002). Liu and Nancollas (1997) produced HAp for drug delivery via the precipitation technique. In an aqueous mode at 25 °C, Feng et al. (2023) precipitated two sets of apatite powders. The result reveals that the nano-crystal dry powders are improperly crystallized. Future applications of apatite made with slightly sub-stoichiometric calcium have the potential to be very exciting in the biological, catalytic, and environmental fields. HAp was produced using the wet precipitation method and using two different drying processes to see if this parameter had a major impact on the qualities of the final product. It was discovered that the way the powders were dried had an impact on both the porosity of the sinters made from them and the form of the grains (Szterner et al., 2023).

Different processing variables, including pH, Ca/P ratio, reaction temperature, sintering temperature, and reaction duration, are needed for the various techniques to produce crystalline HAp. The most important factors are the reaction pH and the balanced Ca/P molar ratio, which the intended process should maintain. Certain processes use chemical modifiers, like emulsion, combustion and sonochemical, to speed up the reaction. The Sol-gel and hydrothermal methods are recommended for the production of HAp from natural sources with high purity at low cost and ease of operation. Table 3 is a summary of the techniques with their advantages, disadvantages and limitations. The sol–gel approach has several advantages over others including good mixing of the starting components, high purity, low synthesis temperature, and great chemical homogeneity. The ratio of Ca to P must be 1.67 in order to synthesise HAp using sol–gel.

4. Comparison of natural to synthetic hydroxyapatite

HAp is composed of the inorganic mineral constituents of hard tissues, for example, the spine (Farkas et al., 2023; Hatim et al., 2023; Niziołek et al., 2023), skull (Von Euw et al., 2019; Litak et al., 2022; Hahn et al., 2013), and teeth (Verheggen and Merten, 2001; Wiltfang et al., 2004; Weissman et al., 1996; Amaechi et al., 2019). Commercial artificial HAp powders can be derived via a synthesis techniques due to the ease and cost-efficiency of these methods (Farkas et al., 2023). However, the resultant product may be short of crucial ions, such as magnesium, zinc, potassium, silicon, strontium, and iron (Nobre et al., 2020; Bossù et al., 2019; Mehta et al., 2014; Liu et al., 2021). These trace elements are important as they: Inhibit osteoclast cell formation (Guerra Bretaña et al., 2017; Zofkova et al., 2017), Circumvent osteoporosis (Qamar et al., 2017), increase the differentiation of estrogenic cells (Webster et al., 2002; Shepherd et al., 2014; Ito et al., 2005) Magnesium Cell adhesion, and boost bioactivity (Ishikawa et al., 2002; Bhattacharjee et al., 2014; Yu et al., 2017) Stimulate cell differentiation (Cai et al., 2013), deter osteoclast production (Ullah et al., 2020), Boost strength and corrosion resistance (Arul and Ramya, 2017), etc.

A xenograft is a favoured option for biomedical applications study due to the ready availability of essential ions in it, such as from human bone or fish bone and scale (Zhu et al., 2023). Due to their great availability and practicality from an economic standpoint, shells are also recognized as excellent calcium resources that can be supplemented with a phosphate precursor to produce hydroxyapatite (Liu et al., 2019). High crystallinity, purity, and environmental friendliness are all characteristics of natural hydroxyapatite (Swadi et al., 2012; Oryan et al., 2013; Vecchio et al., 2007). Synthetic hydroxyapatite is far less biodegradable than tricalcium phosphate and natural hydroxyapatite, according to a prior study (Huang et al., 2011). The advantage of HAp from natural backgrounds makes it more desired for biomedical applications. Table 4 compares the differences between HAp manufactured chemically and HAp derived from natural sources in terms of cost of production, Ca/P ratio, basis/source, trace elements, and treating time.

Table 4
Some comparative factors between natural and synthetic hydroxyapatite.

S/N	Factors	Natural Hydroxyapatite	Synthetic Hydroxyapatite	Refs
1	Costs	Economical	Expensive	(Hussin et al., 2022; Huang et al., 2011)
2	Sources	Animal bones, Fish bones and scales, Shells, Clams	Calcium pyrophosphate ($Ca_2P_2O_7$), Disodium phosphate (Na_2HPO), and Dipotassium phosphate (K_2HPO)	(Hussin et al., 2022; Huang et al., 2011)
3	Ca/P ratio	1.67 and above	1.67	(Hussin et al., 2022; Huang et al., 2011)
4	Processing Time	Fast	Slow	(Hussin et al., 2022; Huang et al., 2011)
5	Trace elements	Mg, Fe, Sr, Zn, Na, K, etc	N/A	
6	Lattice parameters	a = 9.3892 Å; c = 6.8442 Å	a = 9.4455 Å; c = 6.9234 Å	(Assis et al., 2005)
7	Microdeformation	0.1585 ± 0.0527	0.6664 ± 0.3114	(Assis et al., 2005)
8	Morphology	Spherical, Plate-like, Needle-like	Spherical, Plate-like, Rod like, Needle-like	(Mehnath and Jeyaraj, 2021; Mehnath et al., 2022; Arjama et al., 2021; Lett et al., 2015; Ethirajan et al., 2008; Saha et al., 2009)
9	Crystallite size (nm)	27.3–42	42–106	(Osuchukwu et al., 2022d; Mehnath and Jeyaraj, 2021; Ethirajan et al., 2008)
10	Specific surface area (m^2/g)	19.2	4.2–13.7	(Ethirajan et al., 2008)
11	Porosity (%)	40 and above	40 and above	(Ponomareva et al., 2010; Okpe et al., 2024)

4.1. Applications of hydroxyapatite

Over 2.2 million patients need bone grafting surgery each year to address critical-sized big bone deficiencies brought on by accidents, injuries, or diseases (such as tumour removal) (Herliansyah et al., 2007; Sathiyavimal et al., 2020). Healing of these abnormalities is a frequent and important issue in orthopedic surgery. Autologous bone grafts, allografts, and biocompatible synthetic materials are used to reconstruct those defects (Sossa et al., 2018; Horta et al., 2023). Long-lasting implants must be prepared due to the increased life expectancy and the requirement to insert more implants in younger patients. As a result, there is a growing need for innovative technology to produce these implants (Neovius and Engstrand, 2010).

Synthetic hydroxyapatite has been used for some time as a biomaterial for orthopaedic and dental applications for repairing or substituting hard tissues, as well as for drug delivery systems because it has a chemical formula and physical characteristics that are similar to those of the main inorganic constituent of bones and teeth. To create artificial bone grafts made entirely of HAp or merely as the surface coating by HAp, synthetic biomaterials composed of HAp have been thoroughly researched. The mechanical strength and porosity structure

of the device, in addition to its bioactivity and biocompatibility, are crucial when it is implanted into the human body (Guillet et al., 2023; Smeriglio and Zalc, 2023; Mohseni et al., 2014; Huang et al., 2011; Hashemi et al., 2023; Kolekar et al., 2022). Additionally, the material must possess appropriate osteoconductive, osteoinductive, and osteointegrative properties (Xiao et al., 2016; Jia et al., 2022; Cuylear et al., 2023; Kolmas et al., 2016; Anitta and Sekar, 2023). Because hydroxyapatite and the inorganic component of the bone matrix are comparable, manufacturing techniques for synthetic HAp preparations have been developed. These preparations can be used in biomedicine to repair hard tissues or as drug delivery systems. Complete or partial bone augmentation, filling bones and teeth, or covering in orthopaedics and dental implants are all examples of using HAp as a bone substitute or replacement (Anitta and Sekar, 2023; MubarakAli et al., 2023; Murugan et al., 2023; Dorcioman et al., 2023; Sachlos and Czernuszka, 2003). This section centres on the works of recent studies on the applications of HAp for biomedical applications (bone fillers and tissue engineering scaffolds, implant coating arrangement, and drug delivery approaches) (Anitta and Sekar, 2023).

4.1.1. *Bone plasters and tissue engineering scaffolds*

Management of big bone defects occasioning from resection of tumors, shock, or contamination very regularly involves bone implanting surgical treatment. In the case of reconstructive processes with autograft and allograft, the complications of benefactor compatibility, immune rebuff, and pathogen transferal can rise (Ataollahi, 2023; Uddin et al., 2023; Khoshnazar et al., 2023; Miola et al., 2023; de Oliveira et al., 2023). Orthopaedic biomaterials today can approximate real bones in appearance. The resultant porous materials can function briefly as an extracellular medium, stimulating the normal course of tissue growth and regeneration (MubarakAli et al., 2023; Lacambra-Andreu et al., 2023; Miranda-Oporta et al., 2023; Hohmann, 2023; Hollister, 2005; Chen et al., 2010; Ielo et al., 2022; Mou et al., 2011; Ma et al., 2012; Villa et al., 2015). The biocompatibility and osteoconductive properties of HAp is one of the main components of bone that facilitate the interaction, growth, and generation of human osteoblast cells. The incorporation of HAp into a polymeric matrix is therefore of utmost significance. The main factor affecting how such a complex material behaves has to do with how HAp is absorbed into the polymer matrix. Mineral precipitation in the polymer solution is one way to overcome these obstacles (Kim et al., 2015; López-Noriega et al., 2015; Selvakumar et al., 2015).

The HAp constituent increases the compressive strength and the elastic modulus of the composite scaffolds (Mou et al., 2011; Yang et al., 2022; Tang et al., 2023; Said et al., 2023). According to Mou et al. (2011), a higher HAp content enabled composite scaffolds to become more differentiated and mineralized. In research by Li et al. (2023); 10 wt% of HAp and carbonate-exchanged HAp units were combined into a polymer hydrogel, which showed a significantly better biological action of human osteoblast-like cells on the composite than other hydrogels. By combining HAp nanoparticles with the polymer matrix to cproduce an in situ crystallization of HAp (Hollister, 2005; Mou et al., 2011; Li et al., 2023; Wei et al., 2022; Wu et al., 2023; Juhasz et al., 2010; Sultana et al., 2015), by synthesizing HAp inside the polymer matrix (Ielo et al., 2022; Przekora et al., 2016), or even by 3D printing (Younesi et al., 2013; Liao et al., 2016; Chen et al., 2016; Martínez-Vázquez et al., 2015; Verma and Quadros, 2024; Gisbert-Garzarán et al., 2023; Sagare et al., 2023), it is possible to produce nano-hybrid bone tissue scaffolds.

It has been established that porous assembly affords an acceptable gap which encourages bone ingrowth. Macropores expedite osteoid creation and mineralization by snowballing the osteoblasts and osteoprogenitors' passage keen on the scaffold, while interrelated micropores can improve vascularization and nutrient circulation in bone restoration (Jakus and Shah, 2017; Trachtenberg et al., 2017; Senatov et al., 2016; Liu et al., 2016). Bone restoration needs a basis of mesenchyme stem cells that can segregate keen on bone-creating osteoblasts (Jamari et al., 2023; Sinkler et al., 2023; Jakus et al., 2016).

Healing of significant bone abnormalities is still quite difficult. Novel approaches motivated by bone healing mechanisms found in nature are needed to develop novel materials for bone replacement and regeneration (Ishack et al., 2017; Mehnath and Jeyaraj, 2021; Ribas et al., 2019; Winkler et al., 2018; Behzadi et al., 2017; Li et al., 2023; Schulze et al., 2023). In addition to being biocompatible, bone fillers and scaffolds should assist osteoinductive bone repair. Additionally, they should serve as a vehicle for the transfer of various growth factors, as well as anti-inflammatory and antibacterial medications, preventing their rejection after application (Fig. 31) (Wang et al., 2023). Composite bone-like scaffolds made of biodegradable polymers and nanosized HAp are intriguing substitutes for bone and bone regeneration materials (Stahl and Yang, 2021; Verrier et al., 2016).

Huge bone faults therapeutic remains a great task. Production of novel HAp from a blend of bovine and catfish bones for bone replacement and restoration needs fresh approaches motivated by devices of the bone restorative present in the environment. Bone fillers and scaffoldings should be biocompatible and afford osteoinductive sustenance for bone restoration. Composite bone-like scaffoldings containing a nanosized HAp with green polymers are favourable materials for bone replacement and restoration. In their book Chapter, Han et al. (2004) explored the connection between HAp and its biological influence on bone restoration. They also described the effective role of HAp for the repair of impaired bone or restoration of lost bone via *in vitro* and *in vivo* studies. In a study by Han et al. (2009), Snail shells were utilized to fabricate HAp using an improved chemical precipitation process. The HAp was then coated on an interrelated scaffold by the dip-coating method. The result revealed that the produced natural HAp has constituents which are vital for biomedical use. The reinforced HAp greatly increased the mechanical properties and porosity of the scaffolds. The SEM picture illustrated the homogenous distribution of HAp over the scaffold surface.

4.1.2. *Implant*

Due to their excellent mechanical qualities, durability, low density, and chemical stability in human fluids, titanium and its alloys are used to make the majority of implants. Metallic implants offer strong mechanical strength and hardness, but they have poor biocompatibility and osseointegration. Because of its excellent biocompatibility, chemical stability, and osteoconductivity, hydroxyapatite is being thoroughly studied as a covering for metal implants to improve their qualities (Szcześ et al., 2017; Montemurro et al., 2023; Patel and Wairkar, 2023).

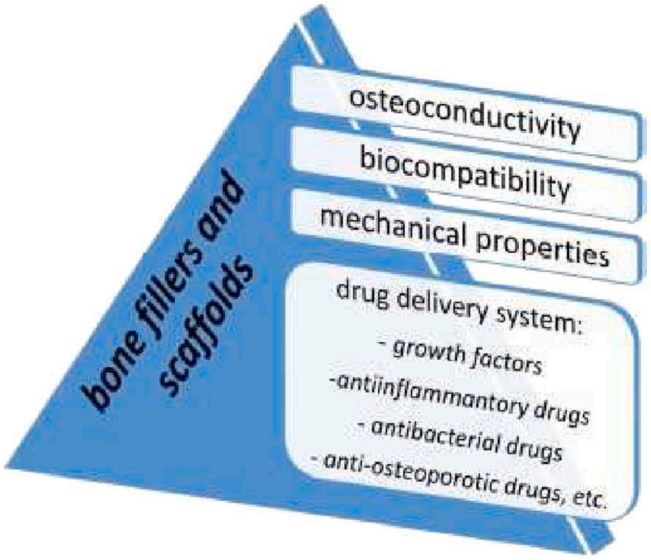

Fig. 31. Characteristics of bone fillers for biomedical uses (Wang et al., 2023).

It was established that this kind of coating aids the osseointegration of grafts with immediate tissues (Szcześ et al., 2017). HAp coatings on the implantation surface can be manufactured by sol–gel deposition (Yuan et al., 2016; Shobana and Swamiappan, 2023; Hussain et al., 2023; He et al., 2014; Singh et al., 2015; Dragomir et al., 2023; Sidane et al., 2015; Sidane et al., 2015) and many other methods. The advantage of biocompatible coatings can powerfully be influenced by the production methods employed (Sidane et al., 2017; Jafari et al., 2016; Jonauske et al., 2016; Wang et al., 2017) and their factors as extensively described by Bița et al. (2022).

Furthermore, the mechanical properties of the graft coatings rely on some considerations such as their density, phase, and chemical structure, as well as crystallinity (Maadani and Salahinejad, 2022; Bairagi and Mandal, 2022; Narayanan et al., 2008). Therefore, excellent HAp coatings on the metal graft surface normally have to exhibit high degree of crystallinity, correct Ca/P ratio, ideal porosity, and excellent bond to the substrate (Snyders et al., 2008; Motelica-Heino et al., 2023; Wu, 2021; Udomluck et al., 2020; Xie et al., 2014; Gherasim et al., 2021). As a thin film processing technology, the sol–gel method enables the production of chemically homogenous films with a fine-grain configuration of the final product. The sol–gel method is comparable to other thin film techniques such that it is straightforward and inexpensive due to the low treatment temperature (Dragomir et al., 2023).

To design a relatively low cost procedure that will enable implants with good coatings and good characteristics, future research on HAp coatings should focus on improving the coating deposition method (Fig. 32). The integration of biologically active components and boosting their therapeutic capacities (drug delivery and osteoinductive agents) is another issue with HAp coatings (Wang et al., 2023).

Mo et al. (2023) coated material in two different concentrations of bioactive SiCa rod-shaped particles produced by the Stöber procedure and dipped it in a chitosan matrix by electrophoretic deposition to increase the bioactivity of stainless steel grafts. Coatings that were thick and uniform were achieved. Additionally, the coating showed quick rates of breakdown, and after dipping for 10 days in SBF, it may be possible to detect the growth of carbonated Ca/P. The electrochemically aided deposition of HAp coatings on the titanium alloy (TiAlNb) was studied by Choudhary et al. (2023). The TiAlNb alloy was secured from corrosion in a harsh environment by the functional electrodeposited HAp layer, which also increased the whole corrosion resistance. The HAp-modified TiAlNb alloy's higher biocompatibility and bioactivity may boost implant strength in the human body, resulting in effective grafting and an extended graft lifespan. To improve bone deposition and osseointegration, titanium-based implant materials are frequently coated with HAp (Tierney et al., 2023; Katunar et al., 2023; Katić et al., 2023; Gao et al., 2018; Paital and Dahotre, 2009). High-strength implant materials like titanium alloys can develop HAp coatings to combine their osteoconductive characteristics with better mechanical properties of metals (Dorozhkin, 2015; Tang et al., 2018; Eliaz and Metoki, 2017).

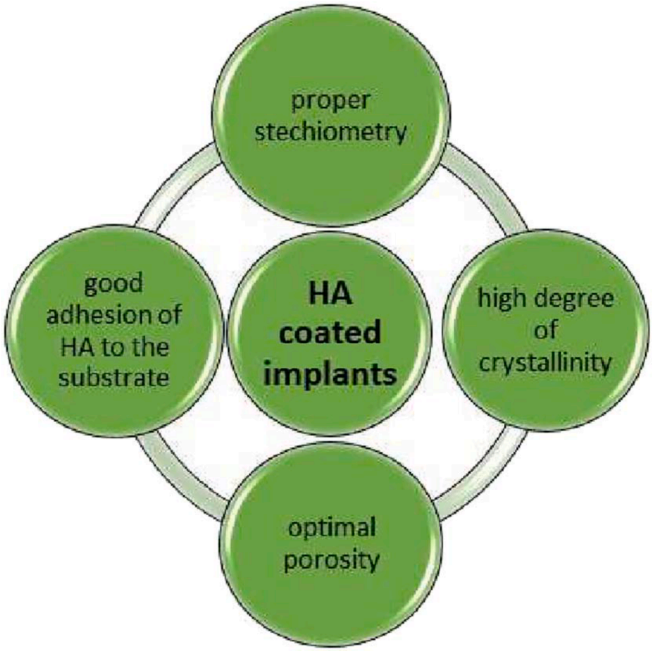

Fig. 32. Some Properties of hydroxyapatite (Wang et al., 2023).

Advance studies of HAp coatings should focus on the enhancements in the coating admission technique to improve a moderately low-cost procedure that will allow to develop grafts with a reliable analysis of acceptable properties. One more concern with regards to HAp coatings is the integration of organic dynamic elements for improving their healing abilities (osteoinductive proxies and delivery of drugs). Jindapon et al. (2023) arranged PCPP functionalized HNT and encapsulated it with AMO and MS. FTIR analysis confirmed the PCPP coating over the HNT by the formation of new peaks at 1640 and 1580 cm^{-1}. The higher stability of HNT nanocomposites was denoted by its zeta value – 45.24 mV. The maximum release of 58 % (AMO) and 62 % (MS) from the nanocomposites was achieved at the acidic pH. PCPP-coated MS-HNT nanocomposites form lumen sizes ranging from 15 to 20 nm with uniform surface morphology. In flow cytometry, biocompatible HNT nanocomposites exhibited lesser dead cells of about 0.56 %. HNT nanocomposites inhibit 96 % (*E.coli*) and 97 % (*S. aureus*) bacterial inhibition and the rate was highercompared to the AMO only. Similarly, with a decline of 78 % of Porphyromonas gingivalis biofilm biomass, the coating was strongly active against both pathogenic microbes and bacterial biofilm of *peri*-implant infection. The nanostructured coating of Ti–6Al–4 V screw has unlimited potential in dental implantology.

4.1.3. Drug delivery

It is of utmost importance to use nanoparticles with a large surface area, high loading capacity, and capacity for intracellular conveyance, as well as those that can be loaded with therapeutic molecules, as drug delivery systems or for imaging and diagnostics in biological approaches (Niinomi, 2008; Senopati et al., 2023; Maciąg et al., 2023; Singh et al., 2014). By combining biomaterials, metal ions, and medications with antibacterial qualities with pharmaceuticals or materials that have osteogenic effects, several synthetic scaffolds with dual functionalities have been produced (Jiang et al., 2023; dos Apostolos et al., 2023; Dubnika et al., 2017; Lu et al., 2016). Porous and nanocrystalline hydroxyapatite, because of its non-toxicity and biocompatibility, is of great importance as a drug delivery method and well-ordered drug release. As the acidic gastric environs can reduce HAp, it is primarily employed as an emaciated drug delivery structure in bone ailments moderately than oral healing methods. Porous HAp laden with the suitable drug permits its specific delivery to the injured part. HAp is mostly employed to deliver directly to hard tissues antibiotics (Lu et al., 2016; Skelly et al., 2014; Pacheco et al., 2014; Xie et al., 2014; Long et al., 2013) and also other drugs, such as anti-cancer substances (Galasso et al., 2023; Verma and Quadros, 2024; Kolanthai et al., 2016; Rong et al., 2016; Chen et al., 2023; Jirofti et al., 2023; Li et al., 2016; Zhang et al., 2023), anti-inflammatory drugs (Pourmadadi et al., 2023; Xiong et al., 2016; Shi et al., 2023; Öner et al., 2011; Shao et al., 2012; Li et al., 2012), anti-osteoporotic substances (Aghaei et al., 2014; Abdian et al., 2023; Sheykholeslami et al., 2023; Seshima et al., 2006; Wang et al., 2011) and others, like vitamins, hormones, proteins, growth factors (Long et al., 2013; Macha et al., 2017; Liu et al., 2016; Khajuria et al., 2016).

The residence and continuous release of drugs permit the reduction of persistent remedies and can hasten the bone healing process, as well as reduce the degree of operation of the injured bone. Hydroxyapatite applied in drug delivery schemes needs distinct morphology that permits great ability for drugs loading. The well configuration of HAp microspheres enables drug packing and their precise release. Several

techniques which include the described techniques, have been established to fabricate artificial HAp with accurate control of its shape (Swain and Sarkar, 2011). The biopolymer/hydroxyapatite composites showed a longer release period of the medication in comparison to the HAp nanoparticles, according to the *in vitro* drug-release analysis (He et al., 2015; Ilie et al., 2016; Akshata et al., 2023; Uskoković and Desai, 2014; Skwira et al., 2023). However, as was found in research (He et al., 2015), chitosan's addition regulated the small-molecule ideal drug's surge release but reduced its antibacterial effectiveness against *S. aureus*. According to Wei et al. (Skwira et al., 2023), the use of a mixture of hydroxyapatite microparticles and a multiple-layer coating made of chitosan and hyaluronic acid may lessen the early rush release of DOX from the porous HAp mix. This is due to the polymer's many-layer coating acting as a barrier to monitor medication exchange.

Fabricated Nanoparticles (FN) receptive to tumor microenvironment considerations such as pH were produced as drug delivery and for Magnetic Resonance Imaging (MRI) as gap agents. From the result, FN with sensitive pH receptiveness had great potency for tumor analysis and treatment interaction (Senopati et al., 2023). Maciąg et al. (2023) produced a pH-sensitive hybrid method dependent on silica and HAp with special attributes for drug delivery. The observations revealed the luminescent and magnetic attributes of the materials and presented appropriate properties for bid in the discharge of pH-profound drugs. A new transporter method for native drug carriage centred on functionalized silver doped HAp with estimated extensive span silver ion drop degrees. The results proposed that the newly produced composite scaffolds have antibacterial action for up to one year as well as regulated anaesthetic drug supply for up to two weeks (Singh et al., 2014).

Wassif et al. (2023) studied the regulated supply of Bortezomib in a new bifunctional scaffold constructed on nano-HAp and sodium alginate nanocomposite. By synchronically directing tumour inhibition and tissue regeneration for the healing of neoplastic bone deformities, this perfect bi-functional scaffold presents a potentially novel method for oncological therapy. To produce scaffolds that is similar to bones for drug delivery, Wei et al. (2015) introduced a unique drug-loaded extrudable feedstock without the requirement for any post-treatment phases. Ilie et al. (2016) designed an implanted drug (ciprofloxacin) delivery method in a scaffold arrangement with an exceptional set of structures for native management of osteomyelitis. The efficiency of HAp as a transporter was investigated by Aghaei et al. (2014) to implement a strategy for the native release of bisphosphonates (Bps), which is currently managed meticulously. The results suggested that Bps-HAp composites might be used as a localized medication delivery method in areas where bone restoration is occurring.

Because of its non-toxicity and biocompatibility, HAp is a favourable material as a pharmaceutical or biological agent delivery method, specifically in orthopaedics and dentistry for osteo tissue restoration. Despite the broad research in the arena of novel and active HAp production techniques, more research should be carried out to formulate drug delivery methods that allow accurate drug release in the aimed place. Besides, one more need is the research of several methods that enable the delivery of more than one antibiotic to support their combination result (Osuchukwu et al., 2023, 2022a, b, c, 2021; Obada et al., 2022; Osuchukwu et al., 2022d, 2023; Swain and Sarkar, 2011). This can be achieved by using different synthsis techniques to produce a novel low-cost HAp from a blend of bovine and catfish bones doped with strontium (Sr) (Sr-HAp). Mehnath and Jeyaraj (2023) produced hydrogel poised of bacterial polysaccharides, and hyaluronic acid, which links filled with hexapeptides, osteogenic stimulants, and trace elements in the form of HAp and FIB protein. The formation of hyaluronic acid −HAP and HA-HAP-Fibron is confirmed by the FTIR and RAMAN studies by a change in the carboxyl group (See Fig. 33). The hydrogel exhibited

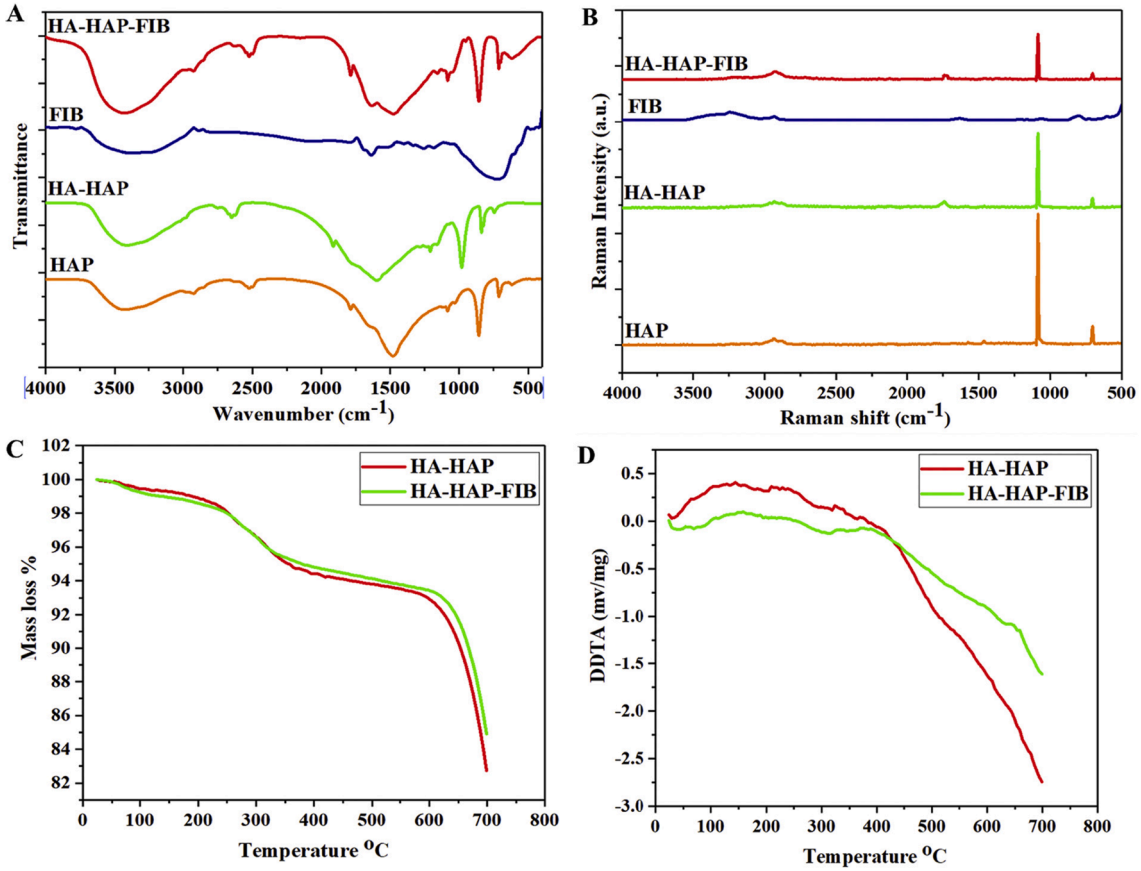

Fig. 33. (A) FTIR spectroscopy (B) Raman spectra (C) TGA pattern of hydrogel (D) DTA studies of HA-HAP and HA-HAP-FIB hydrogel (Mehnath and Jeyaraj, 2023).

Table 5
Properties Hydroxyapatite essential for therapeutic applications (Shafiq et al., 2023; Chen et al., 2023; Soares et al., 2023; Surmenev, 2012; Xu et al., 2005; Tomsia et al., 2011; Mouriño and Boccaccini, 2010; Surmenev et al., 2014).

Property	Definition/Function
Bioactivity	A substance's innate capacity to take part in particular biological processes or have an impact on living tissues
Biocompatibility	The capacity of a material to function in a certain application with a suitable host response
Bioactive fixation	Reactive surfaces chemically bind with bone, reducing the creation of the fibrous capsule.
Biostability	The capacity of a material to keep its qualities when in living tissue.
Crystallinity	A higher degree of crystallinity delays the bioceramic's rapid resorption (dissolution) in bodily fluids.
Interfacial stability and good adhesion	Avoid mechanical problems when a load is borne
Osseointegration	Direct anchoring of an implant through the creation of bone tissue around it without the development of fibrous tissue at the bone/implant interface
Osteoconduction	Being able to act as a scaffold for the growth of new bone
Osteoinduction	The method used to trigger osteogenesis. This phrase describes a process wherein pluripotent, primitive cells are encouraged to differentiate into the bone-forming cell lineage.
Resorption	Gradual breakdown over time to allow the host tissue to take the place of the biomaterial
Therapeutic capabilities	Templates for the time-specific in situ administration of medicines and growth factors
Wettability	The characteristic that reveals a substance's capacity to draw or repel water molecules

a porous structure due to the bending of the FIB β structure, and even delivery of HAp particles was established by SEM analysis.

Immediate cell rehabilitation facilitated by biomaterials has developed a prevailing approach. The application of biomaterials for stem-cell analysis of *in vivo* has the prospective to handle the problems associated with the effectiveness and protection of post- in vivo synthetic cells (Yusoff et al., 2021; Vijayakumar, 2020). According to Catros et al. (2010), the delivery efficacy in directed cells and the safety of the biomaterial are seen as major problems for immediate cell therapy.

5. Essentials of hydroxyapatite for therapeutic applications

HAp are frequently used in medical applications as cement, coatings, scaffolds, and paste; however, they may also be required to have several properties, some of which are listed in Table 5 (Shafiq et al., 2023; Chen et al., 2023; Soares et al., 2023; Surmenev, 2012; Xu et al., 2005; Tomsia et al., 2011; Mouriño and Boccaccini, 2010; Surmenev et al., 2014). The primary mechanism of bioactivity is the partial ionic product release and dissolution in vivo, which increases the local concentrations of calcium and phosphate ions and precipitates a biological apatite on the surface of the ceramics (Lu et al., 2023; Lu et al., 2023; Park et al., 2023; Ben-Nissan, 2014; Veiga et al., 2020). All implantable materials must be biocompatible, which means they can't cause a localized or generalized reaction in the body's tissues or biological systems. It has been determined that all Ca/P ceramics are biocompatible (Lu et al., 2023). This is a result of their profusion, in both dissolved and solid forms, within the body (Georgeanu et al., 2023; Liu et al., 2023; Sheng et al., 2023; Dorozhkin and Epple, 2002). For instance, it was discovered that HAp implantation did not cause any inflammation or a reaction to a foreign body (Ito et al., 2008).

The mechanical properties of Ca/Ps are a serious issue that prevents a larger clinical application (Jindapon et al., 2023). Average hip joint stresses can reach up to three times body weight (3000 N), while peak loads when jumping can reach up to ten times body weight. Depending on the nature of the activities—which can include standing, sitting, jogging, stretching, and climbing—these strains are recurrent and fluctuate. As a result, all prospective biomaterials and bioceramics must be resilient under a variety of circumstances (Han et al., 2004). Ca/Ps are brittle, have poor impact resistance, and only undergo relatively light tensile stresses (6–10 MPa) (Jindapon et al., 2023).

6. Conclusion

Injury therapeutic is an intricate biotic practice to repair the bone arrangement to its unique condition. The purpose of this paper is to review some of the synthesis methods employed to produce HAp from different sources for biomedical applications. HAp has been used in a broad collection of healing applications extending from common dental paddings, and bioactive coatings on grafts to purposefully premeditated drug delivery methods, and even for tissue engineering (TE) applications. The production method is essential in formulating the physico-chemical properties of HAp, which in turn affects its mechanical and biological role. The anticipated physiognomies of HAp can be accomplished using a suitable technique of production and sources. The sol–gel route is preferred over other routes due to its even molecular mixing, high creation purity, low production temperature, and ability to synthesize nanosized particles. The management of bulky quantities of bio-wastes, such as bovine bones and catfish bones from kitchenettes and abattoirs, has since been a challenge. But, by the use of a sol–gel method, it is promising to convert these bio-wastes in mixed proportion into economic materials. A simple consideration of the consequence of the addition of external material as a reinforcement proxy to the mechanical properties of HAp is the basic element for the improvement of a novel biomaterial. As a result, it is provisional that upon the cautious blend of key considerations such as sources, synthesis technique, and production parameters for the fabrication of natural HAp (NHAp), mechanical properties can be improved and the product can be employed as a drug delivery system.

Funding

This research did not receive any funding from any organization or individual by any of the authors.

CRediT authorship contribution statement

Precious Osayamen Etinosa: Writing – review & editing, Formal analysis, Conceptualization. **Obinna Anayo Osuchukwu:** Writing – review & editing, Writing – original draft, Visualization, Methodology, Conceptualization. **Emeka Obiora Anisiji:** Writing – review & editing, Visualization, Supervision. **Mohammed Y. Lawal:** Visualization, Validation. **Sikiru Adepoju Mohammed:** Writing – original draft, Methodology. **Ibitoye Opeyemi Isaac:** Visualization, Validation. **Peter Gbenga Oni:** Visualization, Supervision. **Victor D. Aderibigbe:** Writing – original draft, Validation. **Toyin Aina:** Visualization, Resources. **Damilola Oyebode:** Writing – review & editing, Validation. **Solomon C. Nwigbo:** Validation, Supervision.

Declaration of Competing Interest

The authors declare that they have no known competing financial interests or personal relationships that could have appeared to influence the work reported in this paper.

Acknowledgments

The authors acknowledge the Department of Mechanical Engineering, Worcester Polytechnic Institute, 100 Institute Road, Worcester, USA, Multifunctional Materials Laboratory, Shell Office in Mechanical Engineering, Ahmadu Bello University, Nigeria, the Department of Metallurgical and Materials Engineering, Ahmadu Bello University,

Zaria, and the Department of Mechanical Engineering, Bayero University, Nigeria, for providing facilities to carry out this study.

References

Abdelmoneim, D., Porter, G.C., Coates, D.E., Duncan, W.J., Waddell, J.N., Hammer, N., Li, K.C., 2022. Materials 15 (8), 2798.

Abdian, N., Etminanfar, M., Sheykholeslami, S.O.R., Hamishehkar, H., Khalil-Allafi, J., 2023. Mater. Chem. Phys. 301, 127672.

Abdullah, H.Z., Idris, M.I., Te Chuan, L., Dermawan, S.K., Jaffri, M.Z., 2023. Sustainable Material for Biomedical Engineering Application. Springer Nature Singapore, Singapore, pp. 107–124.

Abifarin, J.K., Obada, D.O., Dauda, E.T., Dodoo-Arhin, D., 2019. Data Brief 26, 104485.

Abukawa, H., Papadaki, M., Abulikemu, M., Leaf, J., Vacanti, J.P., Kaban, L.B., Troulis, M.J., 2006. Dent. Clin. 50, 205–216.

Adak, M.D., Purohit, K.M., 2011. Trends Biomater. Artif. Organs 25 (3), 101–107.

Afriani, F., Tiandho, Y., Evi, J., Indriawati, A., Rafsanjani, R.A., 2019, October. In: IOP Conference Series: Earth and Environmental Science, Vol. 353, No. 1. IOP Publishing, p. 012032.

Afshar, A., Ghorbani, M., Ehsani, N., Saeri, M.R., Sorrell, C.C., 2003. Mater. Des. 24 (3), 197–202.

Agalya, P., Kumar, G.S., Prabu, K.M., Cholan, S., Karunakaran, G., Hakami, J., Ramalingam, S., 2022. Ceram. Int. 48 (19), 28299–28307.

Aghaei, H., Nourbakhsh, A.A., Karbasi, S., JavadKalbasi, R., Rafienia, M., Nourbakhsh, N., Mackenzie, K.J., 2014. Ceram. Int. 40 (5), 7355–7362.

Ahamed, A.F., Manimohan, M., Kalaivasan, N., 2022. J. Inorg. Organomet. Polym Mater. 32 (10), 3902–3922.

Ahmed, H.Y., Safwat, N., Shehata, R., Althubaiti, E.H., Kareem, S., Atef, A., Sami, R., 2022. Membranes 12 (4), 408.

Akpan, E.S., Dauda, M., Kuburi, L.S., Obada, D.O., 2020. MRS Adv. 5, 1357–1366.

Akram, M., Ahmed, R., Shakir, I., Ibrahim, W.A.W., Hussain, R., 2014. J. Mater. Sci. 49, 1461–1475.

Akshata, C.R., Murugan, E., Harichandran, G., 2023. Int. J. Biol. Macromol. 252, 126478.

Alahnoori, A., Badrossamay, M., Foroozmehr, E., 2023. Mater. Chem. Phys. 296, 127316.

Alam, M.K., Hossain, M.S., Kawsar, M., Bahadur, N.M., Ahmed, S., 2024. RSC Adv. 14 (5), 3548–3559.

Aldousari, S.M., Fouda, N., Hedia, H.S., AlThobiani, F.W., 2018. Mater. Test. 60, 142–148.

Alif, M.F., Aprillia, W., Arief, S., 2018. Mater. Lett. 230, 40–43.

Amaechi, B.T., AbdulAzees, P.A., Alshareif, D.O., Shehata, M.A., Lima, P.P.D.C.S., Abdollahi, A., Evans, V., 2019. BDJ open 5 (1), 18.

Anandan, D., Jaiswal, A.K., 2023. J. Aust. Ceram. Soc. 1–17.

Anbalagan Balamurugan, J.M., Faure, J., HichamBenhayoune, L., Sockallingum, G., Banchet, V., Bouthors, S., Balossier, G., 2006. Ceramics-Silikaty 50 (1), 27–31.

Anitta, S., Sekar, C., 2023. Results Chem. 5, 100816.

Anwar, A., Kanwal, Q., Sadiqa, A., Razaq, T., Khan, I.H., Javaid, A., Ouladsmane, M., 2023. Int. J. Mol. Sci. 24 (19), 14527.

Apostu, D., Lucaciu, O., Berce, C., Lucaciu, D., Cosma, D., 2018. J. Int. Med. Res. 46, 2104–2119.

Arjama, M., Mehnath, S., Rajan, M., Jeyaraj, M., 2021. React. Funct. Polym. 160, 104841.

Arul, K.T., Ramya, J.R., 2017. Int. J. Eng. Sci. Res. Technol 6 (8), 15–18.

Aslani, A., Pourmadadi, M., Abdouss, M., Rahdar, A., Díez-Pascual, A.M., 2024. Sustain. Chem. Pharm. 38, 101497.

Assis, C.M.D., Vercik, L.C.D.O., Santos, M.L.D., Fook, M.V.L., Guastaldi, A.C., 2005. Mater. Res. 8, 207–211.

Ataollahi, S., 2023. Bioprinting, e00304.

Atemni, I., Ouafi, R., Hjouji, K., Mehdaoui, I., Ainane, A., Ainane, T., Rais, Z., 2023. Emerg. Mater. 6 (2), 551–560.

Awasthi, S., Pandey, S.K., Arunan, E., Srivastava, C., 2021. J. Mater. Chem. B 9, 228–249.

Azaryan, E., Mortazavi-Derazkola, S., Alemzadeh, E., Emadian Razavi, F., Yousefi, M., Hanafi-Bojd, M.Y., Naseri, M., 2023. Odontology 111 (2), 461–473.

Azis, Y., Jamarun, N., Arief, S., Nur, H., 2015. Orient. J. Chem. 31 (2), 1–7.

Azzallou, R., Ouerghi, O., Geesi, M.H., Riadi, Y., Taleb, M.A., Mamouni, R., Villain, S., 2022. J. Phys. Chem. Solid 163, 110533.

Bairagi, D., Mandal, S., 2022. J. Magnesium Alloys 10 (3), 627–669.

Baladi, M., Amiri, M., Mohammadi, P., Mahdi, K.S., Golshani, Z., Razavi, R., Salavati-Niasari, M., 2023. Arab. J. Chem. 16 (4), 104646.

Bambaeero, A., Bazargan-Lari, R., 2021. Chin. J. Chem. Eng. 33, 221–230.

Barakat, N.A., Khil, M.S., Omran, A.M., Sheikh, F.A., Kim, H.Y., 2009. J. Mater. Process. Technol. 209 (7), 3408–3415.

Barua, E., Deb, P., Das Lala, S., Deoghare, A.B., 2019. Biomaterials in Orthopaedics and Bone Regeneration: Design and Synthesis, pp. 147–158.

Behzadi, S., Luther, G.A., Harris, M.B., Farokhzad, O.C., Mahmoudi, M., 2017. Biomaterials 146, 168–182.

Ben-Nissan, B. (Ed.), 2014. Advances in Calcium Phosphate Biomaterials.

Bezzi, G., Celotti, G., Landi, E., La Torretta, T.M.G., Sopyan, I., Tampieri, A., 2003. Mater. Chem. Phys. 78 (3), 816–824.

Bhattacharjee, P., Begam, H., Chanda, A., Nandi, S.K., 2014. Animal trial on zinc doped hydroxyapatite: a case study. J. Asian Ceram. Soc. 2 (1), 44–51.

Bigi, A., Boanini, E., Rubini, K., 2004. J. Solid State Chem. 177 (9), 3092–3098.

Biţa, A.I., Antoniac, I., Miculescu, M., Stan, G.E., Leonat, L., Antoniac, A., Forna, N., 2022. Materials 15 (9), 3100.

Bordbar-Khiabani, A., Kovrlija, I., Locs, J., Loca, D., Gasik, M., 2023. Int. J. Mol. Sci. 24 (17), 13135.

Bossù, M., Saccucci, M., Salucci, A., Di Giorgio, G., Bruni, E., Uccelletti, D., Polimeni, A., 2019. J. Nanobiotechnol. 17, 1–13.

Bramhe, S., Kim, T.N., Balakrishnan, A., Chu, M.C., 2014. Mater. Lett. 135, 195–198.

Brzezińska-Miecznik, J., Haberko, K., Sitarz, M., Bućko, M.M., Macherzyńska, B., 2015. Ceram. Int. 41 (3), 4841–4846.

Burdusel, A.C., Neacsu, I.A., Birca, A.C., Chircov, C., Grumezescu, A.M., Holban, A.M., Andronescu, E., 2023. J. Funct. Biomater. 14 (7), 378.

Cai, Y., Zhang, S., Ong, S., Zeng, X., Wang, W., 2013. Hydroxyapatite Coatings for Biomedical Applications, pp. 55–144.

Cao, L.Y., Zhang, C.B., Huang, J.F., 2005. Ceram. Int. 31 (8), 1041–1044.

Cao, Q., Zhang, J., Zhang, H., Xu, J., Che, R., 2022. J. Adv. Ceram. 11 (3), 504–514.

Catros, S., Guillemot, F., Lebraud, E., Chanseau, C., Perez, S., Bareille, R., Fricain, J.C., 2010. Irbm 31 (4), 226–233.

Chahal, H.K., Matthews, S., Jones, M.I., 2023. J. Therm. Spray Technol. 1–17.

Chai, C.S., Ben-Nissan, B., 1999. J. Mater. Sci.: Mater. Med. 10, 465–469.

Chen, H., Clarkson, B.H., Sun, K., Mansfield, J.F., 2005. J. Colloid Interface Sci. 288 (1), 97–103.

Chen, L., Hu, J., Ran, J., Shen, X., Tong, H., 2016. Polym. Compos. 37 (1), 81–90.

Chen, J., Nan, K., Yin, S., Wang, Y., Wu, T., Zhang, Q., 2010. Colloids Surf. B: Biointerfaces 81 (2), 640–647.

Chen, J., Wen, J., Fu, Y., Li, X., Huang, J., Guan, X., Zhou, Y., 2023. J. Nanobiotechnol. 21 (1), 174.

Chen, J., Wen, J., Fu, Y., Li, X., Huang, J., Guan, X., Zhou, Y., 2023. J. Nanobiotechnol. 21 (1), 174.

Cheng, M., Hu, L., Pan, P., Liu, Q., Zhang, Z., Wang, C., Chen, J., 2023. Colloids Surf. B: Biointerfaces, 113561.

Choudhary, N., Ghosh, C., Sharma, V., Roy, P., Kumar, P., 2023. Rapid Prototyp. J. 29 (5), 1061–1079.

Cihlar, J., Castkova, K., 2002. Springer Vienna.

Citradewi, P.W., Hidayat, H., Purwiandono, G., Fatimah, I., Sagadevan, S., 2021. Chem. Phys. Lett. 769, 138412.

Condino, S., Turini, G., Parchi, P.D., Viglialoro, R.M., Piolanti, N., Gesi, M., Ferrari, V., 2018. J. Healthc. Eng. 2018.

Cuylear, D.L., Elghazali, N.A., Kapila, S.D., Desai, T.A., 2023. Mol. Pharm. 20 (2), 810–828.

Dang, G.P., Wei, Y., Wan, Q.Q., Gu, J.T., Wang, K.Y., Wan, M.C., Niu, L.N., 2024. BMEMat, e12069.

de Andrade, R., Paim, T.C., Bertaco, I., Naasani, L.S., Buchner, S., Kovářík, T., Wink, M. R., 2023. Appl. Mater. Today 33, 101875.

De Groot, K., 1980. Biomaterials 1 (1), 47–50.

de Oliveira, I.R., dos Santos Gonçalves, I., Wallace dos Santos, K., Lança, M.C., Vieira, T., Carvalho Silva, J., Miranda Ribeiro Borges, J.P., 2023. ACS Mater. Au. 5, 5–55.

Demir-Oğuz, Ö., Boccaccini, A.R., Loca, D., 2023. Bioact. Mater. 19, 217–236.

DileepKumar, V.G., Sridhar, M.S., Aramwit, P., Krut'ko, V.K., Musskaya, O.N., Glazov, I. E., Reddy, N., 2022. J. Biomater. Sci. Polym. Ed. 33 (2), 229–261.

DileepKumar, V.G., Sridhar, M.S., Aramwit, P., Krut'ko, V.K., Musskaya, O.N., Glazov, I. E., Reddy, N., 2022. J. Biomater. Sci. Polym. Ed. 33 (2), 229–261.

Dillon, S., Staines, K.A., Millán, J.L., Farquharson, C., 2019. JBMR plus 3 (7), e10202.

Dorcioman, G., Grumezescu, V., Stan, G.E., Chifiriuc, M.C., Gradisteanu, G.P., Miculescu, F., Duta, L., 2023. Pharmaceutics 15 (4), 1294.

Dorozhkin, S.V., 2015. Mater. Sci. Eng. C 55, 272–326.

Dorozhkin, S.V., Epple, M., 2002. Angew. Chem. Int. Ed. 41 (17), 3130–3146.

dos Apostolos, R.C.R., Andrada, A.D.S., Oliveira, A.F., Neto, E.S.F., de Sousa, E.M.B., 2023. Polymers 15 (12), 2681.

Dragomir, L., Antoniac, A., Manescu, V., Robu, A., Dinu, M., Pana, I., Vladescu, A., 2023. Ceram. Int.

Du, X., Chu, Y., Xing, S., Dong, L., 2009. J. Mater. Sci. 44, 6273–6279.

Dubnika, A., Loca, D., Rudovica, V., Parekh, M.B., Berzina-Cimdina, L., 2017. Ceram. Int. 43 (4), 3698–3705.

Duminis, T., Shahid, S., 2021. Int. J. Dent. Mater. 3 (3), 76–83.

Durucan, C.A.N.E.R., Brown, P.W., 2000. J. Mater. Sci. - Mater. Med. 11 (6), 365–371.

Edralin, E.J.M., Garcia, J.L., dela Rosa, F.M., Punzalan, E.R., 2017. Mater. Lett. 196, 33–36.

Eliaz, N., Metoki, N., 2017. Materials 10 (4), 334.

Eshtiagh-Hosseini, H., Housaindokht, M.R., Chahkandi, M., 2007. Mater. Chem. Phys. 106 (2–3), 310–316.

Ethirajan, A., Ziener, U., Chuvilin, A., Kaiser, U., Cölfen, H., Landfester, K., 2008. Adv. Funct. Mater. 18 (15), 2221–2227.

Farkas, N.I., Turdean, G.L., Bizo, L., Marincaş, L., Cadar, O., Barbu-Tudoran, L., Réka, B., 2023. Ceram. Int.

Farokhi, M., Mottaghitalab, F., Samani, S., Shokrgozar, M.A., Kundu, S.C., Reis, R.L., Kaplan, D.L., 2018. Biotechnol. Adv. 36 (1), 68–91.

Fatimah, I., Audita, R., Purwiandono, G., Hidayat, H., Sagadevan, S., Oh, W.C., Doong, R. A., 2024. Case Stud. Chem. Environ. Eng., 100797

Fedotov, A.Y., Komlev, V.S., 2022. Inorg. Mater. Appl. Res. 13 (4), 985–1004.

Fendi, F., Abdullah, B., Suryani, S., Raya, I., Usman, A.N., Tahir, D., 2023, May. In: AIP Conference Proceedings, Vol. 2719, No. 1. AIP Publishing.

Feng, G., Zheng, E., Jiang, F., Hu, Z., Fu, H., Li, Y., Jiang, W., 2023. Ceram. Int. 49 (18), 30603–30612.

Figueiredo, M., Fernando, A., Martins, G., Freitas, J., Judas, F., Figueiredo, H., 2010. Ceram. Int. 36 (8), 2383–2393.

Fomin, A.S., Barinov, S.M., Ievlev, V.M., Smirnov, V.V., Mikhailov, B.P., Kutsev, S.V., Drozdova, N.A., 2009. Inorg. Mater. 45, 1193–1196.

Fulmer, M.T., Brown, P.W., 1998. J. Mater. Sci. - Mater. Med. 9 (4), 197–202.

Galasso, C., Ruocco, N., Mutalipassi, M., Barra, L., Costa, V., Giommi, C., Pennesi, C., 2023. Int. J. Biol. Macromol., 127145

Gao, A., Hang, R., Bai, L., Tang, B., Chu, P.K., 2018. Electrochim. Acta 271, 699–718.
Gedanken, A., 2004. Ultrason. Sonochem. 11 (2), 47–55.
Georgeanu, V.A., Gingu, O., Antoniac, I.V., Manolea, H.O., 2023. Appl. Sci. 13 (14), 8471.
Gherasim, O., Grumezescu, A.M., Grumezescu, V., Negut, I., Dumitrescu, M.F., Stan, M. S., Andronescu, E., 2021. Antibiotics 10 (2), 160.
Giardina, M.A., Fanovich, M.A., 2010. Ceram. Int. 36 (6), 1961–1969.
Gibson, I.R., Bonfield, W., 2002. J. Biomed. Mater. Res.: Off. J. Soc. Biomater. Jpn. Soc. Biomater. Aust. Soc. Biomater. Kor. Soc. Biomater. 59 (4), 697–708.
Gisbert-Garzarán, M., Gómez-Cerezo, M.N., Vallet-Regí, M., 2023. Int. J. Mol. Sci. 24 (3), 2007.
Gómez-Morales, J., Torrent-Burgues, J., Boix, T., Fraile, J., Rodríguez-Clemente, R., 2001. Cryst. Res. Technol.: J. Exp. Ind. Crystallogr. 36 (1), 15–26.
Goto, T., Sasaki, K., 2014. Ceram. Int. 40, 10777–10785.
Graham, S., Brown, P.W., 1996. J. Cryst. Growth 165 (1–2), 106–115.
Guerra Bretaña, R.M., Guerra-López, J.R., de Sena, L.A., 2017. In: VII Latin American Congress on Biomedical Engineering CLAIB 2016, Bucaramanga, Santander, Colombia, October 26th–28th, 2016. Springer Singapore, pp. 78–81.
Guillet, C., Birgersson, U., Engstrand, T., Åberg, J., Lopes, V.R., Thor, A., Forterre, F., 2023. Biomed. Mater. 18 (3), 035007.
Guo, X., Xiao, P., Liu, J., Shen, Z., 2005. J. Am. Ceram. Soc. 88 (4), 1026–1029.
Gusti, A.W.R., Mahyudin, F., Widiyanti, P., Utomo, D.N., 2023. J. Aust. Ceram. Soc. 1–11.
Hahn, B.D., Park, D.S., Choi, J.J., Ryu, J., Yoon, W.H., Choi, J.H., Jung, I.K., 2013. Appl. Surf. Sci. 283, 6–11.
Han, Y., Li, S., Wang, X., Chen, X., 2004. Mater. Res. Bull. 39 (1), 25–32.
Han, K.S., Sathiyaseelan, A., Saravanakumar, K., Wang, M.H., 2022. J. Environ. Chem. Eng. 10 (1), 106888.
Han, Y., Wang, X., Li, S., Ma, X., 2009. J. Sol-Gel Sci. Technol. 49, 125–129.
Han, Y., Wang, X., Li, S., 2009. J. Nanopart. Res. 11, 1235–1240.
Hao, M., Wang, W., Kumar, A., Kamaruddin, W.H.A., Saidin, S., Malek, N.A.N.N., Liu, H., 2024. BMEMat 2 (1), e12059.
Hariani, P.L., Muryati, M., Said, M., Salni, S., 2020. Key Engineering Materials Vol. 840, 293–299.
Hasan, M.R., Abdullah, C.A.C., Afizah, M.N., Ghazali, M.S.M., Noranizan, M.A., 2024. Food Bioprod. Process. 143, 54–65.
Hashemi, S.S., Mondal, D., Montesano, J., Willett, T.L., 2023. Mater. Des. 225, 111587.
Hassan, T.A., Rangari, V.K., Jeelani, S., 2014. Int. J. Nano Biomater. 5 (2–3), 103–112.
Hassanzadeh-Tabrizi, S.A., Norbakhsh, H., Pournajaf, R., Tayebi, M., 2021. Ceram. Int. 47 (13), 18167–18176.
Hatim, A., Abida, F., Elouahli, A., Abourriche, A., Benhammou, A., El Hafiane, Y., Abouliatim, Y., 2023. J. Aust. Ceram. Soc. 1–10.
He, G., Guo, B., Wang, H., Liang, C., Ye, L., Lin, Y., Cai, X., 2014. Cell Prolif. 47 (3), 258–266.
He, Q., Pan, L., Wang, Y., Meldrum, F.C., 2015. Cryst. Growth Des. 15 (2), 723–731.
Heidari, F., Tabatabaei, F.S., Razavi, M., Lari, R.B., Tavangar, M., Romanos, G.E., Tayebi, L., 2020. J. Mater. Sci. - Mater. Med. 31, 1–14.
Hench, L., 1998. Bioceramics. J. Am. Ceram. Soc. 81, 1705–11172.
Herawaty, L., 2014. Synthesis of Hydroxyapatite Nanoparticle from Tutut (Bellamyâ Javanica) Shells by Using Precipitation and Hydrothermal Method.
Herliansyah, M.K., Nasution, D.A., Bin Abdul Shukor, M.H., Ide-Ektessabi, A., Wildan, M. W., Tontowi, A.E., 2007, October. In: Materials Science Forum, Vol. 561. Trans Tech Publications Ltd., pp. 1441–1444.
Hohmann, E., 2023. Arthroscopy 39 (7), 1758–1760.
Hollister, S.J., 2005. Nat. Mater. 4 (7), 518–524.
Horta, M.K.D.S., Westin, C., Rocha, D.N.D., Campos, J.B.D., Souza, R.F.M.D., Aguilar, M. S., Moura, F.J., 2023. Mater. Res. 26, e20220466.
Hosseinzadeh, E., Davarpanah, M., Nemati, N.H., Tavakoli, S.A., 2014. Int. J. Organ Transpl. Med. 5 (1), 23.
Hsieh, M.F., Perng, L.H., Chin, T.S., Perng, H.G., 2001. Biomaterials 22 (19), 2601–2607.
Hsu, H.C., Wu, S.C., Lin, C.Y., Ho, W.F., 2023. Coatings 13 (2), 228.
Huang, Y.C., Hsiao, P.C., Chai, H.J., 2011. Ceram. Int. 37 (6), 1825–1831.
Huang, Y.T., Imura, M., Nemoto, Y., Cheng, C.H., Yamauchi, Y., 2011. Sci. Technol. Adv. Mater. 12 (4), 045005.
Hussain, S., Sabiruddin, K., 2023. J. Aust. Ceram. Soc. 1–16.
Hussain, S., Shah, Z.A., Sabiruddin, K., Keshri, A.K., 2023. J. Mech. Behav. Biomed. Mater. 137, 105550.
Hussin, M.S.F., Abdullah, H.Z., Idris, M.I., Wahap, M.A.A., 2022. Heliyon 8 (8), e10356.
Iafisco, M., Delgado-López, J.M., Gómez-Morales, J., Hernández-Hernández, M.A., Rodríguez-Ruiz, I., Roveri, N., 2011. Cryst. Res. Technol. 46 (8), 841–846.
Ielo, I., Calabrese, G., De Luca, G., Conoci, S., 2022. Int. J. Mol. Sci. 23 (17), 9721.
Ilie, A., Ghiţulică, C., Andronescu, E., Cucuruz, A., Ficai, A., 2016. Int. J. Pharm. 510 (2), 501–507.
Ioku, K., Yamauchi, S., Fujimori, H., Goto, S., Yoshimura, M., 2002. Solid State Ion. 151 (1–4), 147–150.
Irfan, M., Suprajaa, P.S., Praveen, R., Reddy, B.M., 2021. Mater. Lett. 282, 128685.
Ishack, S., Mediero, A., Wilder, T., Ricci, J.L., Cronstein, B.N., 2017. J. Biomed. Mater. Res. B Appl. Biomater. 105 (2), 366–375.
Ishikawa, K., Miyamoto, Y., Yuasa, T., Ito, A., Nagayama, M., Suzuki, K., 2002. Biomaterials 23 (2), 423–428.
Ito, H., Oaki, Y., Imai, H., 2008. Cryst. Growth Des. 8 (3), 1055–1059.
Ito, A., Otsuka, M., Kawamura, H., Ikeuchi, M., Ohgushi, H., Sogo, Y., Ichinose, N., 2005. Curr. Appl. Phys. 5 (5), 402–406.
Jafari, H., Hessam, H., Shahri, S.M.G., Assadian, M., Shairazifard, S.H.P., Idris, M.H., 2016. J. Mater. Eng. Perform. 25, 901–909.
Jaganathan, G., Sithique, M.A., 2023. Inorg. Chem. Commun. 147, 110248.
Jahangir, M.U., Islam, F., Jahan, R.A., Matin, M.A., Arafat, M.T., 2019, July. In: AIP Conference Proceedings, Vol. 2121, No. 1. AIP Publishing LLC, p. 140012.
Jakus, A.E., Rutz, A.L., Shah, R.N., 2016. Biomed. Mater. 11 (1), 014102.
Jakus, A.E., Shah, R.N., 2017. J. Biomed. Mater. Res. A 105 (1), 274–283.
Jamari, J., Fitriyana, D.F., Ramadhan, P.S., Nugroho, S., Ismail, R., Bayuseno, A.P., 2023. Mater. Manuf. Process. 38 (9), 1093–1103.
Jarudilokkul, S., Tanthapanichakoon, W., Boonamnuayvittaya, V., 2007. Colloids Surf. A: Physicochem. Eng. Asp. 296 (1–3), 149–153.
Javaid, M.A., Kaartinen, M.T., 2013. Int. Dent. J. Students Res. 1, 24–35.
Jevtic, M., Mitric, M., Skapin, S., Jancar, B., Ignjatovic, N., Uskokovic, D., 2008. Cryst. Growth Des. 8 (7), 2217–2222.
Jia, X., Zhou, J., Ning, J., Li, M., Yao, Y., Wang, X., Zhao, K., 2022. Regener. Biomater. 9, rbac035.
Jiang, W., Wang, Q., Cui, D., Han, L., Chen, L., Xu, J., Niu, N., 2023. Colloids Surf. B: Biointerfaces 222, 113076.
Jillavenkatesa, A., Hoelzer, D.T., Condrate, R.A., 1999. J. Mater. Sci. 34, 4821–4830.
Jindapon, N., Klinmalai, P., Surayot, U., Tanadchangsaeng, N., Pichaiaukrit, W., Phimolsiripol, Y., Wangtueai, S., 2023. Int. J. Mol. Sci. 24 (3), 2776.
Jirofti, N., Ebrahimzadeh, M.H., Moradi, A., 2023. J. Sol-Gel Sci. Technol. 1–13.
Jirofti, N., Ebrahimzadeh, M.H., Moradi, A., 2023. J. Sol-Gel Sci. Technol. 1–13.
Jirofti, N., Hashemi, M., Moradi, A., Kalalinia, F., 2023. Int. J. Biol. Macromol. 252, 126279.
Jonauske, V., Prichodko, A., Skaudžius, R., Kareiva, A., 2016. Chemija 27 (4), 192–201.
Juhasz, J.A., Best, S.M., Bonfield, W., 2010. Sci. Technol. Adv. Mater. 11 (1), 014103.
Kamalanathan, P., Ramesh, S., Bang, L.T., Niakan, A., Tan, C.Y., Purbolaksono, J., Teng, W.D., 2014. Ceram. Int. 40 (10), 16349–16359.
Kandori, K., Takeguchi, K., Fukusumi, M., Morisada, Y., 2009. Polyhedron 28 (14), 3036–3042.
Karalkeviciene, R., Raudonyte-Svirbutaviciene, E., Zarkov, A., Yang, J.C., Popov, A.I., Kareiva, A., 2023. Crystals 13 (2), 265.
Katić, J., Krivačić, S., Petrović, Ž., Mikić, D., Marciuš, M., 2023. Coatings 13 (3), 640.
Katunar, M.R., Diaz, F., Boccaccini, A.R., Ballarre, J., 2023. Ceram. Int.
Khajuria, D.K., Disha, C., Vasireddi, R., Razdan, R., Mahapatra, D.R., 2016. Mater. Sci. Eng. C 63, 78–87.
Khoshnazar, S.M., Asadi, A., Roshancheshm, S., Karimian, A., Abdolmaleki, A., 2023. Cell Tissue Biol. 17 (5), 454–464.
Kim, H., Camata, R.P., Vohra, Y.K., Lacefield, W.R., 2005. J. Mater. Sci. - Mater. Med. 16, 961–966.
Kim, H.L., Jung, G.Y., Yoon, J.H., Han, J.S., Park, Y.J., Kim, D.G., Kim, D.J., 2015. Mater. Sci. Eng. C 54, 20–25.
Kim, W., Saito, F., 2001. Ultrason. Sonochem. 8 (2), 85–88.
Kimura, I., 2007. Adv. Mater. Sci. Eng. 2007.
King'Ori, A.M., 2011. Int. J. Poult. Sci. 10 (11), 908–912.
Kolanthai, E., Ganesan, K., Epple, M., Kalkura, S.N., 2016. Mater. Today Commun. 8, 31–40.
Kolekar, T.V., Bandgar, S.S., Yadav, H.M., Kim, D.Y., Magalad, V.T., 2022. Inorg. Chem. Commun. 137, 109172.
Kolmas, J., Krukowski, S., Laskus, A., Jurkitewicz, M., 2016. Ceram. Int. 42 (2), 2472–2487.
Kong, L.B., Ma, J., Boey, F., 2002. J. Mater. Sci. 37, 1131–1134.
Kongsri, S., Janpradit, K., Buapa, K., Techawongstien, S., Chanthai, S., 2013. Chem. Eng. J. 215, 522–532.
Koumoulidis, G.C., Vaimakis, T.C., Sdoukos, A.T., Boukos, N.K., Trapalis, C.C., 2001. J. Am. Ceram. Soc. 84 (6), 1203–1208.
Koutsopoulos, S., 2002. J. Biomed. Mater. Res.: Off. J. Soc. Biomater. Jpn. Soc. Biomater. Aust. Soc. Biomater. Kor. Soc. Biomater. 62 (4), 600–612.
Kris-Etherton, P.M., Harris, W.S., Appel, L.J., 2002. Circulation 106 (21), 2747–2757.
Krishnamra, N., Tang, I.M., 2016. Mater. Sci. Eng. C 62, 183–189.
Kumar, A.R., Kalainathan, S., 2010. Phys. B Condens. Matter 405 (13), 2799–2802.
Kumar, G.S., Sathish, L., Govindan, R., Girija, E.K., 2015. RSC Adv. 5 (49), 39544–39548.
Kumar, G.S., Karunakaran, G., Girija, E.K., Kolesnikov, E., Van Minh, N., Gorshenkov, M. V., Kuznetsov, D., 2018. Ceram. Int. 44 (10), 11257–11264.
Kumta, P.N., Sfeir, C., Lee, D.H., Olton, D., Choi, D., 2005. Acta Biomater. 1 (1), 65–83.
Kuriakose, T.A., Kalkura, S.N., Palanichamy, M., Arivuoli, D., Dierks, K., Bocelli, G., Betzel, C., 2004. J. Cryst. Growth 263 (1–4), 517–523.
Kuznetsov, A.V., Fomin, A.S., Veresov, A.G., Putlyaev, V.I., Fadeeva, I.V., Barinov, S.M., 2008. Russ. J. Inorg. Chem. 53, 1–5.
Lacambra-Andreu, X., Maazouz, A., Lamnawar, K., Chenal, J.M., 2023. Biomimetics 8 (1), 81.
Lai, C., Wang, Y.J., Wei, K., 2008. Colloids Surf. A: Physicochem. Eng. Asp. 315 (1–3), 268–274.
Lakrat, M., Jodati, H., Mejdoubi, E.M., Evis, Z., 2023. Powder Technol. 413, 118026.
Laky, M., Egelja, M., Kurzmann, C., Laky, B., Arslan, M., Shokoohi-Tabrizi, H., Moritz, A., 2023. Lasers Med. Sci. 38 (1), 1–7.
Laonapakul, T., 2015. Eng. Appl. Sci. Res. 42, 269–275.
Layrolle, P., Ito, A., Tateishi, T., 1998. J. Am. Ceram. Soc. 81 (6), 1421–1428.
Lee, S.W., Kim, S.G., Balázsi, C., Chae, W.S., Lee, H.O., 2012. Oral Surg. Oral Med. Oral Pathol. Oral Radiol. 113 (3), 348–355.
Lee, D.K., Park, J.Y., Kim, M.R., Jang, D.J., 2011. CrstEngComm 13 (17), 5455–5459.
Lee, S., Sugimoto, Y., Kato, K., Miyajima, T., Sakurai, M., Nagata, F., 2022. J. Asian Ceram. Soc. 10 (4), 744–754.
Lett, J.A., Ravichandran, K., Sundareswari, M., 2015. J. Chem. Pharm. Res. 7 (2), 231–239.
Li, P., De Groot, K., 1994. J. Sol-Gel Sci. Technol. 2, 797–801.
Li, D., Huang, X., Wu, Y., Li, J., Cheng, W., He, J., Huang, Y., 2016. Biomater. Sci. 4 (2), 272–280.

Li, J., Li, W., Kong, M., Li, Z., Yang, T., Wang, Q., Teng, W., 2023. J. Nanobiotechnol. 21 (1), 1–20.
Li, S., Wang, K., Chang, K.C.A., Zong, M., Wang, J., Cao, Y., Zhang, Z., 2012. Sci. China Chem. 55, 1134–1139.
Li, C., Wang, H., Georgakopoulou, A., Gil, S., Yannaki, E., Lieber, A., 2021. Mol. Ther. 29 (2), 822–837.
Li, W., Wu, Y., Zhang, X., Wu, T., Huang, K., Wang, B., Liao, J., 2023. RSC Adv. 13 (25), 16773–16788.
Liang, T., Qian, J., Yuan, Y., Liu, C., 2013. J. Mater. Sci. 48, 5334–5341.
Liao, J., Li, Y., Zou, Q., Duan, X., Yang, Z., Xie, Y., Liu, H., 2016. Mater. Sci. Eng. C 63, 285–291.
Lin, K., Liu, X., Chang, J., Zhu, Y., 2011. Nanoscale 3 (8), 3052–3055.
Liou, S.C., Chen, S.Y., Lee, H.Y., Bow, J.S., 2004. Biomaterials 25 (2), 189–196.
Litak, J., Czyzewski, W., Szymoniuk, M., Pastuszak, B., Litak, J., Litak, G., Kamieniak, P., 2022. Materials 15 (8), 2906.
Liu, X., Bao, C., Xu, H.H., Pan, J., Hu, J., Wang, P., Luo, E., 2016. Acta Biomater. 42, 378–388.
Liu, C., Huang, Y., Shen, W., Cui, J., 2001. Biomaterials 22 (4), 301–306.
Liu, X., Huang, H., Zhang, J., Sun, T., Zhang, W., Li, Z., 2023. Bioengineering 10 (4), 414.
Liu, Y., Nancollas, G.H., 1997. J. Phys. Chem. B 101 (18), 3464–3468.
Liu, R., Wang, Y., Lee, J., Shen, C., 2018. Astrophys J 870 (1), 15.
Liu, A., Xue, G.H., Sun, M., Shao, H.F., Ma, C.Y., Gao, Q., He, Y., 2016. Sci. Rep. 6 (1), 21704.
Liu, C.P., Yang, Y.X., 2014. Asian J. Chem. 26, 5466–5468.
Liu, J., Yao, R., Guo, J., Gao, T., He, J., Meng, G., Wu, F., 2021. Colloids Surf. B: Biointerfaces 204, 111822.
Liu, S., Zhou, H., Liu, H., Ji, H., Fei, W., Luo, E., 2019. Cell Prolif. 52 (3), e12613.
Londoño-Restrepo, S.M., Ramirez-Gutierrez, C.F., del Real, A., Rubio-Rosas, E., Rodriguez-García, M.E., 2016. J. Mater. Sci. 51, 4431–4441.
Long, T., Guo, Y.P., Liu, Y.Z., Zhu, Z.A., 2013. RSC Adv. 3 (46), 24169–24176.
Loo, S.C.J., Siew, Y.E., Ho, S., Boey, F.Y.C., Ma, J., 2008. J. Mater. Sci. - Mater. Med. 19, 1389–1397.
López-Noriega, A., Quinlan, E., Celikkin, N., O'Brien, F.J., 2015. APL Mater. 3 (1).
Lu, H., Liu, Y., Guo, J., Wu, H., Wang, J., Wu, G., 2016. Int. J. Mol. Sci. 17 (3), 334.
Lu, T., Ma, N., He, F., Liang, Y., Ye, J., 2023. J. Biomater. Appl. 37 (6), 1007–1017.
Lu, L., Mikos, A.G., 1996. MRS Bull. 21 (11), 28–32.
Lu, T., Yuan, X., Zhang, L., He, F., Wang, X., Ye, J., 2023. Mater. Today Chem. 29, 101410.
Lukina, Y., Kotov, S., Bionyshev-Abramov, L., Serejnikova, N., Chelmodeev, R., Fadeev, R., Sivkov, S., 2023. Ceramics 6 (1), 168–194.
Ma, H., Su, W., Tai, Z., Sun, D., Yan, X., Liu, B., Xue, Q., 2012. Chin. Sci. Bull. 57, 3051–3058.
Maadani, A.M., Salahinejad, E., 2022. J. Controll. Rel. 351, 1–7.
Macha, I.J., Cazalbou, S., Shimmon, R., Ben-Nissan, B., Milthorpe, B., 2017. J. Tissue Eng. Regen. Med. 11 (6), 1723–1731.
Maciąg, F., Moskalewicz, T., Cholewa-Kowalska, K., Hadzhieva, Z., Dziadek, M., Łukaszczyk, A., Boccaccini, A.R., 2023. Metall. Mater. Trans. A 54 (1), 241–260.
Madanayake, N.H., Adassooriya, N.M., Salim, N., 2021. Environmental Nanotechnology. Monit. Manag. 15, 100404.
Mai, H.D., Rafiq, K., Yoo, H., 2017. Chem.–A: Eur. J. 23 (24), 5631–5651.
Manafi, S.A., Joughehdoust, S., 2009. Iran. J. Pharm. Sci. 5 (2), 89–94.
Manafi, S., Rahimipour, M.R., 2011. Chem. Eng. Technol. 34 (6), 972–976.
Martínez-Vázquez, F.J., Cabañas, M.V., Paris, J.L., Lozano, D., Vallet-Regí, M., 2015. Acta Biomater. 15, 200–209.
Md Dali, S.S., Wong, S.K., Chin, K.Y., Ahmad, F., 2023. Int. J. Mol. Sci. 24 (8), 7161.
Medvecky, L., Stulajterova, R., Giretova, M., Sopcak, T., Girman, V., 2022. Ceram. Int. 48 (12), 17776–17788.
Mehnath, S., Jeyaraj, M., 2021. Functional Nanomaterials for Regenerative Tissue Medicines. CRC Press, pp. 195–238.
Mehnath, S., Jeyaraj, M., 2021. Functional Nanomaterials for Regenerative Tissue Medicines. CRC Press, pp. 195–238.
Mehnath, S., Jeyaraj, M., 2023. Mater. Chem. Phys. 295, 127061.
Mehnath, S., Muthuraj, V., Jeyaraj, M., 2022. Eur. Polym. J. 175, 111387.
Mehta, D., George, S., Mondal, P., 2014. Int. J. Res. Advent Technol. 2 (4), 159–161.
Memarpour, M., Shafiei, F., Rafiee, A., Soltani, M., Dashti, M.H., 2019. BMC Oral Health 19 (1), 1–14.
Mendez-Lozano, N., Apatiga-Castro, M., Soto, K.M., Manzano-Ramírez, A., Zamora-Antunano, M., Gonzalez-Gutierrez, C., 2022. J. Saudi Chem. Soc. 26 (4), 101513.
Méndez-Lozano, N., Pérez-Ramírez, E.E., de la Luz-Asunción, M., 2024. Ceramics 7 (2), 735–742.
Milovac, D., Ferrer, G.G., Ivankovic, M., Ivankovic, H., 2014. Mater. Sci. Eng. C 34, 437–445.
Minaev, N.V., Minaeva, S.A., Sherstneva, A.A., Chernenok, T.V., Sedova, Y.K., Minaeva, E.D., Demina, T.S., 2022. Polymers 14 (20), 4309.
Minim, P.R., Silva, L.A., Ferrairo, B.M., Pereira, L.F., Goulart, C.A., Monteiro, R.S., Rubo, J.H., 2023. J. Mech. Behav. Biomed. Mater., 105993
Miola, M., Lucchetta, G., Vernè, E., 2023. J. Non Cryst. Solids 618, 122527.
Miranda-Oporta, C., Araya-Calvo, M., Araya-Sibaja, A.M., Vega-Baudrit, J.R., Arguello-Rivera, C., Loaiza-Montoya, R., Guillén-Girón, T., 2023. Bioprinting 33, e00283.
Miyatake, N., Kishimoto, K.N., Anada, T., Imaizumi, H., Itoi, E., Suzuki, O., 2009. Biomaterials 30 (6), 1005–1014.
Mo, X., Zhang, D., Liu, K., Zhao, X., Li, X., Wang, W., 2023. Int. J. Mol. Sci. 24 (2), 1291.
Mohd Pu'ad, N.A.S., Latif, A.F.A., Ramli, N.D., Muhamad, M.S., Abdullah, H.Z., Idris, M. I., Lee, T.C., 2020. Materials Science Forum Vol. 1010, 579–583.
Mohseni, E., Zalnezhad, E., Bushroa, A.R., 2014. Int. J. Adhes. Adhes. 48, 238–257.
Monma, H., Kamiya, T., 1987. J. Mater. Sci. 22, 4247–4250.
Monteiro, M., Medina, L., Casanova, P., Espinola, M., Machado, A., Ribeiro, A.A., Nogueira, R.E.Q., 2023. Ceram. Int.
Montemurro, N., Pierozzi, E., Inchingolo, A.M., Pahwa, B., De Carlo, A., Palermo, A., Rapone, B., 2023. Eur. Rev. Med. Pharmacol. Sci. 27 (16).
Morey, G.W., Niggli, P., 1913. J. Am. Chem. Soc. 35 (9), 1086–1130.
Morgan, H., Wilson, R.M., Elliott, J.C., Dowker, S.E.P., Anderson, P., 2000. Biomaterials 21 (6), 617–627.
Motelica-Heino, M., Predoi, M.V., Ciobanu, S.C., Iconaru, S.L., Predoi, D., 2023. Coatings 13 (2), 472.
Mou, Z.L., Zhao, L.J., Zhang, Q.A., Zhang, J., Zhang, Z.Q., 2011. J. Supercrit. Fluids 58 (3), 398–406.
Mouriño, V., Boccaccini, A.R., 2010. J. R. Soc. Interface 7 (43), 209–227.
MubarakAli, D., Arunachalam, K., Lakshmanan, M., Badar, B., Kim, J.W., Lee, S.Y., 2023. Pharmaceutics 15 (2), 463.
Murata, H., Kawanabe, R., Tada, A., Tokudome, Y., Nakahira, A., 2023. J. Ceram. Soc. Jpn. 131 (2), 17–21.
Murray, M.G.S., Wang, J., Ponton, C.B., Marquis, P.M., 1995. J. Mater. Sci. 30, 3061–3074.
Murugan, L., Kim, S.M., Rajesh, A., Arunachalam, K., Davoodbasha, M., Kim, J.W., Lee, S.Y., 2023. BioNanoScience 1–10.
Muthu, D., Kumar, G.S., Gowri, M., Prasath, M., Viswabaskaran, V., Kattimani, V.S., Girija, E.K., 2022. Ceram. Int. 48 (1), 1326–1339.
Narayanan, R., Seshadri, S.K., Kwon, T.Y., Kim, K.H., 2008. J. Biomed. Mater. Res. Part B: Appl. Biomater.: Off. J. Soc. Biomater. Jpn. Soc. Biomater. Aust. Soc. Biomater. Kor. Soc. Biomater. 85 (1), 279–299.
Naseri, K., Khademi, E., Mortazavi-Derazkola, S., 2023. Arab. J. Chem. 16 (1), 104404.
Nayak, A.K., 2010. Int. J. ChemTech Res. 2 (2), 903–907.
Neira, I.S., Guitián, F., Taniguchi, T., Watanabe, T., Yoshimura, M., 2008. J. Mater. Sci. 43, 2171–2178.
Neovius, E., Engstrand, T., 2010. J. Plast. Reconstr. Aesthet. Surg. 63 (10), 1615–1623.
Nguyen, N.M., Kakarla, A.B., Nukala, S.G., Kong, C., Baji, A., Kong, I., 2023. Polymers 15 (19), 3980.
Niakan, A., Ramesh, S., Ganesan, P., Tan, C.Y., Purbolaksono, J., Chandran, H., Teng, W. D., 2015. Ceram. Int. 41, 3024–3029.
Niakan, A., Ramesh, S., Naveen, S.V., Mohan, S., Kamarul, T., 2017. Mater. Lett. 197, 83–86.
Niinomi, M., 2008. J. Mech. Behav. Biomed. Mater. 1 (1), 30–42.
Niu, X., Chen, S., Tian, F., Wang, L., Feng, Q., Fan, Y., 2017. Mater. Sci. Eng. C 70, 1120–1124.
Niziołek, K., Słota, D., Sadlik, J., Łachut, E., Florkiewicz, W., Sobczak-Kupiec, A., 2023. Materials 16 (19), 6431.
Nobre, C.M.G., Pütz, N., Hannig, M., 2020. Scanning 2020, 1–12.
Noruzi, M., Hadian, P., Soleimanpour, L., Ma'mani, L., Shahbazi, K., 2023. Chem. Biol. Technol. Agric. 10 (1), 1–18.
Núñez, D., Serrano, J.A., Mancisidor, A., Elgueta, E., Varaprasad, K., Oyarzún, P., Rivas, B.L., 2019. RSC Adv. 9 (40), 22883–22890.
Nurbaiti, N., Herliansyah, M.K., Tontowi, A.E., Widiastuti, M.G., Hoten, H.V., 2024. Int. J. Eng. 37 (9), 1755–1762.
Obada, D.O., Dauda, E.T., Abifarin, J.K., Dodoo-Arhin, D., Bansod, N.D., 2020. Mater. Chem. Phys. 239, 122099.
Obada, D.O., Aliyu, A., Kuta, U.M., Lisiyas, A., Ogenyi, V.F., Aquatar, M.O., Adam, I., 2022. WIT Trans. Ecol. Environ. 257, 199–210.
Obada, D.O., Salami, K.A., Alabi, A.A., Oyedeji, A.N., Csaki, S., Hulan, T., Meher, A.K., 2023. J. Korean Ceram. Soc. 60 (1), 99–112.
Odusote, J.K., Danyuo, Y., Baruwa, A.D., Azeez, A.A., 2019. J. Appl. Biomater. Funct. Mater. 17 (2), 2280800019836829.
Oizumi, I., Hamai, R., Shiwaku, Y., Mori, Y., Anada, T., Baba, K., Suzuki, O., 2021. Acta Biomater. 124, 358–373.
Okada, M., Furuzono, T., 2007. J. Nanopart. Res. 9, 807–815.
Okpe, P.C., Folorunso, O., Aigbodion, V.S., Obayi, C., 2024. J. Biomed. Mater. Res. Part B: Appl. Biomat. 112 (7), e35440.
Öner, M., Yetiz, E., Ay, E., Uysal, U., 2011. Ceram. Int. 37 (7), 2117–2125.
Oonishi, H., 1991. Biomaterials 12 (2), 171–178.
Oryan, A., Alidadi, S., Moshiri, A., 2013. Hard Tissue 2 (2), 1–12.
Oryan, A., Alidadi, S., Moshiri, A., Maffulli, N., 2014. J. Orthop. Surg. Res. 9, 1–27.
Osuchukwu, O.A., Salihi, A., Abdullahi, I., Abdulkareem, B., Nwannenna, C.S., 2021. SN Appl. Sci. 3, 1–23.
Osuchukwu, O.A., Salihi, A., Abdullahi, I., Obada, D.O., Abolade, S.A., Akande, A., Csaki, S., 2022a. Mater. Lett. 326, 132977.
Osuchukwu, O.A., Salihi, A., Abdullahi, I., Obada, D.O., 2022b. Sci. Rep. 12 (1), 17968.
Osuchukwu, O.A., Salihi, A., Abdullahi, I., Obada, D.O., 2022c. Data Brief 42, 108305.
Osuchukwu, O.A., Salihi, A., Abdullahi, I., Obada, D.O., 2022d. Mater. Today:. Proc. 62, 4182–4187.
Osuchukwu, O.A., Salihi, A., Abdullahi, I., Obada, D.O., Abolade, S.A., Akande, A., Dodoo-Arhin, D., 2023. Data Brief 48, 109075.
Osuchukwu, O.A., Salihi, A., Abdullahi, I., Etinosa, P.O., Obada, D.O., 2023. Mater. Chem. Phys., 127434
Osuchukwu, O.A., Salihi, A., Abdullahi, I., Etinosa, P.O., Obada, D.O., 2023. Results Mater. 18, 100394.
Ozawa, M., Suzuki, S., 2002. J. Am. Ceram. Soc. 85 (5), 1315–1317.
Pacheco, H., Vedantham, K., Aniket, Young, A., Marriott, I., El-Ghannam, A., 2014. J. Biomed. Mater. Res. A 102 (12), 4213–4223.
Paital, S.R., Dahotre, N.B., 2009. Mater. Sci. Eng. R. Rep. 66 (1–3), 1–70.
Pal, A., Paul, S., Choudhury, A.R., Balla, V.K., Das, M., Sinha, A., 2017. Mater. Lett. 203, 89–92.

Pal, A., Nasker, P., Paul, S., Chowdhury, A.R., Sinha, A., Das, M., 2019. J. Mech. Behav. Biomed. Mater. 90, 328–336.
Palazzo, B., Walsh, D., Iafisco, M., Foresti, E., Bertinetti, L., Martra, G., Roveri, N., 2009. Acta Biomater. 5 (4), 1241–1252.
Pamungkas, A., Dhelika, R., Saragih, A.S., 2019. In: AIP Conference Proceedings, Vol. 2092, No. 1, AIP Publishing LLC, p. 020034.
Panda, N.N., Pramanik, K., Sukla, L.B., 2014. Bioprocess Biosyst. Eng. 37, 433–440.
Park, J.E., Jang, Y.S., Seo, J.M., Lee, M.H., 2023. Biointerphases 18 (3).
Patel, D., Wairkar, S., 2023. Drug Deliv. Transl. Res. 13 (2), 419–432.
Petrakova, N.V., Teterina, A.Y., Mikheeva, P.V., Akhmedova, S.A., Kuvshinova, E.A., Sviridova, I.K., Komlev, V.S., 2021. ACS Omega 6 (11), 7487–7498.
Pieters, I.Y., De Maeyer, E.A., Verbeeck, R.M., 1998. Inorg. Chem. 37 (24), 6392–6395.
Poinern, G.J.E., Brundavanam, R.L.X.T., Le, X.T., Djordjevic, S., Prokic, M., Fawcett, D., 2011. Int. J. Nanomed. 2083–2095.
Ponomareva, N.I., Poprygina, T.D., Karpov, S.I., Lesovoi, M.V., Agapov, B.L., 2010. Russ. J. Gen. Chem. 80, 905–908.
Pon-On, W., Suntornsaratoon, P., Charoenphandhu, N., Thongbunchoo, J., Krishnamra, N., Ming Tang, I., 2016. Mater. Sci. Eng. C: Mater. Biol. Appl. 62, 183–189.
Pourmadadi, M., Yazdian, F., Koulivand, A., Rahmani, E., 2023. Int. J. Biol. Macromol. 240, 124345.
Pramono, D.D., Puspitasari, P., 2024, June. In: AIP Conference Proceedings, Vol. 2991, No. 1. AIP Publishing.
Prasad, P.S., Marupalli, B.C., Das, S., Das, K., 2023. J. Mater. Sci. 58 (14), 6076–6105.
Przekora, A., Palka, K., Ginalska, G., 2016. Mater. Sci. Eng. C 58, 891–899.
Pu'ad, N.M., Haq, R.A., Noh, H.M., Abdullah, H.Z., Idris, M.I., Lee, T.C., 2020. Mater. Today:. Proc. 29, 233–239.
Qamar, Z., Har, Z.B., Chew, H.P., Fatima, T., 2017. J. Pak. Med. Assoc. 67 (1), 116–120.
Qiao, S.Z., Liu, J., Lu, G.Q.M., 2011. Modern Inorganic Synthetic Chemistry. Elsevier, pp. 479–506.
Raghavendra, G.M., Varaprasad, K., Jayaramudu, T., 2015. Nanotechnology Applications for Tissue Engineering. William Andrew Publishing, pp. 21–44.
Ramesh, S., Tolouei, R., Hamdi, M., Purbolaksono, J., Tan, Y., Amiriyan, M., Teng, W., 2011. Curr. Nanosci. 7 (6), 845–849.
Ramesh, S., Natasha, A.N., Tan, C.Y., Bang, L.T., Ching, C.Y., Chandran, H., 2016. Ceram. Int. 42, 7824–7829.
Ramirez-Gutierrez, C.F., Londoño-Restrepo, S.M., Del Real, A., Mondragón, M.A., Rodriguez-García, M.E., 2017. Ceram. Int. 43, 7552–7559.
Ravaglioli, A., Krajewski, A., 1991. Bioceramics: Materials·Properties·Applications. Springer Science & Business Media.
Razali, N.M., Pramanik, S., Osman, N.A., Radzi, Z., Pingguan-Murphy, B., 2016. J. Ceram. Process. Res. 17, 699–706.
Ressler, A., Ivanković, T., Ivanišević, I., Cvetnić, M., Antunović, M., Urlić, I., Ivanković, M., 2023. Ceram. Int. 49 (7), 11005–11017.
Ribas, R.G., Schatkoski, V.M., do Amaral Montanheiro, T.L., de Menezes, B.R.C., Stegemann, C., Leite, D.M.G., Thim, G.P., 2019. Ceram. Int. 45 (17), 21051–21061.
Rivera, E.M., Araiza, M., Brostow, W., Castano, V.M., Dıaz-Estrada, J.R., Hernández, R., Rodrıguez, J.R., 1999. Mater. Lett. 41 (3), 128–134.
Rong, Z.J., Yang, L.J., Cai, B.T., Zhu, L.X., Cao, Y.L., Wu, G.F., Zhang, Z.J., 2016. J. Mater. Sci. - Mater. Med. 27, 1–12.
Roohani, I., Cheong, S., Wang, A., 2021. Open Ceramics 6, 100092.
Rouhani, P., Taghavinia, N., Rouhani, S., 2010. Ultrason. Sonochem. 17 (5), 853–856.
Roy, S.D., Das, K.C., Dhar, S.S., 2023. Biomass Convers. Biorefin. 1–11.
Sachlos, E., Czernuszka, J.T., 2003. Eur. Cell. Mater. 5 (29), 39–40.
Sadat-Shojai, M., 2009. J. Iran. Chem. Soc. 6, 386–392.
Sadat-Shojai, M., Khorasani, M.T., Jamshidi, A., Irani, S., 2013. Mater. Sci. Eng. C 33 (5), 2776–2787.
Sagare, R.D., Dasankoppa, F.S., Sholapur, H.N., Banapurmath, N.R., Umarfarooq, M.A., 2023. J. Drug Delivery Sci. Technol., 104637
Saha, S.K., Banerjee, A., Banerjee, S., Bose, S., 2009. Mater. Sci. Eng. C 29 (7), 2294–2301.
Said, H.A., Mabroum, H., Lahcini, M., Oudadesse, H., Barroug, A., Youcef, H.B., Noukrati, H., 2023. Int. J. Biol. Macromol., 125150
Sankar, J., Kumar, S.S., 2021. INCAS Bull. 13 (1), 173–181.
Sano, Y., Kobayashi, S., Shirai, K., Takahata, N., Matsumoto, K., Watanabe, T., Iwai, K., 2012. Nat. Commun. 3 (1), 761.
Sanosh, K.P., Chu, M.C., Balakrishnan, A., Kim, T.N., Cho, S.J., 2009. Bull. Mater. Sci. 32, 465–470.
Santhosh, S., Prabu, S.B., 2013. Mater. Lett. 97, 121–124.
Santos, M.H., Oliveira, M.D., Souza, L.P.D.F., Mansur, H.S., Vasconcelos, W.L., 2004. Mater. Res. 7, 625–630.
Sathiskumar, S., Vanaraj, S., Sabarinathan, D., Bharath, S., Sivarasan, G., Arulmani, S., Ponnusamy, V.K., 2019. Ceram. Int. 45 (6), 7804–7810.
Sathiyavimal, S., Vasantharaj, S., Shanmugavel, M., Manikandan, E., Nguyen-Tri, P., Brindhadevi, K., Pugazhendhi, A., 2020. Prog. Org. Coat. 148, 105890.
Sathiyavimal, S., Vasantharaj, S., LewisOscar, F., Selvaraj, R., Brindhadevi, K., Pugazhendhi, A., 2020. Prog. Org. Coat. 147, 105858.
Schulze, F., Lang, A., Schoon, J., Wassilew, G.I., Reichert, J., 2023. Biomedicines 11 (2), 325.
Selvakumar, M., Jaganathan, S.K., Nando, G.B., Chattopadhyay, S., 2015. J. Biomed. Nanotechnol. 11 (2), 291–305.
Senatov, F.S., Niaza, K.V., Zadorozhnyy, M.Y., Maksimkin, A.V., Kaloshkin, S.D., Estrin, Y.Z., 2016. J. Mech. Behav. Biomed. Mater. 57, 139–148.
Senopati, G., Rahman Rashid, R.A., Kartika, I., Palanisamy, S., 2023. Metals 13 (2), 194.
Seredin, P., Goloshchapov, D., Buylov, N., Kashkarov, V., Emelyanova, A., Eremeev, K., Ippolitov, Y., 2022. Nanomaterials 12 (24), 4453.
Seredin, P.V., Goloshchapov, D.L., Buylov, N.S., Kashkarov, V.M., Emelyanova, A.A., Eremeev, K.A., Ippolitov, Y.A., 2023. Results Eng. 17, 100900.
Service, R.F., 2000. Science 1498–1500.
Seshima, H., Yoshinari, M., Takemoto, S., Hattori, M., Kawada, E., Inoue, T., Oda, Y., 2006. J. Biomed. Mater. Res. Part B: Appl. Biomater.: Off. J. Soc. Biomater. Jpn. Soc. Biomater. Aust. Soc. Biomater. Kor. Soc. Biomater. 78 (2), 215–221.
Shafiq, F., Liu, C., Zhou, H., Chen, H., Yu, S., Qiao, W., 2023. Colloids Surf. A: Physicochem. Eng. Asp. 672, 131713.
Shao, F., Liu, L., Fan, K., Cai, Y., Yao, J., 2012. J. Mater. Sci. 47, 1054–1058.
Shariffuddin, J.H., Jones, M.I., Patterson, D.A., 2013. Chem. Eng. Res. Des. 91 (9), 1693–1704.
Shavandi, A., Bekhit, A.E.D.A., Ali, A., Sun, Z., 2015. Mater. Chem. Phys. 149, 607–616.
Sheng, X., Li, C., Wang, Z., Xu, Y., Sun, Y., Zhang, W., Wang, J., 2023. Mater. Today Biol., 100636
Shepherd, D.V., Kauppinen, K., Brooks, R.A., Best, S.M., 2014. J. Biomed. Mater. Res. A 102 (11), 4136–4141.
Sheykholeslami, S.O.R., Khalil-Allafi, J., Etminanfar, M., Khalili, V., Parsa, A.B., 2023. Surf. Coat. Technol. 459, 129410.
Shi, X., Ai, X., Zhang, Q., Lu, X., Gu, S., Su, L., Jiang, W., 2020. J. Adv. Ceram. 9, 424–431.
Shi, P., Cheng, Z., Zhao, K., Chen, Y., Zhang, A., Gan, W., Zhang, Y., 2023. J. Nanobiotechnol. 21 (1), 1–27.
Shih, W.J., Chen, Y.F., Wang, M.C., Hon, M.H., 2004. J. Cryst. Growth 270 (1–2), 211–218.
Shih, W.J., Wang, M.C., Hon, M.H., 2005. J. Cryst. Growth 275 (1–2), e2339–e2344.
Shirkhanzadeh, M., 1998. J. Mater. Sci. - Mater. Med. 9, 67–72.
Shobana, K., Swamiappan, S., 2023. Inorg. Chem. Commun. 148, 110347.
Shum, H.C., Bandyopadhyay, A., Bose, S., Weitz, D.A., 2009. Chem. Mater. 21 (22), 5548–5555.
Sidane, D., Chicot, D., Yala, S., Ziani, S., Khireddine, H., Iost, A., Decoopman, X., 2015. Thin Solid Films 593, 71–80.
Sidane, D., Khireddine, H., Yala, S., Ziani, S., Bir, F., Chicot, D., 2015. Metall. Mater. Trans. B 46, 2340–2347.
Sidane, D., Rammal, H., Beljebbar, A., Gangloff, S.C., Chicot, D., Velard, F., Kerdjoudj, H., 2017. Mater. Sci. Eng. C 72, 650–658.
Singh, R.K., Kim, T.H., Patel, K.D., Mahapatra, C., Dashnyam, K., Kang, M.S., Kim, H.W., 2014. J. Am. Ceram. Soc. 97 (10), 3071–3076.
Singh, S., Manoj Kumar, R., Kuntal, K.K., Gupta, P., Das, S., Jayaganthan, R., Lahiri, D., 2015. JOM 67, 702–712.
Sinkler, M.A., Furdock, R.J., McMellen, C.J., Calcei, J.G., Voos, J.E., 2023. J. Arthrosc. Relat. Surg. 39 (2), 166–175.
Sirajunisha, H., Balakrishnan, T., Sakthivel, P., Krishnaveni, A., 2023. Chem. Phys. Impact 6, 100159.
Skelly, J.D., Lange, J., Filion, T.M., Li, X., Ayers, D.C., Song, J., 2014. Clin. Orthopaed. Relat. Res.® 472, 4015–4023.
Skwira, A., Szewczyk, A., Barros, J., Laranjeira, M., Monteiro, F.J., Sądej, R., Prokopowicz, M., 2023. Int. J. Pharm. 645, 123408.
Smeriglio, P., Zalc, A., 2023. Curr. Osteoporos. Rep. 21 (5), 624–631.
Snyders, R., Bousser, E., Music, D., Jensen, J., Hocquet, S., Schneider, J.M., 2008. Plasma Processes Polym. 5 (2), 168–174.
Soares, F., Ribeiro, N., Baião, A., Sarmento, B., Olhero, S.M., 2023. J. Drug Delivery Sci. Technol. 88, 104906.
Sobczak, A., Kida, A., Kowalski, Z., Wzorek, Z., 2009. Pol. J. Chem. Technol. 11 (1), 37–43.
Sobczak, A., Kowalski, Z., Wzorek, Z., 2009. Acta Bioeng. Biomech. 11 (4), 23–28.
Sofronia, A.M., Baies, R., Anghel, E.M., Marinescu, C.A., Tanasescu, S., 2014. Mater. Sci. Eng. C 43, 153–163.
Song, J., Li, L., Fang, L., Zhang, E., Zhang, Y., Zhang, Z., Xue, J., 2023. BMEMat 1 (4), e12046.
Sossa, P.A.F., Giraldo, B.S., Garcia, B.C.G., Parra, E.R., Arango, P.J.A., 2018. Matéria (Rio de Janeiro) 23.
Stahl, A., Yang, Y.P., 2021. Tissue Eng. B Rev. 27 (6), 539–547.
Stea, S., Visentin, M., Savarino, L., Donati, M.E., Pizzoferrato, A., Moroni, A., Caja, V., 1995. J. Mater. Sci. - Mater. Med. 6, 455–459.
Štulajterová, R., Medvecký, Ľ., 2008. Colloids Surf. A: Physicochem. Eng. Asp. 316 (1–3), 104–109.
Sturgeon, J.L., Brown, P.W., 2009. J. Mater. Sci. - Mater. Med. 20, 1787–1794.
Suchanek, W.L., Riman, R.E., 2006. Adv. Sci. Technol. 45, 184–193.
Sultana, S., Hossain, M.S., Mahmud, M., Mobarak, M.B., Kabir, M.H., Sharmin, N., Ahmed, S., 2021. UV-assisted synthesis of hydroxyapatite from eggshells at ambient temperature: cytotoxicity, drug delivery and bioactivity. RSC Adv. 11 (6), 3686–3694.
Sultana, N., Mokhtar, M., Hassan, M.I., Jin, R.M., Roozbahani, F., Khan, T.H., 2015. Mater. Manuf. Process. 30 (3), 273–278.
Sun, Y., Guo, G., Tao, D., Wang, Z., 2007. J. Phys. Chem. Solid 68 (3), 373–377.
Sun, R.X., Lv, Y., Niu, Y.R., Zhao, X.H., Cao, D.S., Tang, J., Chen, K.Z., 2017. Ceram. Int. 43 (18), 16792–16798.
Sunil, B.R., Jagannatham, M., 2016. Mater. Lett. 185, 411–414.
Suresh Kumar, C., Dhanaraj, K., Vimalathithan, R.M., Ilaiyaraja, P., Suresh, G., 2020. J. Asian Ceram. Soc. 8 (2), 416–429.
Surmenev, R.A., 2012. Surf. Coat. Technol. 206 (8–9), 2035–2056.
Surmenev, R.A., Surmeneva, M.A., Ivanova, A.A., 2014. Acta Biomater. 10 (2), 557–579.
Surya, P., Nithin, A., Sundaramanickam, A., Sathish, M., 2021. J. Mech. Behav. Biomed. Mater. 119, 104501.
Swadi, A.K., Jassim, Z.W., Kadum, M.U., Ali, M.R.M., 2012. Baghdad Sci. J. 9 (3), 541–547.

Swain, S.K., Sarkar, D., 2011. Ceram. Int. 37 (7), 2927–2930.
Szcześ, A., Hołysz, L., Chibowski, E., 2017. Adv. Colloid Interface Sci. 249, 321–330.
Szterner, P., Antosik, A., Pagacz, J., Tymowicz-Grzyb, P., 2023. Crystals 13 (5), 793.
Tan, C.Y., Yaghoubi, A., Ramesh, S., Adzila, S., Purbolaksono, J., Hassan, M.A., Kutty, M. G., 2013. Ceram. Int. 39 (8), 8979–8983.
Tang, W.W., 2021. Am. J. Med. 134 (6), 713–720.
Tang, Z., Li, X., Tan, Y., Fan, H., Zhang, X., 2018. Regener. Biomater. 5 (1), 43–59.
Tang, M., Xu, K., Shang, H., Li, X., He, X., Ke, L., Xu, H., 2023. Int. J. Biol. Macromol. 226, 1273–1283.
Tao, J., Jiang, W., Pan, H., Xu, X., Tang, R., 2007. J. Cryst. Growth 308 (1), 151–158.
Tas, A.C., 2000. Synthesis of biomimetic Ca-hydroxyapatite powders at 37 C in synthetic body fluids. Biomaterials 21 (14), 1429–1438.
TenHuisen, K.S., Brown, P.W., 1998. Biomaterials 19 (23), 2209–2217.
Teoh, M.W., Ng, C.K., Lee, K.Y., Ramesh, S., Ting, C.H., Chuah, Y.D., Sutharsini, U., 2023, January. In: AIP Conference Proceedings, Vol. 2643, No. 1. AIP Publishing.
Thamaraiselvi, T.V., Prabakaran, K., Rajeswari, S., 2006. Trends Biomater. Artif. Organs 19 (2), 81–83.
Tierney, J., Jackman, E., Holder, C., Wall, C.J., Wilson, C.J., 2023. J. Arthroplasty.
Tomsia, A.P., Launey, M.E., Lee, J.S., Mankani, M.H., Wegst, U.G., Saiz, E., 2011. Int. J. Oral Maxillofac. Implants 26 (Suppl), 25.
Torres-Mansilla, A., Álvarez-Lloret, P., Fernández-Penas, R., D'Urso, A., Baldión, P.A., Oltolina, F., Gómez-Morales, J., 2023. Nanomaterials 13 (16), 2299.
Trachtenberg, J.E., Placone, J.K., Smith, B.T., Fisher, J.P., Mikos, A.G., 2017. J. Biomater. Sci. Polym. Ed. 28 (6), 532–554.
Tsai, W.T., Yang, J.M., Lai, C.W., Cheng, Y.H., Lin, C.C., Yeh, C.W., 2006. Bioresour. Technol. 97 (3), 488–493.
Tsiourvas, D., Tsetsekou, A., Kammenou, M.I., Boukos, N., 2011. J. Am. Ceram. Soc. 94 (7), 2023–2029.
Uddin, M.N., Jamal, M.S.I., Ali, M.Y., Darda, M.A., Mahedi, S.I., 2023. Emerg. Mater. 1–13.
Udomluck, N., Lee, H., Hong, S., Lee, S.H., Park, H., 2020. Appl. Surf. Sci. 520, 146311.
Ulfah, I.M., Herdianto, N., Aisah, N., Fitriani, D.A., Kurniawati, F., Gustiono, D., Masruroh, M., 2024. Res. Biomed. Eng. 1–10.
Ullah, I., Siddiqui, M.A., Kolawole, S.K., Liu, H., Zhang, J., Ren, L., Yang, K., 2020. Ceram. Int. 46 (10), 14448–14459.
Uskoković, V., Desai, T.A., 2014. J. Pharm. Sci. 103 (2), 567–579.
Vecchio, K.S., Zhang, X., Massie, J.B., Wang, M., Kim, C.W., 2007. Acta Biomater. 3 (6), 910–918.
Veiga, A., Castro, F., Rocha, F., Oliveira, A.L., 2020. Front. Mater. 7, 24.
Verheggen, R., Merten, H.A., 2001. Acta Neurochir. 143, 919–926.
Verma, G., Quadros, M., 2024. In: Engineered Biomaterials: Progress and Prospects, pp. 229–258.
Verma, G., Quadros, M., 2024. In: Engineered Biomaterials: Progress and Prospects, pp. 229–258.
Verrier, S., Alini, M., Alsberg, E., Buchman, S.R., Kelly, D., Laschke, M.W., Evans, C., 2016. Eur. Cell. Mater. 32, 87–110.
Verwilghen, C., Chkir, M., Rio, S., Nzihou, A., Sharrock, P., Depelsenaire, G., 2009. Mater. Sci. Eng. C 29 (3), 771–773.
Vijayakumar, P., 2020. Biocatal. Agric. Biotechnol. 25, 101612.
Villa, M.M., Wang, L., Huang, J., Rowe, D.W., Wei, M., 2015. J. Biomed. Mater. Res. B Appl. Biomater. 103 (2), 243–253.
Vinayagam, R., Kandati, S., Murugesan, G., Goveas, L.C., Baliga, A., Pai, S., Selvaraj, R., 2023. J. Mater. Res. Technol. 22, 169–180.
Von Euw, S., Wang, Y., Laurent, G., Drouet, C., Babonneau, F., Nassif, N., Azaïs, T., 2019. Sci. Rep. 9 (1), 8456.
Wang, G., Babadagli, M.E., Uludag, H., 2011. Mol. Pharm. 8 (4), 1025–1034.
Wang, H., Georgakopoulou, A., Psatha, N., Li, C., Capsali, C., Samal, H.B., Lieber, A., 2019. J. Clin. Invest. 129 (2), 598–615.
Wang, H., Chang, X., Ma, Q., Sun, B., Li, H., Zhou, J., Song, J., 2023. Bioact. Mater. 21, 324–339.
Wang, F., Li, D., Gu, Y., Wei, S., 2023. Crystals 13 (4), 642.
Wang, J., Shaw, L.L., 2007. Adv. Mater. 19 (17), 2364–2369.
Wang, Z., Wang, C., Li, C., Qin, Y., Zhong, L., Chen, B., Wang, J., 2017. J. Alloys Compd. 717, 271–285.
Wang, C., Wang, S., Kang, D.D., Dong, Y., 2023. BMEMat 1 (3), e12039.
Wang, A., Yin, H., Liu, D., Wu, H., Wada, Y., Ren, M., Cheng, X., 2007. Appl. Surf. Sci. 253 (6), 3311–3316.
Wang, J., Yu, Z., Xiao, X., Chen, Z., Huang, J., Liu, Y., 2023. Desalination 565, 116864.
Wardani, S.C., Sujuti, H., Mustamsir, E., Hapsari, D.N., 2020. Journal of Physics: Conference Series, Vol. 1665, No. 1. IOP Publishing, p. 012032.
Wassif, R.K., Elkheshen, S.A., Shamma, R.N., Amer, M.S., Elhelw, R., El-Kayal, M., 2023. Drug Delivery and Translational Research, pp. 1–23.
Webster, T.J., Ergun, C., Doremus, R.H., Bizios, R., 2002. J. Biomed. Mater. Res.: Off. J. Soc. Biomater. Jpn. Soc. Biomater. Aust. Soc. Biomater. Kor. Soc. Biomater. 59 (2), 312–317.
Wei, J., Shi, J., Wu, Q., Yang, L., Cao, S., 2015. J. Mater. Chem. B 3 (41), 8162–8169.
Wei, M., Tang, Y., Chen, L., Zhang, B., Zhang, S., Zhao, K., Wu, Z., 2022. Ceram. Int. 48 (23), 35185–35197.
Weissman, J.L., Snyderman, C.H., Hirsch, B.E., 1996. Am. J. Neuroradiol. 17 (8), 1569–1574.
Wiltfang, J., Kessler, P., Buchfelder, M., Merten, H.A., Neukam, F.W., Rupprecht, S., 2004. J. Oral Maxillofac. Surg. 62 (1), 29–35.
Winkler, T., Sass, F.A., Duda, G.N., Schmidt-Bleek, K., 2018. Bone Joint Res. 7 (3), 232–243.
Wu, X., 2021. Discret. Dyn. Nat. Soc. 2021, 1–8.
Wu, K., Zhou, H., Yang, L., 2023. Woodhead Publishing.
Wu, S.C., Tsou, H.K., Hsu, H.C., Hsu, S.K., Liou, S.P., Ho, W.F., 2013. Ceram. Int. 39 (7), 8183–8188.
Wu, S.C., Hsu, H.C., Hsu, S.K., Tseng, C.P., Ho, W.F., 2017. Adv. Powder Technol. 28, 1154–1158.
Wu, S.C., Kao, Y.L., Lu, Y.C., Hsu, H.C., Ho, W.F., 2021. J. Aust. Ceram. Soc. 57, 1541–1551.
Wu, S.C., Hsu, H.C., Wang, H.F., Liou, S.P., Ho, W.F., 2023. Molecules 28 (13), 4926.
Xiao, W., Bal, B.S., Rahaman, M.N., 2016. Mater. Sci. Eng. C 60, 324–332.
Xie, C.M., Lu, X., Wang, K.F., Meng, F.Z., Jiang, O., Zhang, H.P., Fang, L.M., 2014. ACS Appl. Mater. Interfaces 6 (11), 8580–8589.
Xie, C.M., Lu, X., Wang, K.F., Meng, F.Z., Jiang, O., Zhang, H.P., Fang, L.M., 2014. ACS Appl. Mater. Interfaces 6 (11), 8580–8589.
Xiong, H., Du, S., Ni, J., Zhou, J., Yao, J., 2016. Biomaterials 94, 70–83.
Xu, H., Chen, Y., Zhang, S.F., 2011. Synthesis and reactivity in inorganic, metal-organic, and nano-metal. Chemistry 41 (1), 31–35.
Xu, S., Long, J., Sim, L., Diong, C.H., Ostrikov, K., 2005. Plasma Processes Polym. 2 (5), 373–390.
Yang, Y., Geng, Y., Liu, M., Liu, K., Lv, X., Yu, H., Chen, J., 2022. Compos. B Eng. 247, 110325.
Yang, G., Park, S.J., 2019. Materials 12 (7), 1177.
Yasukawa, A., Matsuura, T., Nakajima, M., Kandori, K., Ishikawa, T., 1999. Mater. Res. Bull. 34 (4), 589–601.
Yoshimura, M., Suda, H., 2017. Hydroxyapatite and Related Materials. CRC Press, pp. 45–72.
Younesi, D., Mehravaran, R., Akbarian, S., Younesi, M., 2013. Mater. Des. 43, 549–559.
Yu, B., Huang, J.C., Zhou, C., He, S., Zhou, W., 2020. Sci. Total Environ. 742, 140661.
Yu, Q., Liu, H., Lv, G., Liu, X., Wang, L., Liao, L., 2023. Sci. Total Environ. 900, 165910.
Yu, W., Sun, T.W., Qi, C., Ding, Z., Zhao, H., Zhao, S., He, Y., 2017. Int. J. Nanomed. 2293–2306.
Yuan, Q., Qin, C., Wu, J., Xu, A., Zhang, Z., Liao, J., Zhang, P., 2016. Mater. Chem. Phys. 182, 365–371.
Yusoff, M.F.M., Kasim, N.H.A., Himratul-Aznita, W.H., Saidin, S., Genasan, K., Kamarul, T., Radzi, Z., 2021. Mater. Charact. 178, 111169.
Zhang, H., Darvell, B.W., 2010. Acta Biomater. 6 (8), 3216–3222.
Zhang, H., Darvell, B.W., 2011. Acta Biomater. 7 (7), 2960–2968.
Zhang, R., Ding, J., Lu, X., Yao, A., Wang, D., 2023. Ceram. Int. 49 (3), 5161–5168.
Zhang, Y., Kong, F., Wu, D., Zhu, J., Yang, S., Kong, X., 2023. Tissue Eng. (ja).
Zhang, Y., Lu, J., 2007. J. Nanopart. Res. 9, 589–594.
Zhang, J., Zhan, X., Wen, X., Song, B., Ma, L., Peng, W., 2009. Inorg. Mater. 45, 1362–1365.
Zhang, H., Zhang, M., 2011. Ceram. Int. 37 (1), 279–286.
Zhang, H., Zhang, M., 2011. Mater. Chem. Phys. 126 (3), 642–648.
Zhang, H., Yan, Y., Wang, Y., Li, S., 2002. Adv. Eng. Mater. 4 (12), 916–919.
Zhang, H.B., Zhou, K.C., Li, Z.Y., Huang, S.P., 2009. J. Phys. Chem. Solid 70 (1), 243–248.
Zhang, H.G., Zhu, Q., 2005. Mater. Lett. 59 (24–25), 3054–3058.
Zhao, X.Y., Zhu, Y.J., Lu, B.Q., Chen, F., Qi, C., Zhao, J., Wu, J., 2014. Mater. Res. Bull. 55, 67–70.
Zhou, W.Y., Wang, M., Cheung, W.L., Guo, B.C., Jia, D.M., 2008. J. Mater. Sci. - Mater. Med. 19, 103–110.
Zhu, W., Li, C., Yao, M., Wang, X., Wang, J., Zhang, W., Lv, H., 2023. Regen. Biomater., rbad030
Zhu, K., Yanagisawa, K., Onda, A., Kajiyoshi, K., Qiu, J., 2009. Mater. Chem. Phys. 113 (1), 239–243.
Zinicovscaia, I., Yushin, N., Humelnicu, D., Ignat, M., Humelnicu, I., Grozdov, D., Vershinina, T., 2023. Separations 10 (7), 401.
Zofkova, I., Davis, M., Blahos, J., 2017. Physiol. Res. 66 (3), 391.
Zubieta-Otero, L.F., Rodriguez-Garcia, M.E., 2023. Next Materials 1 (3), 100019.
Zubieta-Otero, L.F., Rodriguez-Garcia, M.E., 2023. Next Mater. 1 (3), 100019.
Zuliantoni, Z., Suprapto, W., Setyarini, P.H., Gapsari, F., 2022. Results Eng. 14, 100390.